ORIGINAL RESEARCH

Mitochondrial-Mediated Oxidative Ca^{2+}/Calmodulin-Dependent Kinase II Activation Induces Early Afterdepolarizations in Guinea Pig Cardiomyocytes: An In Silico Study

Ruilin Yang, MS; Patrick Ernst, BS; Jiajia Song, PhD; Xiaoguang M. Liu, PhD; Sabine Huke, PhD; Shuxin Wang, PhD; Jianyi Jay Zhang, MD, PhD; Lufang Zhou, PhD

***Background*—**Oxidative stress–mediated Ca^{2+}/calmodulin-dependent protein kinase II (CaMKII) phosphorylation of cardiac ion channels has emerged as a critical contributor to arrhythmogenesis in cardiac pathology. However, the link between mitochondrial-derived reactive oxygen species (mdROS) and increased CaMKII activity in the context of cardiac arrhythmias has not been fully elucidated and is difficult to establish experimentally.

***Methods and Results*—**We hypothesize that pathological mdROS can cause erratic action potentials through the oxidation-dependent CaMKII activation pathway. We further propose that CaMKII-dependent phosphorylation of sarcolemmal slow Na^+ channels alone is sufficient to elicit early afterdepolarizations. To test the hypotheses, we expanded our well-established guinea pig cardiomyocyte *e*xcitation-*c*ontraction coupling, *m*itochondrial *e*nergetics, and *R*OS-*i*nduced-*R*OS-*r*elease model by incorporating oxidative CaMKII activation and CaMKII-dependent Na^+ channel phosphorylation in silico. Simulations show that mdROS mediated-CaMKII activation elicits early afterdepolarizations by augmenting the late Na^+ currents, which can be suppressed by blocking L-type Ca^{2+} channels or Na^+/Ca^{2+} exchangers. Interestingly, we found that oxidative CaMKII activation–induced early afterdepolarizations are sustained even after mdROS has returned to its physiological levels. Moreover, mitochondrial-targeting antioxidant treatment can suppress the early afterdepolarizations, but only if given in an appropriate time window. Incorporating concurrent mdROS-induced ryanodine receptors activation further exacerbates the proarrhythmogenic effect of oxidative CaMKII activation.

***Conclusions*—**We conclude that oxidative CaMKII activation–dependent Na channel phosphorylation is a critical pathway in mitochondria-mediated cardiac arrhythmogenesis. **(*J Am Heart Assoc*. 2018;7:e008939. DOI: 10.1161/JAHA.118.008939.)**

Key Words: arrhythmias • computational modeling • mitochondrial dysfunction • oxidative CaMKII activation

Cardiovascular disease is a major health problem in the United States and its incidence increases steadily as the general population ages.[1] Despite advances in diagnosis and treatment, cardiovascular disease mortality remains high, accounting for nearly 500 000 American deaths each year.[1] About one half of cardiovascular disease–related deaths occur suddenly because of sudden cardiac death resulting from ventricular arrhythmias.[2,3] Although the incidence rate is high, the precise molecular mechanisms underlying cardiac arrhythmogenesis are not fully understood, hindering the development of effective therapeutic strategies.

Recently, loss of mitochondrial function, which is often observed in many disease processes such as heart failure, ischemic cardiomyopathy, hypertrophic cardiomyopathy, and metabolic diseases, has emerged as a key contributor to the arrhythmogenic substrate. While the detailed mechanistic pathways remain incompletely understood, work from our laboratory and others[4–7] suggest that the proarrhythmic

From Key Laboratory for Mechanism Theory and Equipment Design of Ministry of Education, Tianjin University, Tianjin, China (R.Y., S.W.); Departments of Medicine (R.Y., J.S., S.H., L.Z.) and Biomedical Engineering (P.E., X.M.L., J.J.Z., L.Z.), University of Alabama at Birmingham, AL.

Accompanying Tables S1 through S28 and Figures S1 through S4 are available at http://jaha.ahajournals.org/content/7/15/e008939/DC1/embed/inline-supplementary-material-1.pdf

Correspondence to: Lufang Zhou, PhD, Division of Cardiovascular Disease, University of Alabama School of Medicine, 703 19th Street South, ZRB 306, Birmingham, AL 35294. Email: lfzhou@uab.edu

Received February 26, 2018; accepted June 7, 2018.

© 2018 The Authors. Published on behalf of the American Heart Association, Inc., by Wiley. This is an open access article under the terms of the Creative Commons Attribution-NonCommercial-NoDerivs License, which permits use and distribution in any medium, provided the original work is properly cited, the use is non-commercial and no modifications or adaptations are made.

Clinical Perspective

What Is New?

- We developed a multiscale computational model linking cardiomyocyte mitochondrial energetics to Ca^{2+}/calmodulin-dependent protein kinase II activity and Ca^{2+} handling.
- Mitochondrial-mediated oxidative Ca^{2+}/calmodulin-dependent protein kinase II activation is sufficient to elicit early afterdepolarizations solely through enhanced late Na^+ current.
- Oxidative Ca^{2+}/calmodulin-dependent protein kinase II activation–elicited early afterdepolarizations are sustained even after mitochondrial-derived reactive oxygen species has returned to its physiological levels.

What Are the Clinical Implications?

- It is critically important to consider mitochondria when designing novel antiarrhythmic therapies.
- It appears that there is a treatment window for antioxidants to suppress Ca^{2+}/calmodulin-dependent protein kinase II–mediated pathological effects.

effect of mitochondria dysfunction is at least partially attributed to the organellar-derived reactive oxygen species (ROS), which can influence multiple redox-sensitive ion channels/transporters underlying Ca^{2+} handling such as ryanodine receptors (RyRs)[6–9] and sarcoplasmic reticulum (SR) Ca^{2+} ATPase (SERCA).[10,11] Beside Ca^{2+} handling proteins, excessive ROS can also affect sarcolemmal voltage–gated Na^+ channels,[12,13] K^+ channels, Na^+/Ca^{2+} exchanger, and L-type Ca^{2+} channels (LCCs).[11,14–18] In addition to direct modulation of redox-sensitive ion channels, mitochondrial-derived ROS (mdROS) may indirectly influence Ca^{2+} handling and action potentials (APs) via redox signaling pathways such as oxidation-mediated Ca^{2+}/calmodulin-dependent kinase II (CaMKII) phosphorylation. CaMKII is a multifunctional protein kinase ubiquitously expressed in cardiomyocytes and is activated by binding to Ca^{2+}/CaM and subsequent autophosphorylation.[19,20] A growing body of evidence has demonstrated that CaMKII can also be activated by ROS.[21–24] Once activated, CaMKII can phosphorylate a wide range of key Ca^{2+} and Na^+ regulatory proteins such as LCCs,[25–28] RyRs,[29–35] phosphalamban,[29,34,36] and Na^+ channels.[37,38] Importantly, Xie et al[39] showed that H_2O_2 perfusion–induced oxidative CaMKII activation leads to afterdepolarizations in isolated rabbit cardiomyocytes, likely by phosphorylation of Na^+ channels and LCCs. Given those advances, the detailed mechanistic pathways by which oxidation-dependent CaMKII activation creates a proarrhythmia substrate in diseased hearts remain unclear, partially because of the multidirectional interaction loops between CaMKII activation and ion handling. As a powerful tool complementary to experimental measurement, computational modeling has been applied to elucidate how CaMKII activation may influence cardiac ion handling and electrophysiology. For instance, Onal et al[40] explored the CaMKII-dependent regulation of late Na^+ current ($I_{Na,L}$), Ca^{2+} homeostasis, and cellular excitability in atrial myocytes using a computer model. In another computational study, Dai et al[41] showed that CaMKII overexpression facilitates early afterdepolarization (EAD) by prolonging the deactivation of the $I_{Na,L}$, and combination with β-adrenergic activation further increases EAD risk. Modeling studies also suggested that CaMKII activation–mediated SR Ca^{2+} overload and increased cytosolic Na^+ elicit post-acidosis arrhythmias in human myocytes.[42] To examine the role of oxidation-dependent CaMKII activation in regulating cardiac cell excitability following myocardial infarction, Christensen et al[43] developed a mathematical model of CaMKII activity, which, for the first time, includes both oxidative and autophosphorylation activation pathways. More recently, an integrative cardiomyocyte model has been developed by Foteinou et al[44] to study the mechanistic role of oxidized CaMKII in the genesis of H_2O_2-induced EADs in the heart. In a similar study, Zhang et al[45] developed a new Markov chain model of CaMKII δ-isoform that involves both of the autophosphorylation and oxidation pathways to simulate CaMKII activation and its effect on APs under oxidative stress in cardiomyocytes.

Given the advances, how endogenous ROS, especially those derived from mitochondria (mdROS), affect CaMKII activity and consequently ion homeostasis and AP remains largely unexplored. Dissecting direct mdROS effects and indirect effects caused by CaMKII phosphorylation is difficult to address experimentally, as is defining the contribution of individual targets to arrhythmogenesis. As the voltage-gated Na^+ currents (I_{Na}) are a significant contributor to the initiation and duration of the cardiac AP and a well-recognized substrate of CaMKII phosphorylation, we hypothesize that mdROS-mediated oxidative CaMKII activation could elicit abnormal APs by enhancing I_{Na}. To test the hypothesis, we expanded our well-established cardiomyocyte *e*xcitation-*c*ontraction coupling, *m*itochondrial *e*nergetics, and *R*OS-*i*nduced-*R*OS-*r*elease (ECME-RIRR)[5,46,47] model by incorporating oxidative CaMKII activation and slow Na^+ channel phosphorylation. Our simulations show that mdROS bursts–mediated oxidative CaMKII activation significantly augments $I_{Na,L}$, which alone is sufficient to cause EADs. Moreover, we show that under certain conditions the oxidative CaMKII activation–induced EADs persist even after mdROS have returned to physiological levels, an event that is likely attributed to CaMKII's property as a "memory molecule." Finally, model simulations suggest that timing is critical for antioxidant treatments to effectively eliminate mdROS-CaMKII activation–induced EADs.

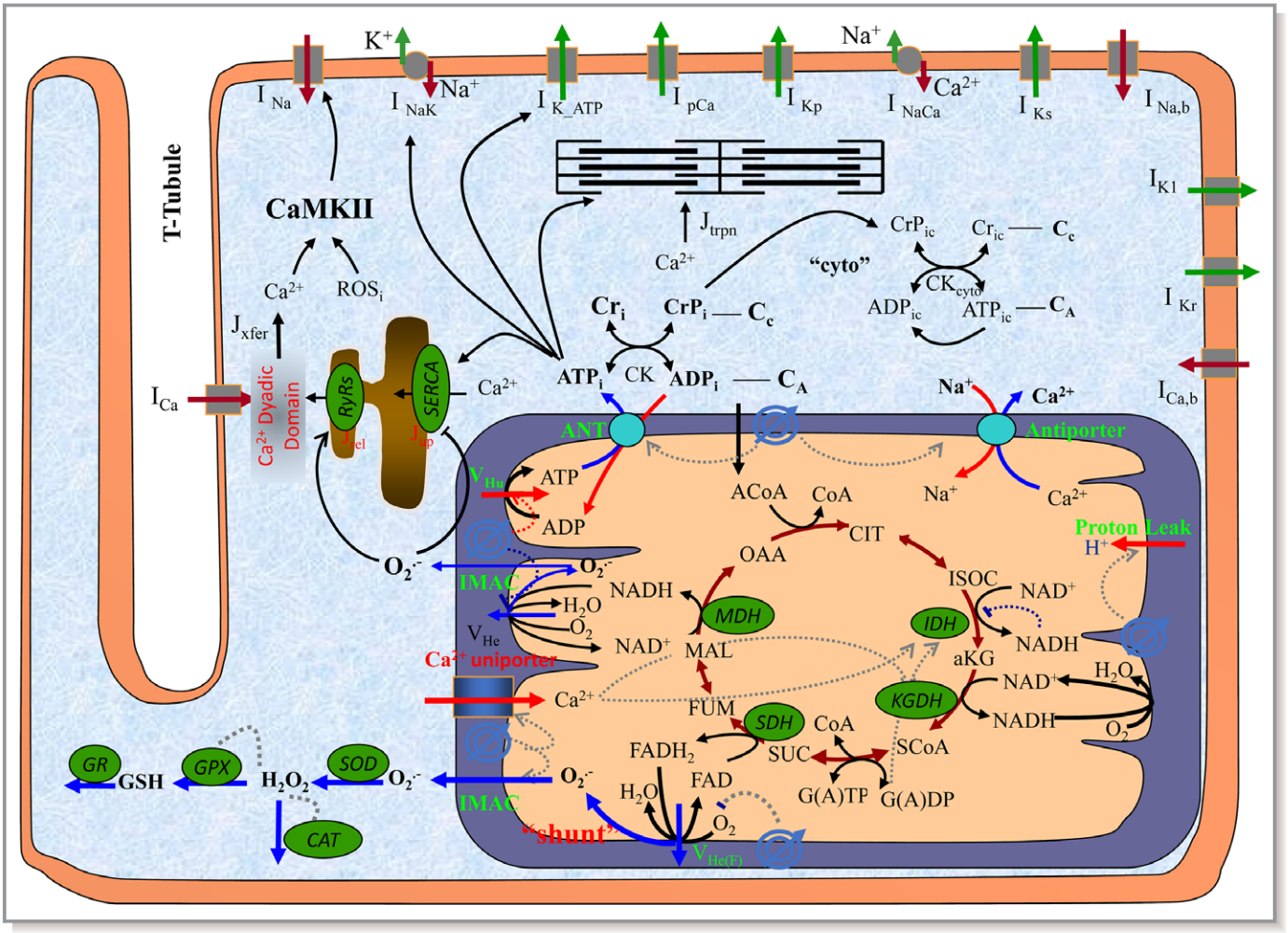

Figure 1. Scheme of the expanded *e*xcitation-contraction *c*oupling, *m*itochondrial *e*nergetics, and *R*OS-*i*nduced-*R*OS-*r*elease (RIRR) model that incorporates oxidative Ca^{2+}/calmodulin-dependent protein kinase II (CaMKII) activation. The electrophysiological module describes the major ion channels underlying the action potential (eg, fast Na^+ channel and Na^+/Ca^{2+} exchanger) and processes involved in Ca^{2+} handling (eg, local Ca^{2+} control and transport of Ca^{2+} across the sarcoplasmic reticulum). The mitochondrial module accounts for major components of mitochondrial energetics such as tricarboxylic acid cycle and oxidative phosphorylation, as well as mitochondrial membrane ion channels (eg, Ca^{2+} uniport). The RIRR module describes reactive oxygen species (ROS) production (from the electron transport chain), transport (through inner membrane anion channel [IMAC]), and scavenging (eg, by the superoxide dismutase and glutathione peroxidase enzymes).

Methods

No human or animal subject was involved in this theoretical study. Thus, there was no institutional review board approval required. The data, analytic methods, and codes will be made available to other researchers for purposes of reproducing the results or replicating the procedure. Model equations and parameters are available within the article or Tables S1 through S28.

Model Development

In this in silico study, we aimed to examine the effect of mitochondrial-derived oxidative stress on CaMKII activation to induce arrhythmias. The model was based on our recently published guinea pig cardiomyocyte ECME-RIRR model[47] and incorporated several new model components including a CaMKII activity module, a Markov slow Na^+ channel module, and an Na^+ channel phosphorylation module. The scheme of the expanded ECME-RIRR model is shown in Figure 1, and the newly added model components are described below.

CaMKII activity module

The CaMKII module model was built based on the Markov chain models constructed by Foteinou et al[44] and Zhang et al,[45] which comprises CaMKII activation by ROS and experimental data from Erickson et al.[22] For simplification, we assumed that Ca^{2+}/CaM-dependent activity, phosphorylation-dependent activity, and oxidation-dependent activity are homogeneous across the cell. With this assumption, the total activated CaMKII is defined as the sum of these activated

CaMKII (ie, binding Ca^{2+}/CaM, phosphorylated, and oxidized). The fraction of activated CaMKII can be calculated as:

$$CaMKII_{active} = \frac{[CaMKII_{active}]}{[CaMKII_{total}]} \times 100\% \quad (1)$$

where $[CaMKII_{active}]$ is the concentration of total activated CaMKII and $[CaMKII_{total}]$ is the concentration of total CaMKII. The complete CaMKII activation model is described in Figure S1 and Tables S4 and S25.

The Markov slow Na^+ channel module

Experimental studies showed that the effect of CaMKII activation on Na^+ channels is mainly on the slow component, ie, augmenting the $I_{Na,L}$. As our ECME-RIRR model consists only of the fast I_{Na} model, we adopted the Markov framework of the Na^+ channel model developed by Grandi et al[48] to incorporate the $I_{Na,L}$:

$$I_{Na,L} = G_{Na,L} \cdot P_{LO} \cdot (V - E_{Na}) \quad (2)$$

where $G_{Na,L}$ is the conductance of the late Na^+ channels (mS/μF) and P_{LO} is the open possibility of the late Na^+ channels. The complete Markov slow Na^+ channel model and parameters are listed in Tables S1 and S26, respectively.

Slow Na^+ channel dynamic phosphorylation module

For modeling purposes, we contended that Na^+ channels are either phosphorylated by activated CaMKII or not. The transition between the unphosphorylated and phosphorylated Na^+ channels can be described by a 2-state Markov model (Figure S1). Specifically, the fraction of phosphorylated Na^+ channels is governed by

$$\frac{d\phi_{Na,CaMKII}}{dt} = K_{Phos} \cdot (1 - \phi_{Na,CaMKII}) - K_{Dephos} \cdot \phi_{Na,CaMKII} \quad (3)$$

where $\phi_{Na,CaMKII}$ is the fraction of phosphorylated Na^+ channels, K_{Phos} is the phosphorylation rate, which is proportional to the fraction of activated CaMKII, and K_{Dephos} is a constant, which can be determined by the experimental data as described previously.[48] The total $I_{Na,L}$ $I^*_{Na,L}$ is calculated by the following equations:

$$I^*_{Na,L} = (1 - \phi_{Na,CaMKII}) \cdot I_{Na,L} + \phi_{Na,CaMKII} \cdot I'_{Na,L} \quad (4)$$

$$I'_{Na,L} = G_{Na,L} \cdot P'_{LO} \cdot (V - E_{Na}) \quad (5)$$

In these equations, $I'_{Na,L}$ represents the late Na^+ current caused by CaMKII activation, and P'_{LO} is the open probability of phosphorylated late Na^+ channels. The model parameters for the phosphorylated and unphosphorylated Na^+ channels by activated CaMKII were refit with experimental data by Aiba et al[49] and are listed in Table S27.

Simulation Protocol

The CaMKII activity and slow Na^+ channel module models were integrated into the guinea pig ventricular myocytes ECME-RIRR model[47] after parameterization. To focus on the effect of mdROS-mediated oxidative CaMKII activation on AP and dissect the underlying ionic mechanisms, we did not consider the direct effect of mdROS on redox-sensitive ion handling proteins such as RyRs, SERCA, and Na^+ channels in the present study unless otherwise specified. The formulas of other processes, such as ion channels and metabolic reactions, and model parameters were the same as those in the ECME-RIRR model[47] (Tables S1 through S28). The code of the new cell model was written in C^{++} (Visual Studio, Microsoft). The nonlinear ordinary differential equations were integrated numerically with CVODE as previously described.[5,50]

The cardiomyocyte was stimulated at 0.25 Hz until the steady state was reached. The steady state values were then used as initial conditions for subsequent simulations. For model validation, we first simulated the effect of pacing cycle lengths (PCLs; 500, 1000, 2000, and 4000 ms) on AP duration (APD), then the ROS-induced $I_{Na,L}$ augmentation, and finally EAD incidence rate dependence on PCL under oxidative stress. Model simulations were compared with experimental data from the literature. After model validation, we simulated the effect of mdROS on CaMKII activation, $I_{Na,L}$, cytosolic Na^+ and Ca^{2+} handling, and AP under various conditions. The production of mdROS was modeled as a fraction, or *shunt*, of electrons from the electron transport chain into the matrix, as previously described.[5,47,51,52] Studies have shown that under physiological conditions, up to 2% of the electron flowing the respiratory chain are partially reduced to form the superoxide,[53] thus the physiological value of *shunt* was set as 2%. Pathological *shunt* was set as 10% or 14% to induce sustained mitochondrial oscillations, which is consistent with our previous computational studies.[5,47,52] The simulation results were postprocessed and plotted using Origin software (OriginLab).

Results

Model Validation

To validate the built guinea pig cardiomyocyte ECME-RIRR model that incorporates new model modules, we first simulated the effects of CaMKII phosphorylation and PCL on APD and compared the results with experimental data. Our simulations showed that increasing the PCL (from 500 to 4000 ms) caused stepwise APD elongation (Figure 2A, gray), which was further enhanced by CaMKII phosphorylation (data not shown). Those model predictions were comparable to experimental data reported by Aiba et al[49] (Figure 2A, black).

We then simulated the effect of oxidative stress on the voltage-gated I_{Na} (Figure 2B). In an experimental study, Wagner et al[38] showed that H_2O_2 (200 μmol/L) perfusion caused a remarkable increase (≈177 A ms/F) in $I_{Na,L}$ integral in wild-type mouse ventricular myocytes and this enhancement was substantially reduced in CaMKII knockout cardiomyocytes (≈48.7 A ms/F). Our model simulations showed a similar trend: reducing CaMKII by 95% (estimated based on Western blot data in Backs et al[54]) notably reduced the oxidative stress–induced $I_{Na,L}$ augmentation.

Finally, we examined the effect of ROS on APs at different PCLs. To be consistent with experimental studies by Xie et al[39] and Zhao et al,[55] the concentration of cytosolic ROS was set as 200 μmol/L in this simulation. Our simulations showed that oxidative stress–induced EAD incidence rate is PCL dependent: EADs could be induced readily when PCL was long (eg, 6 seconds) but hardly when PCL was relatively short (eg, 1 second) (Figure 2C). Those simulations were in agreement with previous experimental[39,55] (Figure 2D) and computational studies.[44]

Effect of mdROS on CaMKII and Ion Handling During Mitochondrial Oscillations

After model validation, we simulated how mitochondrial-derived oxidative stress could influence CaMKII activity and ion handling in a "beating" guinea pig cardiomyocyte. As previously reported,[5,46,47,52,56] increasing *shunt*, the fraction of the electrons of the respiratory chain towards the generation of $O_{2^-}^{-}$ from 0.02 to 0.10 triggered sustained

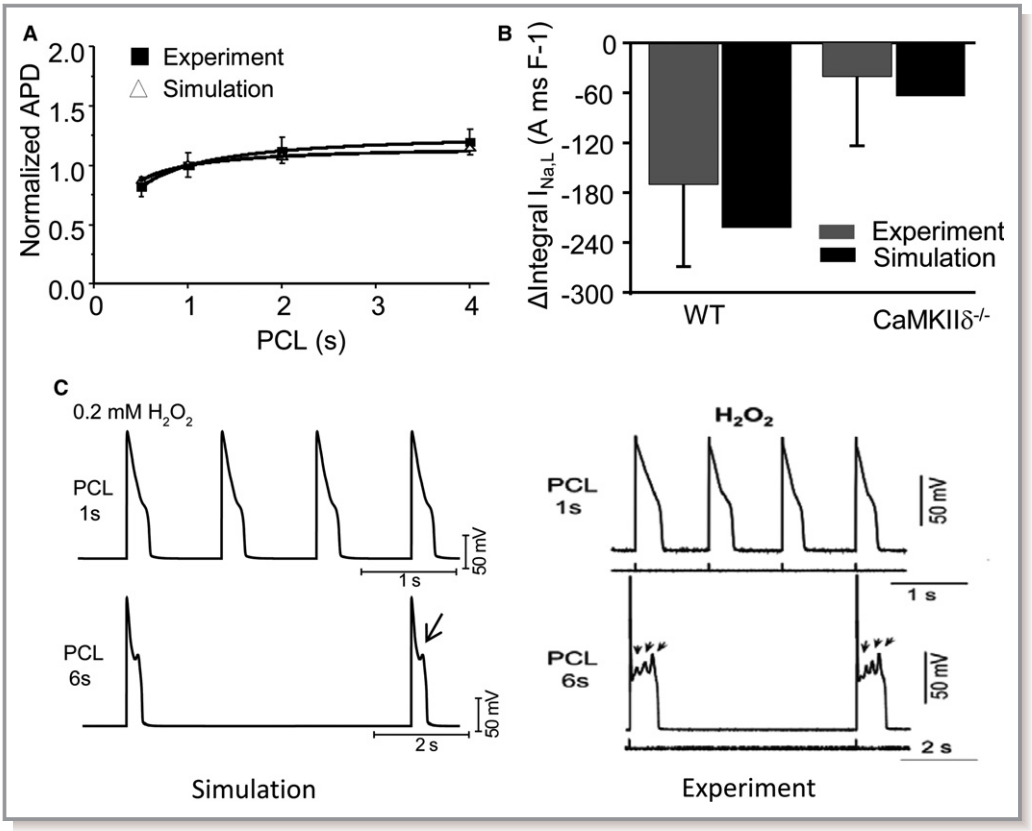

Figure 2. Validation of cardiomyocyte *e*xcitation-contraction *c*oupling, *m*itochondrial *e*nergetics, and *R*OS-*i*nduced-*R*OS-*r*elease model that incorporates oxidative Ca^{2+}/calmodulin-dependent protein kinase II (CaMKII) activation and slow Na^+ channels phosphorylation modules. A, The effect of pacing cycle length (PCL) on the duration of action potential (APD). For comparison, the APDs at different PCLs were normalized to the APD at PCL=1 second. Blank triangles are model simulations and black squares represent experimental data from Aiba et al.[49] B, The effects of oxidative CaMKII activation on late Na^+ current ($I_{Na,L}$). The integral of $I_{Na,L}$ was calculated between 50 and 500 ms after the onset of depolarization. The CaMKII activation–induced $I_{Na,L}$ change (ie, Δ integral $I_{Na,L}$) was obtained by subtracting the baseline $I_{Na,L}$ integral from the CaMKII $I_{Na,L}$ integral. Simulation was run with PCL=2 seconds. Experimental data are from Wagner et al.[38] C, Effect of cytosolic H_2O_2 on action potential at different PCLs (1000 and 6000 seconds). Left panel shows model simulations and right panel shows experimental data from isolated rabbit ventricular myocytes (modified from Zhao et al[55] with permission. Copyright© 2012, The American Physiological Society). WT indicates wild-type.

mitochondrial oscillations and cyclic ROS production (Figure S2A). The results indicate that addition of new model components (eg, mdROS-mediated oxidative CaMKII activation and CaMKII-dependent Na^+ channels phosphorylation) did not alter the dynamics of the existing model subsystems. Simulations also show that $\Delta\Psi_m$ depolarization (and the associated mdROS bursting) led to sustained EADs during each oscillatory cycle (Figure 3A, for better visualization only the first depolarization was shown). Cytosolic Na^+ concentration ($[Na^+]_i$) climbed gradually during mitochondrial depolarization (Figure 3B). Cytosolic Ca^{2+} transient rose slightly and exhibited a large increase during the decay phase (Figure 3C). The dynamics of the fraction of activated CaMKII were similar to that of $[Na^+]_i$ (Figure 3D).

To examine the ionic mechanisms underlying mdROS-mediated EADs, we analyzed the dynamics of major Ca^{2+} and Na^+ handling currents/fluxes before and after mitochondrial depolarization, and with or without mdROS-induced oxidative CaMKII activation. In the absence of CaMKII activation, the mdROS bursts slightly elongated APD and Ca^{2+} transient, enhanced $I_{Na,L}$, and shifted the Na^+-Ca^{2+} exchanger current (I_{NaCa}) forward component to the right (Figure 4, red lines). The effects on L-type calcium channel current (I_{CaL}), SR Ca^{2+} release, and SERCA Ca^{2+} uptake were small. Addition of CaMKII activation had negligible effects on APD and cytosolic Ca^{2+} concentration ($[Ca^{2+}]_i$), as well as I_{NaCa}, I_{CaL}, and SR Ca^{2+} handling under physiological mdROS conditions (ie, polarized $\Delta\Psi_m$) (Figure 4, blue lines). The $I_{Na,L}$ integral was slightly increased, likely caused by $[Ca^{2+}]_i$-induced CaMKII activation. During mitochondrial depolarization, mdROS-mediated CaMKII activation did not change the peak I_{Na} but caused substantial $I_{Na,L}$ augmentation (Figure 4C, olive line arrow #1), resulting in APD prolongation and AP reverse (Figure 4A, olive lines). The AP reverse reactivated I_{CaL} (Figure 4E, olive line), which triggered Ca^{2+}-induced Ca^{2+} release (Figure 4F, olive lines), leading to a larger Ca^{2+} elevation (Figure 4B, olive line) and a second $I_{Na,L}$ surge (Figure 4C, olive line arrow #2). The forward mode I_{NaCa} was initially inhibited and reversed (arrow #1) and then largely amplified (arrow #2) (Figure 4C, olive line), caused by AP reverse and altered Na^+ and Ca^{2+} homeostasis. It is worth mentioning that oxidative CaMKII activation alone could not induce delayed afterdepolarizations (DADs; data not shown), which is consistent with the findings of Foteinou et al.[44]

One unique characteristic of our ECME-RIRR model is its capability to simulate sustained mitochondrial oscillations[50,56] (Figure S2A), allowing examination of the dynamics of AP

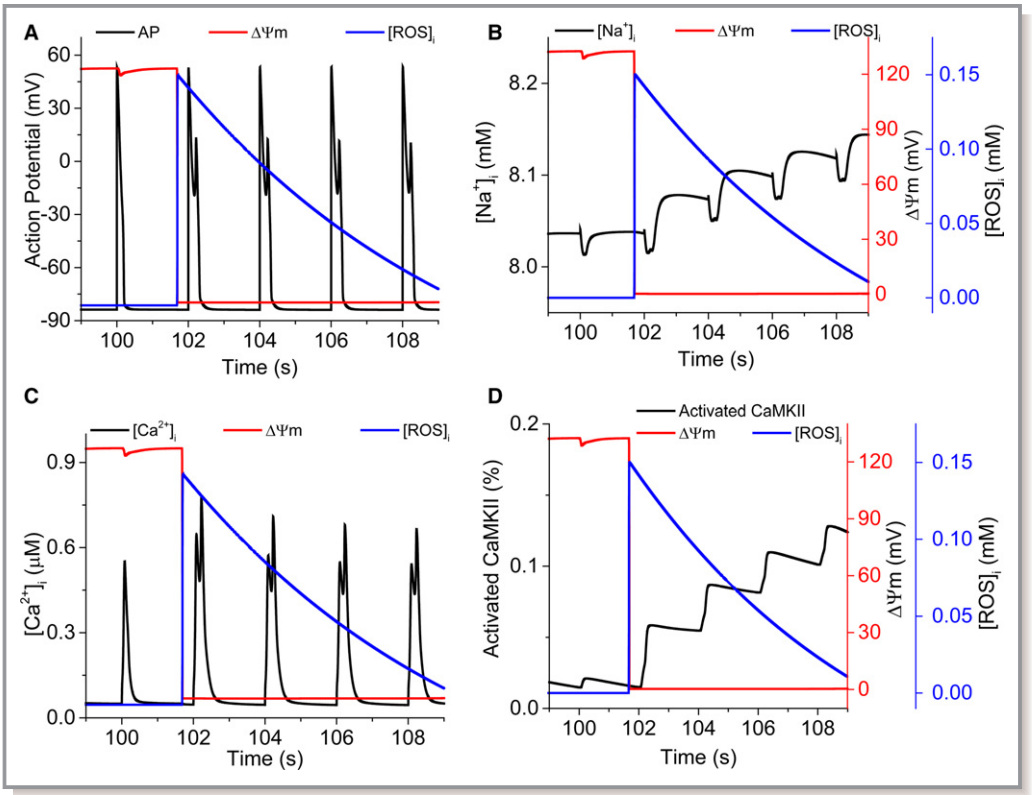

Figure 3. Effect of mitochondrial depolarization and mitochondrial-derived reactive oxygen species (ROS) bursts on action potential (A), cytosolic Na^+ ($[Na^+]_i$) (B), cytosolic Ca^{2+} concentration ($[Ca^{2+}]_i$) (C), and fraction of activated Ca^{2+}/calmodulin-dependent protein kinase II (CaMKII) (D). *shunt*=0.1 and pacing cycle length=2 seconds.

upon mitochondrial repolarization.[5,52] As shown in Figure 5A, after $\Delta\Psi_m$ repolarization, AP EADs surprisingly remained on the first several (eg, 7 in this simulation) beats, even though mdROS had reduced to basal levels (Figure S2A). The sustained EADs then turned to intermittent EADs and eventually became normal APs. $[Ca^{2+}]_i$ (Figure 5B) and activation of $I_{Na,L}$ (Figure 5C) followed the same pattern. $[Na^+]_i$ (Figure 5D) and fraction of phosphorylated Na^+ channels (Frac_NaP) (Figure 5E) gradually decreased during the repolarization phase. However, $[Na^+]_i$ did not completely return to the predepolarization level, causing gradual $[Na^+]_i$ accumulation along the progression of mitochondrial oscillations (Figure S2B). In the absence of mdROS-induced oxidative CaMKII activation, $[Na^+]_i$ remained relatively constant during mitochondrial oscillations (Figure S2C).

Importantly, with the progression of mitochondrial oscillations, the time needed for AP to return to normal morphology during $\Delta\Psi_m$ repolarization increased. When *shunt* was further increased to 0.14, EADs (constant and intermittent) were maintained throughout the whole repolarization phase after the third depolarization (Figure S3). This behavior seemed to be attributed to the elevated CaMKII

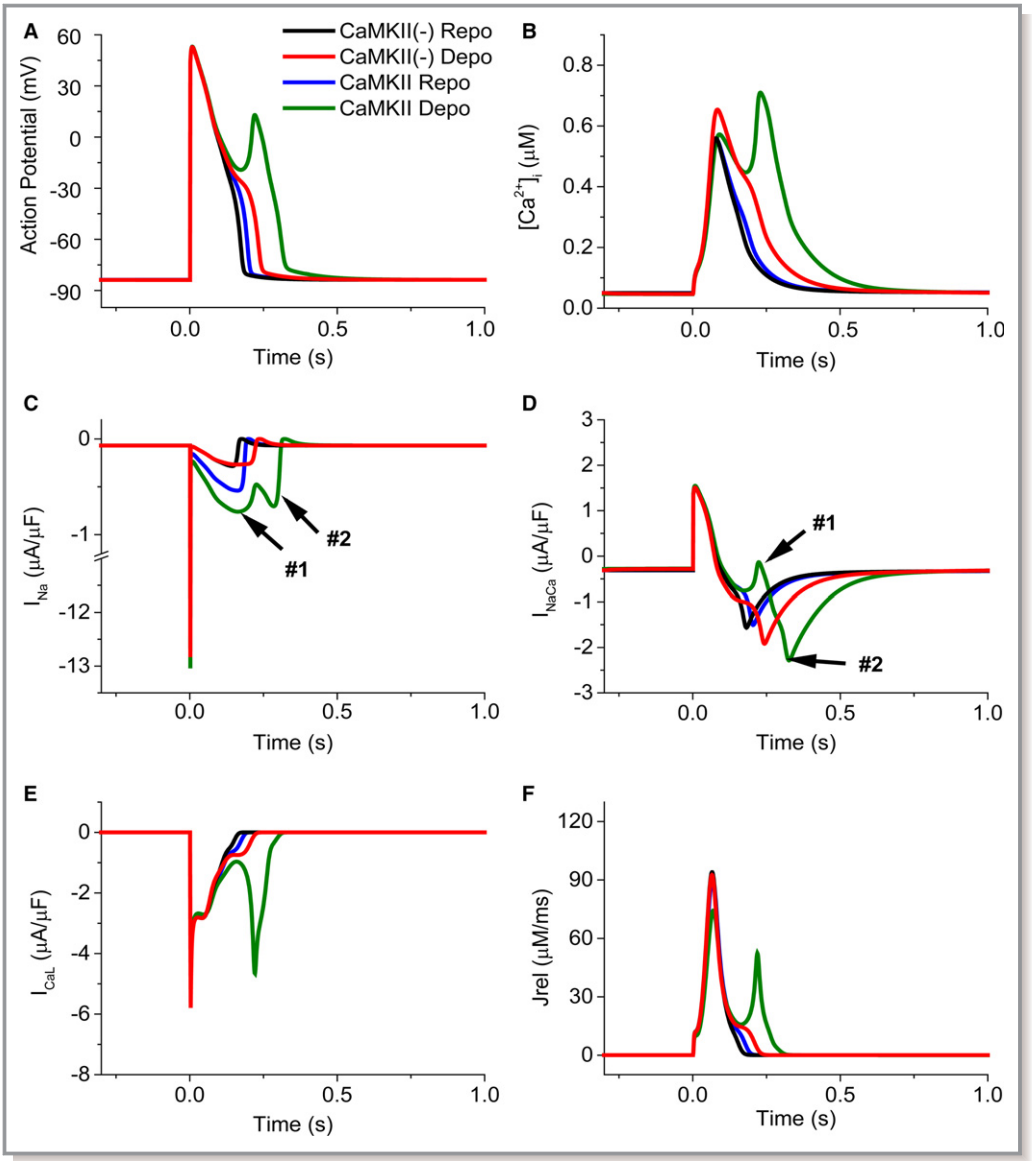

Figure 4. Dynamics of action potential (A), cytosolic Ca^{2+} concentration ($[Ca^{2+}]_i$) (B), Na^+ current (I_{Na}) (C), Na^+-Ca^{2+} exchanger current (I_{NaCa}) (D), L-type calcium channel current (I_{CaL}) (E), and sarcoplasmic reticulum Ca^{2+} release (J_{rel}) (F) before (Repo) and after (Depo) mitochondrial depolarization. Ca^{2+}/calmodulin-dependent protein kinase II (CaMKII) (+) represents the new excitation-contraction *c*oupling, *m*itochondrial *e*nergetics, and *R*OS-*i*nduced-*R*OS-*r*elease (ECME-RIRR) model consisting of the oxidative CaMKII activation module, whereas CaMKII (−) represents the previous ECME-RIRR model that does not incorporate the oxidative CaMKII activation module. *shunt*=0.1 and pacing cycle length=2 seconds.

activation and augmentation of $I_{Na,L}$. Thus, we analyzed the correlation between the number of sustained or intermittent EADs and the peak $[Na^+]_i$ during the state transition (eg, from sustained EADs to intermittent EADs). Results show that the numbers of sustained EADs and intermittent EADs were both closely correlated with the peak $[Na^+]_i$, especially under more severe stressed conditions (ie, *shunt*=0.14) (Figure 6).

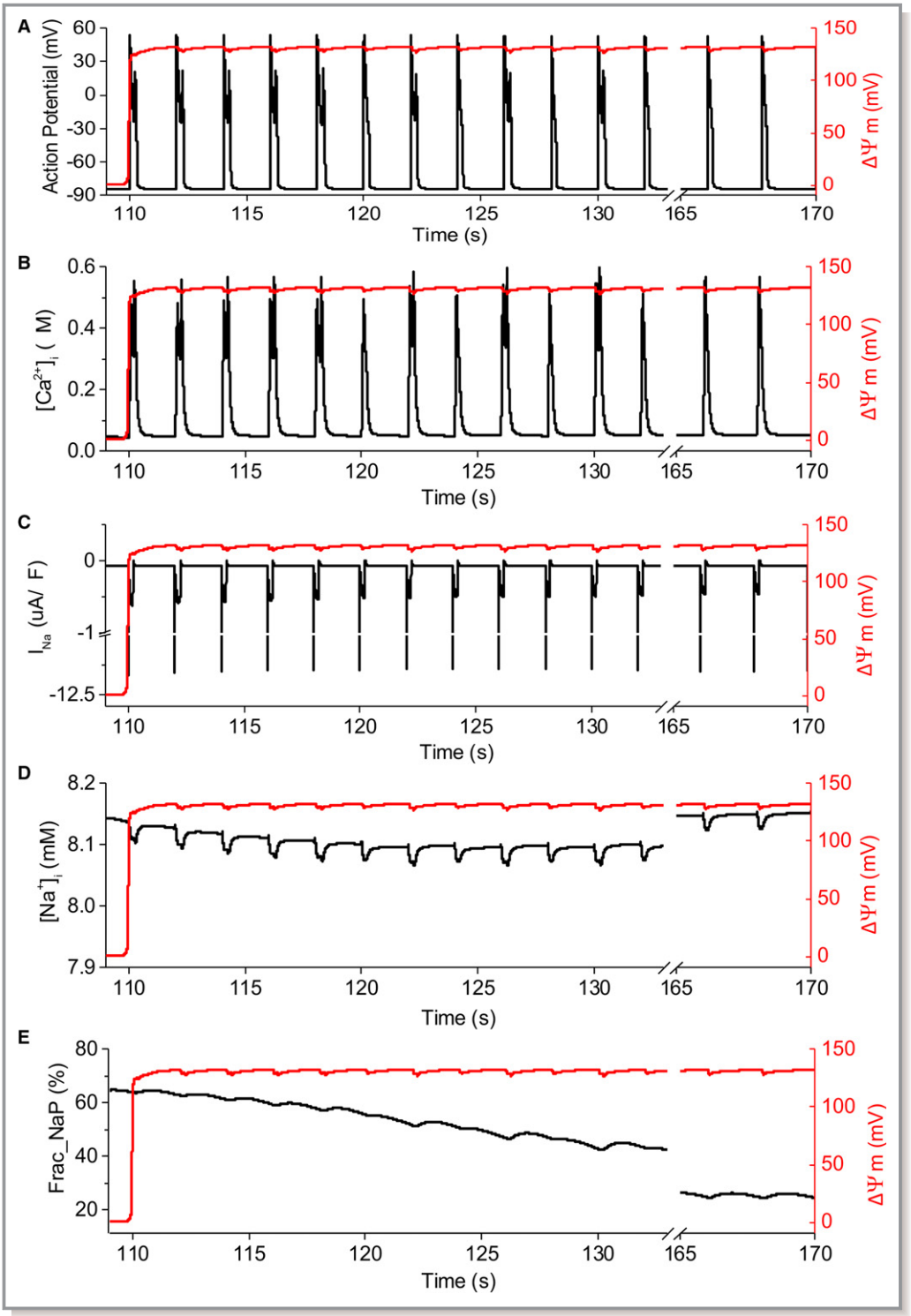

Figure 5. Dynamics of action potential (A), cytosolic Ca^{2+} concentration ($[Ca^{2+}]_i$) (B), Na^+ current (I_{Na}) (C), cytosolic Na^+ concentration ($[Na^+]_i$) (D), and fraction of phosphorylated Na^+ channels (Frac_NaP) (E) during the first mitochondrial repolarization. *shunt*=0.1 and pacing cycle length=2 seconds.

Effect of Blocking Na^+ or Ca^{2+} Handling Channel on mdROS-CaMKII Activation–Induced EADs

Next, we examined the effect of completely blocking individual Na^+ or Ca^{2+} handling channel on mdROS-mediated oxidative CaMKII activation–induced AP abnormality during mitochondrial depolarization. Under control conditions (ie, physiological mdROS production or *shunt*=0.02), blocking $I_{Na,L}$ had no effect on AP upstroke but slightly shortened APD. The effects on $[Ca^{2+}]_i$, $[Na^+]_i$, I_{NaCa}, I_{CaL}, and the peak of I_{Na} were negligible (data not shown). Under pathological mdROS production conditions (eg, *shunt*=0.14), 100% elimination of $I_{Na,L}$ abolished EADs, transient I_{NaCa} reverse, and I_{CaL} reactivation, accompanied by reduced $[Ca^{2+}]_i$ and $[Na^+]_i$ overload (Figure 7A, blue lines).

Similar to $I_{Na,L}$ inhibition, completely blocking I_{NaCa} suppressed I_{CaL} reactivation and the subsequent Ca^{2+}-induced Ca^{2+} release, which prevented Ca^{2+} elevation and abolished the EADs (Figure 7B, blue lines). I_{NaCa} blockage also reduced $I_{Na,L}$ enhancement and $[Na^+]_i$ (Figure 7B), which was consistent with published data.[55] It is worth mentioning that although transient blockage seems beneficial, long-term I_{NaCa} inhibition may cause significant alteration of $[Ca^{2+}]_i$ and $[Na^+]_i$ homeostasis and eventually lead to abnormal APs (such as EADs).

Our model simulations show that blocking I_{CaL} also eliminated the oxidative CaMKII activation–induced EADs, which was consistent with previous experimental data showing that L-type Ca^{2+} channel inhibitor suppressed oxidative stress–induced EADs.[39] Lack of I_{CaL} activation facilitated phase 2 AP repolarization, resulting in significant APD shortening that hindered the subsequent Ca^{2+}-induced Ca^{2+} release and Ca^{2+} overload. Consequently, Na^+/Ca^{2+} exchanger inward current enhancement was suppressed (Figure 7C). The outcome of I_{CaL} blockade in the absence of mdROS bursts were shortened APD, abolished AP plateau, and diminished Ca^{2+} transients (data not shown), which agreed with previous studies.[57,58]

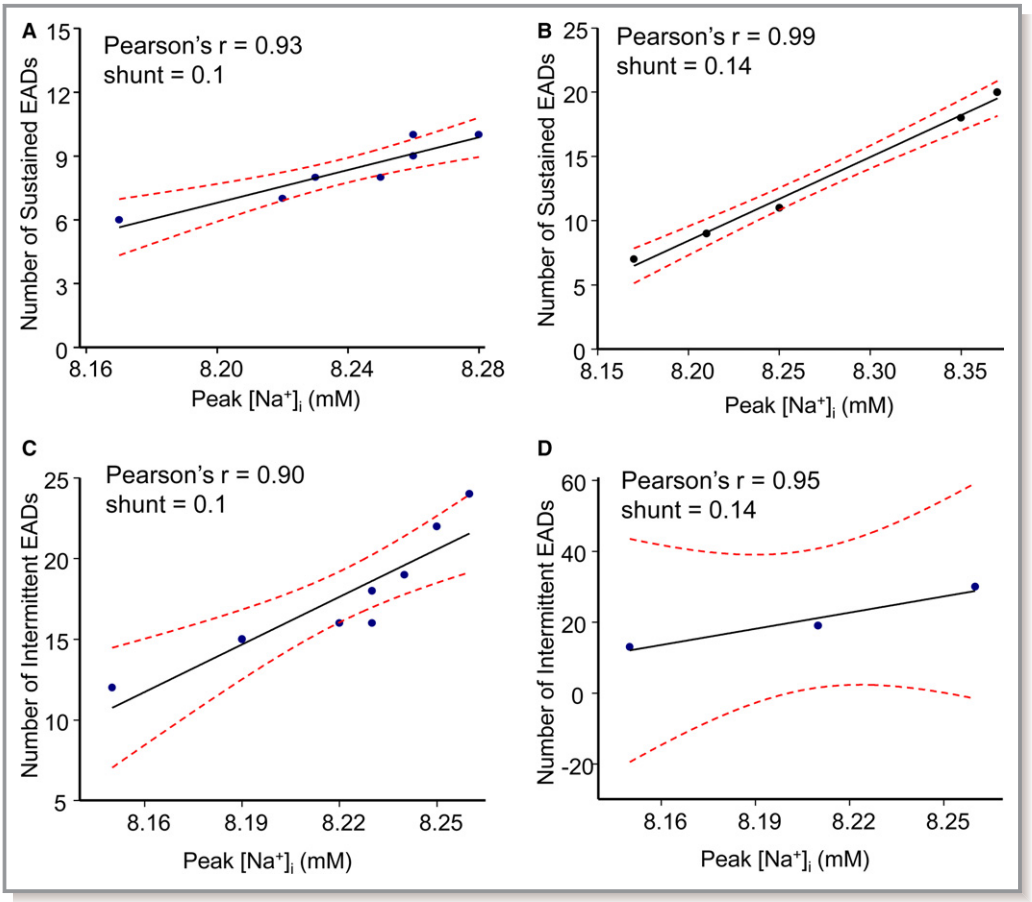

Figure 6. Correlation between the number of sustained early afterdepolarizations (EADs) (A and B) or intermittent EADs (C and D) and peak Na^+ concentration during mitochondrial repolarization at different *shunts* (0.1 for A and C and 0.14 for B and D). Black solid lines represent regression and red dash lines represent 95% confidence bands; pacing cycle length=2 seconds.

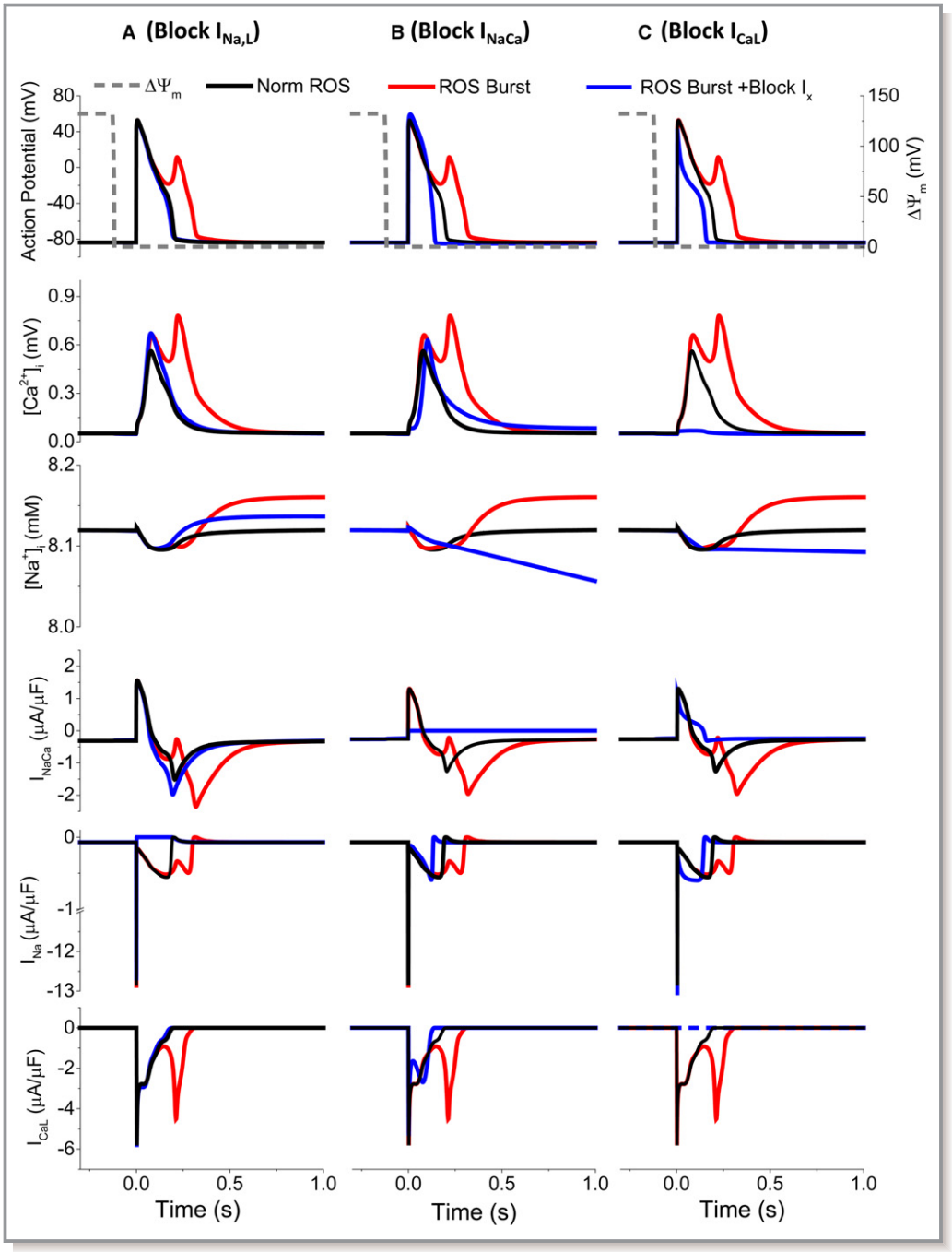

Figure 7. Effect of complete blockage of late Na^+ current ($I_{Na,L}$) (A), Na^+-Ca^{2+} exchanger current (I_{NaCa}) (B), or L-type calcium channel current (I_{CaL}) (C) on action potential (1), cytosolic Ca^{2+} concentration ($[Ca^{2+}]_i$) (2), cytosolic Na^+ concentration ($[Na^+]_i$) (3), I_{NaCa} (4), I_{Na} (5), and I_{CaL} (6) under normal and mitochondrial depolarization conditions. *shunt*=0.14 and pacing cycle length=2 seconds.

Effect of Antioxidant Treatment on mdROS-CaMKII Activation–Induced EADs

We then examined whether antioxidant treatment, such as reducing mitochondrial ROS production or increasing ROS scavenging could eliminate mdROS-CaMKII activation–induced EADs. In the simulations shown in Figure 8, *shunt* was initially set to the basal level (0.02) for 5 seconds, then increased to 0.1 or 0.14, and finally reduced to 0.02 at 700 seconds. Increasing *shunt* caused sustained mitochondrial oscillations and correlated fluctuations of $[Na^+]_i$ and Frac_NaP. Interestingly, both $[Na^+]_i$ and Frac_NaP increased gradually with the progression of mitochondrial oscillations, with the increases more evident at higher *shunt* (Figure 8A and 8B). Reducing *shunt* from 0.1 to the basal level rendered $[Na^+]_i$ and Frac_NaP to their initial values and eliminated EADs

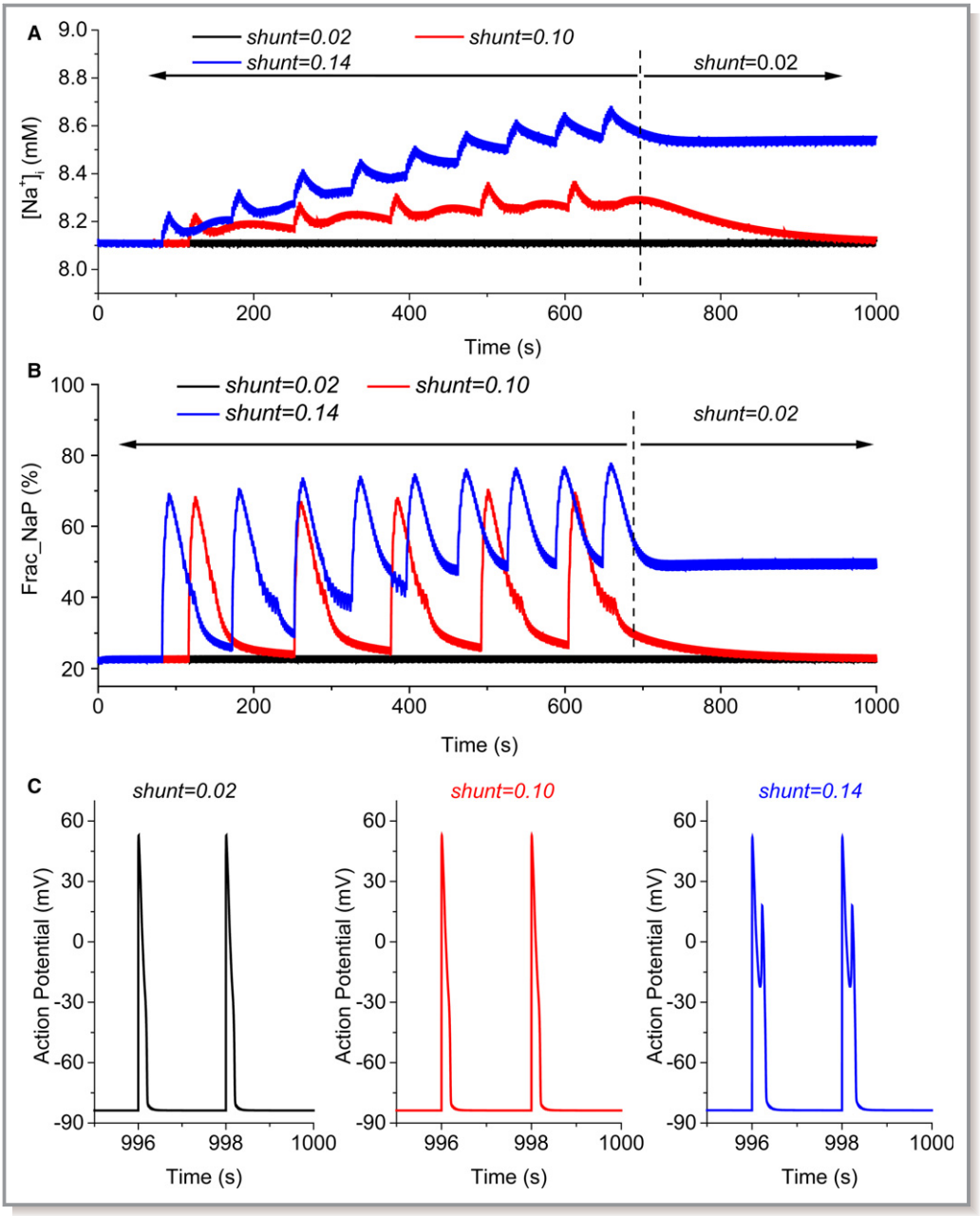

Figure 8. Effect of reducing *shunt* on mitochondrial-derived reactive oxygen species (mdROS)-Ca^{2+}/calmodulin-dependent protein kinase II (CaMKII) activation–induced early afterdepolarizations (EADs). In these simulations, *shunt* was set as 0.02 (black line), 0.10 (red line), or 0.14 (blue line) during 0 to 700 seconds and 0.02 thereafter. A, Cytosolic Na^+ concentration ($[Na^+]_i$), (B) fraction of phosphorylated Na^+ channels (Frac_NaP), and (C) action potentials of the last 2 beats. Pacing cycle length=2 seconds.

(Figure 8, red lines). However, when the preceding *shunt* was higher (ie, 0.14), reducing ROS production at 700 seconds failed to normalize the elevated $[Na^+]_i$ and Frac_NaP and suppress EADs (Figure 8, blue lines). Interestingly, we found that reducing mdROS production (*shunt*, from 0.14 to 0.02) earlier (eg, at 350 seconds) converted sustained EADs to intermittent EADs. When *shunt* reduction was induced earlier still (eg, 200 seconds), $[Na^+]$ overload and the oxidative stress–induced EADs were eliminated (Figure 9).

Another strategy to reduce oxidative stress is to use antioxidant scavengers. In our model, this can be achieved by increasing *et_SOD*, a parameter that represents the total amount of superoxide dismutase. Similar to reducing *shunt*, increasing *et_SOD*, when introduced sufficiently soon after mitochondrial depolarization (eg, at 200 seconds), successfully reduced elevated $[Na^+]_i$ and suppressed EADs. However, increasing ROS scavenging later (eg, 300 and 700 seconds) failed to eliminate EADs (Figure S4). Taken together, those

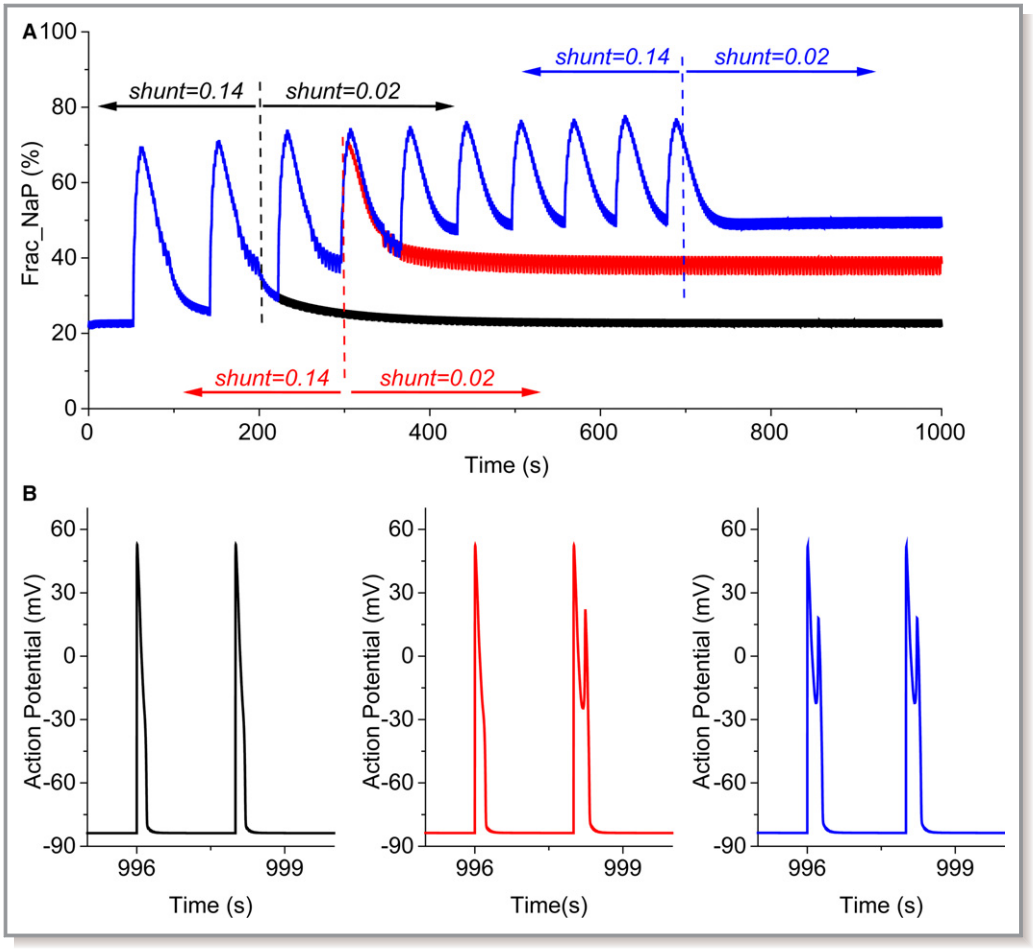

Figure 9. Effect of timing of reducing *shunt* on mitochondrial-derived reactive oxygen species-Ca^{2+}/calmodulin-dependent protein kinase II (CaMKII) activation–induced early afterdepolarizations (EADs). In these simulations, *shunt* was initially set as 0.14 and then reduced to 0.02 at 200 seconds (black line), 300 seconds (red line), or 700 seconds (blue lines). A, Fraction of phosphorylated Na^+ channels (Frac_NaP). B, Action potentials of the last 2 beats. Pacing cycle length=2 seconds.

simulations imply that: (1) altered ion (eg, $[Na^+]_i$ and $[Ca^{2+}]_i$) homeostasis plays a critical role in mdROS-CaMKII activation–induced EADs, and (2) timely antioxidant treatment is critical for its antiarrhythmic effect with the sooner the better.

RyRs Oxidation Effect for Inducing Arrhythmias

In a recent computational study, we showed that mdROS can induce abnormal Ca^{2+} cycling and elicit erratic APs by directly activating RyRs and inhibiting SERCA. Here, we examined whether concurrent oxidative RyRs activation would exacerbate the effect of oxidative CaMKII activation on Ca^{2+} mishandling and AP abnormality. As shown in Figure 10A, mdROS induced during phase 2 of the AP, when modeled to activate CaMKII only, caused an EAD. Adding the effect of mdROS on SR Ca^{2+} handling (eg, RyRs activation and SERCA inhibition) converted the single EAD to multiple EADs. Notably, when the mdROS burst was induced during phase 4 of the AP, concurrent oxidative RyRs and CaMKII activation elicited a DAD, which was otherwise barely seen with oxidative CaMKII activation alone (Figure 10B). Concurrent RyRs oxidation by mdROS also exacerbated Na^+ and Ca^{2+} overload during mitochondrial depolarization (Figure 10C through 10F).

Discussion

In the present study, we expanded our recently published guinea pig cardiomyocyte ECME-RIRR model[47] by incorporating mdROS-induced oxidative CaMKII activation and slow Na^+ channel phosphorylation. Our new model was able to replicate previous model simulations (eg, sustained mitochondrial oscillations) and experimental data (eg, rate dependence of H_2O_2-induced EADs and ROS-induced increases in intracellular Na^+ and Ca^{2+}). We then simulated how the endogenous mitochondrial-derived oxidative stress (ie, mdROS) may influence CaMKII activity and subsequently alter cardiomyocyte ion homeostasis and APs. Our main findings are: (1) mdROS-mediated oxidative CaMKII activation–induced

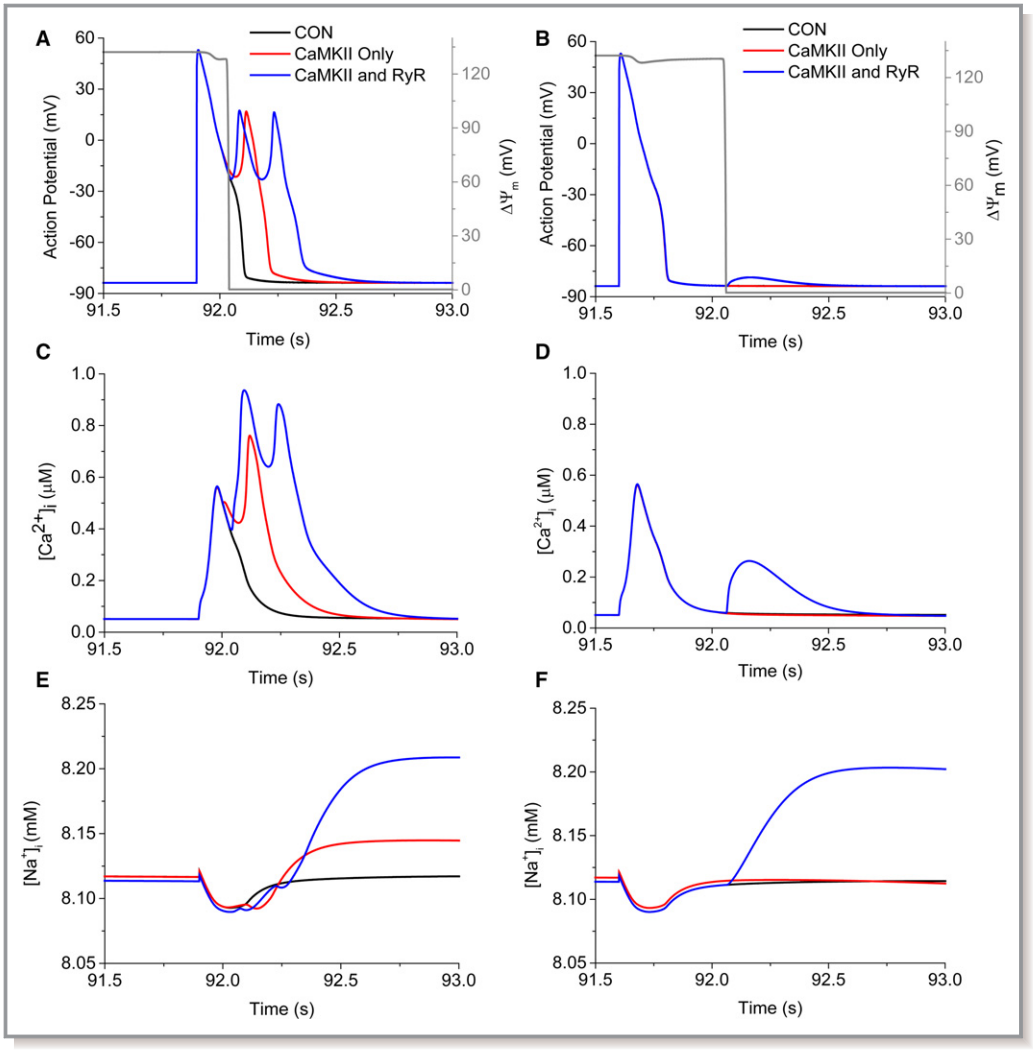

Figure 10. Concurrent mitochondrial-derived reactive oxygen species (mdROS)–mediated oxidative ryanodine receptor (RyR) activation and oxidative Ca^{2+}/calmodulin-dependent protein kinase II (CaMKII) activation on action potential (A and B), cytosolic Ca^{2+} concentration ($[Ca^{2+}]_i$) (C and D), and cytosolic Na^+ concentration ($[Na^+]_i$) (E and F). In simulations of (A, C, and E) mdROS bursting was induced at phase 2 of the action potential and in (B, D, and F) mdROS bursting was induced at phase 4 of the action potential. Pacing cycle length=2 seconds and *shunt*=0.1. CON: shunt = 0.02, or no mitochondrial-derived reactive oxygen species bursting.

augmentation of $I_{Na,L}$ alone is sufficient to elicit EADs; (2) mdROS-CaMKII activation–induced EADs can be sustained even when mdROS reduces to a physiological level; and (3) mdROS burst-induced EADs can be suppressed by antioxidant treatment only when it is given within a timely window.

It has been proposed that the proarrhythmic effect of oxidative CaMKII activation is attributed to its capability to phosphorylate multiple ion channels/transporters underlying Ca^{2+} handling and AP. However, the detailed mechanistic pathways remain incompletely understood, partially because of the difficulty in experimentally dissecting the contribution of individual ion currents. For instance, although CaMKII activation of $I_{Na,L}$ has been implicated to be involved in oxidative stress–induced EADs,[39,44,59] whether this $I_{Na,L}$ augmentation alone can induce EADs under oxidative stress has never been examined. Therefore, in this computational study, we developed an ECME-RIRR model that considered only the direct modulatory effect of CaMKII oxidation on I_{Na}. Model simulations showed that oxidative CaMKII activation–induced augmentation of $I_{Na,L}$, which is comparable to experimental data (Figure 2B), successfully elicits EADs in a cardiomyocyte exposure to increased mdROS. Further analysis suggests that the augmented $I_{Na,L}$ causes EADs by altering both membrane potential and intracellular ion (eg, Na^+ and Ca^{2+}) homeostasis. In particular, our simulations revealed that the mdROS-CaMKII activation–induced EADs

involve the following: (1) increased $I_{Na,L}$ leads to APD prolongation and AP reverse; (2) the AP reverse causes a shift in Na^+/Ca^{2+} exchanger activity (reverse mode) and I_{CaL} reactivation; (3) reactivation of I_{CaL} triggers Ca^{2+}-induced Ca^{2+} release and results in a larger Ca^{2+} transient, which further augments I_{CaL} via a dynamic positive feedback mechanism; and (4) the large Ca^{2+} increase activates the forward mode I_{NaCa} and CaMKII-mediated $I_{Na,L}$, collectively resulting in EADs.

It is worth mentioning that while our model suggests that direct CaMKII activation of I_{CaL} is not required in mdROS-CaMKII activation–induced EADs, I_{CaL} reactivation, caused by AP reverse, plays a critical role in the EAD generation, as blocking I_{CaL} eliminates the mdROS-CaMKII activation–induced EADs. Interestingly, blocking I_{CaL} also caused APD shortening. This finding is different from that reported in our recent computational studies[47] focusing on mdROS-induced abnormal SR Ca^{2+} handling, in which blocking I_{CaL} suppressed EADs but did not reduce AP prolongation (as compared with normal mdROS). This suggests that the ionic mechanisms underlying oxidative CaMKII activation and oxidative RyRs activation–mediated arrhythmogenesis are different. We also found that oxidative CaMKII activation alone cannot generate DADs but concurrent oxidative RyRs and CaMKII activations can. As previous experimental studies[38,39] have recorded both EADs and DADs in H_2O_2-perfused isolated cardiomyocytes, it is likely that both pathways are presented in cardiomyocytes undergoing oxidative stress. In addition, our channel blocking simulations indicated that I_{NaCa} activation is also involved in the generation of oxidative CaMKII activation–induced EADs. Thus, although we showed that oxidative CaMKII activation–induced $I_{Na,L}$ augmentation is capable of eliciting EAD, the actual arrhythmogenic effects of mdROS are clearly multifactorial and new antiarrhythmic treatments targeting both ion channels/transporters/proteins and mitochondria are essential.

Another intriguing finding from the present modeling study is that the mdROS-CaMKII activation–induced EADs may not terminate immediately upon mitochondrial repolarization, even though mdROS has been reduced to basal physiological levels. While the phenomenon of sustained EADs postmitochondrial repolarization in cardiomyocytes needs further experimental verification, it may indeed occur in cells undergoing oxidative stress such as ischemia reperfusion, as a result of the specific property of CaMKII as "a memory molecule."[60] The memory refers to the autophosphorylation-mediated sustained CaMKII activation even after the dissociation of Ca^{2+}/CaM or the fall of Ca^{2+} concentration to baseline levels, which is essential for memory storage in the brain. Recently, Song et al[61] showed that short-term (5 minutes) ROS exposure caused persistent (more than 60 minutes) activation of I_{CaL} in isolated rat cardiomyocytes, likely via the oxidative stress–induced sustained CaMKII activation, indicating that CaMKII may act as a redox-sensitive "memory molecule" in cardiomyocytes. Notably, our model simulations showed that the duration of persistent EADs, or the proarrhythmic "memory" of CaMKII activation, is linked to the severity of mitochondrial dysfunction: the higher the mdROS bursting, the stronger the memory. Permanent memory might form if mitochondrial malfunction lasts long enough; in this case persistent arrhythmias will occur (Figure 8). Thus, as suggested by our antioxidant treatment simulations (Figure 9 and Figure S4) the ideal antiarrhythmic treatment would require the intervention be given timely and before the permanent memory of CaMKII is formed. Our computational analysis further showed that there is a close correlation between peak $[Na^+]_i$ and the robustness of CaMKII's memory, or the durations of the sustained and intermittent EADs during mitochondrial repolarization, suggesting that cytosolic $[Na^+]_i$ may be used as a risk factor of oxidative CaMKII activation–mediated arrhythmogenesis. The gradual $[Na^+]_i$ accumulation and sustained EADs facilitated by the oxidative stress–induced CaMKII-dependent $I_{Na,L}$ augmentation has also been reported by Wagner et al.[38]

In addition to antioxidant treatment, we also examined several other possible antiarrhythmic strategies such as blocking Na^+ or Ca^{2+} channels. Although our simulations showed that blocking I_{NaCa}, I_{CaL}, or $I_{Na,L}$ all eliminated the mdROS-mediated oxidative CaMKII activation–induced EADs, their antiarrhythmic roles should be further assessed experimentally, as long-term ion channel inhibition may break ion homeostasis and induce new arrhythmogenic substrates. For instance, it has been shown that inhibition of Na^+/Ca^{2+} exchanger–mediated Ca^{2+} extrusion increases Ca^{2+} spark frequency in resting cardiac myocytes. Long-term I_{CaL} inhibition, especially by nondihydropyridine Ca^{2+} channel blockers, can cause a shortening of APD and reduce cardiac contractility and conduction. In addition, the role of Ca^{2+} channel blockers in ventricular arrhythmias is limited and less well defined.[62–64] Compared with I_{NaCa} and I_{CaL} inhibition, blocking the $I_{Na,L}$ reduces depolarizing current during the plateau phase of the AP and thus may be more potent and safer. In line with this, it has been reported that a selective $I_{Na,L}$ inhibitor, GS-458967, prevents APD prolongation without affecting AP upstroke velocity in guinea pig ventricular myocytes.[65,66] Ranolazine, another Na^+ channel blocker, has been shown to reduce EAD and DAD occurrence in various settings where I_{NaL} is enhanced.[59]

Model Limitations

As our major goal was to examine whether, and if so, mdROS-CaMKII activation–induced I_{NaL} augmentation can induce EADs, the present model only incorporates CaMKII-dependent phosphorylation of Na^+ channels. However, it is well

appreciated that many other ion channels/transporters such as LCCs, RyRs, and K^+ channels can be phosphorylated by CaMKII.[67,68] CaMKII can increase I_{CaL} and SR Ca^{2+} release, thereby exacerbating Ca^{2+} overload and increasing the risk of arrhythmogenesis. Moreover, the activity of LCCs, RyRs, Na^+ channels, and K^+ channels can be directly influenced by mdROS.[69] The effects of oxidative CaMKII activation and direct oxidation on ion channels and homeostasis as well as AP may or may not overlap. Furthermore, previous studies from our laboratory and others have shown that deregulated cytosolic ion handling perturbs mitochondrial energetics and leads to oxidative stress, which can positively feedback on CaMKII activity. Finally, recent studies suggested that CaMKII may directly phosphorylate mitochondrial ion channels such as the Ca^{2+} uniporter,[23] thus altering mitochondrial ion homeostasis and bioenergetics.[23] Those components can be added to the ECME-RIRR model in the future. That being said, lack of these mechanisms should have little impact on the present study, as our main goal was to develop a computational model to examine whether the mdROS-mediated CaMKII activation can induce EADs in cardiomyocytes and to understand the underlying ionic mechanisms.

Conclusions

The present study provides a novel computational tool to quantitatively investigate the proarrhythmic effects of mdROS-mediated oxidative CaMKII activation in cardiomyocytes. The results indicate that CaMKII activation is sufficient to initiate downstream molecular events that promote aberrant Ca^{2+} handling and abnormal APs by sensing elevated mitochondrial-derived oxidative stress. Our simulations also underscore the importance of timely treatments in the context of oxidative CaMKII activation–induced arrhythmias.

Acknowledgments

We thank Dr Qince Li for suggestive discussion.

Sources of Funding

The authors acknowledge funding support from China Scholarships Council (grant No. 201506250131) and Key Technologies Research and Development Program of China (grant No. 2017YFC0110400) (to Yang) and National Institutes of Health/National Heart, Lung, and Blood Institute R01HL121206A1 (to Zhou).

Disclosures

None.

References

1. Abraham MR, Henrikson CA, Tung L, Chang MG, Aon M, Xue T, Li RA, O'Rourke B, Marban E. Antiarrhythmic engineering of skeletal myoblasts for cardiac transplantation. *Circ Res*. 2005;97:159–167.
2. Cohn JN. Prognosis in congestive heart failure. *J Card Fail*. 1996;2:S225–S229.
3. Cohn JN, Archibald DG, Ziesche S, Franciosa JA, Harston WE, Tristani FE, Dunkman WB, Jacobs W, Francis GS, Flohr KH, Goldman S, Cobb F, Shah P, Saunders R, Fletcher R, Loeb H, Hughes V, Baker B. Effect of vasodilator therapy on mortality in chronic congestive heart failure. Results of a Veterans Administration Cooperative Study. *N Engl J Med*. 1986;314:1547–1552.
4. Maack C, O'Rourke B. Excitation-contraction coupling and mitochondrial energetics. *Basic Res Cardiol*. 2007;102:369–392.
5. Zhou L, Cortassa S, Wei AC, Aon MA, Winslow RL, O'Rourke B. Modeling cardiac action potential shortening driven by oxidative stress-induced mitochondrial oscillations in guinea pig cardiomyocytes. *Biophys J*. 2009;97:1843–1852.
6. Zhou L, Aon MA, Liu T, O'Rourke B. Dynamic modulation of Ca(2+) sparks by mitochondrial oscillations in isolated guinea pig cardiomyocytes under oxidative stress. *J Mol Cell Cardiol*. 2011;51:632–639.
7. Yan Y, Liu J, Wei C, Li K, Xie W, Wang Y, Cheng H. Bidirectional regulation of Ca^{2+} sparks by mitochondria-derived reactive oxygen species in cardiac myocytes. *Cardiovasc Res*. 2008;77:432–441.
8. Eager KR, Roden LD, Dulhunty AF. Actions of sulfhydryl reagents on single ryanodine receptor Ca(2+)-release channels from sheep myocardium. *Am J Physiol*. 1997;272:C1908–C1918.
9. Gen W, Tani M, Takeshita J, Ebihara Y, Tamaki K. Mechanisms of Ca^{2+} overload induced by extracellular H_2O_2 in quiescent isolated rat cardiomyocytes. *Basic Res Cardiol*. 2001;96:623–629.
10. Morris TE, Sulakhe PV. Sarcoplasmic reticulum Ca(2+)-pump dysfunction in rat cardiomyocytes briefly exposed to hydroxyl radicals. *Free Radic Biol Med*. 1997;22:37–47.
11. Zima AV, Blatter LA. Redox regulation of cardiac calcium channels and transporters. *Cardiovasc Res*. 2006;71:310–321.
12. Jeong EM, Liu M, Sturdy M, Gao G, Varghese ST, Sovari AA, Dudley SC Jr. Metabolic stress, reactive oxygen species, and arrhythmia. *J Mol Cell Cardiol*. 2012;52:454–463.
13. Liu M, Liu H, Dudley SC Jr. Reactive oxygen species originating from mitochondria regulate the cardiac sodium channel. *Circ Res*. 2010;107:967–974.
14. Barrington PL, Meier CF Jr, Weglicki WB. Abnormal electrical activity induced by free radical generating systems in isolated cardiocytes. *J Mol Cell Cardiol*. 1988;20:1163–1178.
15. Ward CA, Giles WR. Ionic mechanism of the effects of hydrogen peroxide in rat ventricular myocytes. *J Physiol*. 1997;500(pt 3):631–642.
16. Kourie JI. Interaction of reactive oxygen species with ion transport mechanisms. *Am J Physiol*. 1998;275:C1–C24.
17. Coetzee WA, Opie LH. Effects of oxygen free radicals on isolated cardiac myocytes from guinea-pig ventricle: electrophysiological studies. *J Mol Cell Cardiol*. 1992;24:651–663.
18. Nakaya H, Takeda Y, Tohse N, Kanno M. Mechanism of the membrane depolarization induced by oxidative stress in guinea-pig ventricular cells. *J Mol Cell Cardiol*. 1992;24:523–534.
19. Zhang T, Brown JH. Role of Ca^{2+}/calmodulin-dependent protein kinase II in cardiac hypertrophy and heart failure. *Cardiovasc Res*. 2004;63:476–486.
20. Wagner S, Rokita AG, Anderson ME, Maier LS. Redox regulation of sodium and calcium handling. *Antioxid Redox Signal*. 2013;18:1063–1077.
21. Erickson JR, He BJ, Grumbach IM, Anderson ME. CaMKII in the cardiovascular system: sensing redox states. *Physiol Rev*. 2011;91:889–915.
22. Erickson JR, Joiner ML, Guan X, Kutschke W, Yang J, Oddis CV, Bartlett RK, Lowe JS, O'Donnell SE, Aykin-Burns N, Zimmerman MC, Zimmerman K, Ham AJ, Weiss RM, Spitz DR, Shea MA, Colbran RJ, Mohler PJ, Anderson ME. A dynamic pathway for calcium-independent activation of CaMKII by methionine oxidation. *Cell*. 2008;133:462–474.
23. Joiner ML, Koval OM, Li J, He BJ, Allamargot C, Gao Z, Luczak ED, Hall DD, Fink BD, Chen B, Yang J, Moore SA, Scholz TD, Strack S, Mohler PJ, Sivitz WI, Song LS, Anderson ME. CaMKII determines mitochondrial stress responses in heart. *Nature*. 2012;491:269–273.
24. Huke S, Knollmann BC. Oxidized CaMKII: a "heart stopper" for the sinus node? *J Clin Invest*. 2011;121:2975–2977.
25. Grueter CE, Abiria SA, Dzhura I, Wu Y, Ham AJ, Mohler PJ, Anderson ME, Colbran RJ. L-type Ca^{2+} channel facilitation mediated by phosphorylation of the beta subunit by CaMKII. *Mol Cell*. 2006;23:641–650.

26. Hudmon A, Schulman H, Kim J, Maltez JM, Tsien RW, Pitt GS. CaMKII tethers to L-type Ca^{2+} channels, establishing a local and dedicated integrator of Ca^{2+} signals for facilitation. *J Cell Biol*. 2005;171:537–547.

27. Dzhura I, Wu Y, Colbran RJ, Balser JR, Anderson ME. Calmodulin kinase determines calcium-dependent facilitation of L-type calcium channels. *Nat Cell Biol*. 2000;2:173–177.

28. Blaich A, Welling A, Fischer S, Wegener JW, Kostner K, Hofmann F, Moosmang S. Facilitation of murine cardiac L-type Ca(v)1.2 channel is modulated by calmodulin kinase II-dependent phosphorylation of S1512 and S1570. *Proc Natl Acad Sci USA*. 2010;107:10285–10289.

29. Maier LS, Bers DM. Role of Ca^{2+}/calmodulin-dependent protein kinase (CaMK) in excitation-contraction coupling in the heart. *Cardiovasc Res*. 2007;73:631–640.

30. Maier LS, Zhang T, Chen L, DeSantiago J, Brown JH, Bers DM. Transgenic CaMKIIdeltaC overexpression uniquely alters cardiac myocyte Ca^{2+} handling: reduced SR Ca^{2+} load and activated SR Ca^{2+} release. *Circ Res*. 2003;92:904–911.

31. Wehrens XH, Lehnart SE, Reiken SR, Marks AR. Ca^{2+}/calmodulin-dependent protein kinase II phosphorylation regulates the cardiac ryanodine receptor. *Circ Res*. 2004;94:e61–e70.

32. Guo T, Zhang T, Mestril R, Bers DM. Ca^{2+}/calmodulin-dependent protein kinase II phosphorylation of ryanodine receptor does affect calcium sparks in mouse ventricular myocytes. *Circ Res*. 2006;99:398–406.

33. Kohlhaas M, Zhang T, Seidler T, Zibrova D, Dybkova N, Steen A, Wagner S, Chen L, Brown JH, Bers DM, Maier LS. Increased sarcoplasmic reticulum calcium leak but unaltered contractility by acute CaMKII overexpression in isolated rabbit cardiac myocytes. *Circ Res*. 2006;98:235–244.

34. Sag CM, Wolff HA, Neumann K, Opiela MK, Zhang J, Steuer F, Sowa T, Gupta S, Schirmer M, Hunlich M, Rave-Frank M, Hess CF, Anderson ME, Shah AM, Christiansen H, Maier LS. Ionizing radiation regulates cardiac Ca handling via increased ROS and activated CaMKII. *Basic Res Cardiol*. 2013;108:385.

35. Ho HT, Liu B, Snyder JS, Lou Q, Brundage EA, Velez-Cortes F, Wang H, Ziolo MT, Anderson ME, Sen CK, Wehrens XH, Fedorov VV, Biesiadecki BJ, Hund TJ, Gyorke S. Ryanodine receptor phosphorylation by oxidized CaMKII contributes to the cardiotoxic effects of cardiac glycosides. *Cardiovasc Res*. 2014;101:165–174.

36. Bassani RA, Mattiazzi A, Bers DM. CaMKII is responsible for activity-dependent acceleration of relaxation in rat ventricular myocytes. *Am J Physiol*. 1995;268:H703–H712.

37. Wagner S, Dybkova N, Rasenack EC, Jacobshagen C, Fabritz L, Kirchhof P, Maier SK, Zhang T, Hasenfuss G, Brown JH, Bers DM, Maier LS. Ca^{2+}/calmodulin-dependent protein kinase II regulates cardiac Na^+ channels. *J Clin Invest*. 2006;116:3127–3138.

38. Wagner S, Ruff HM, Weber SL, Bellmann S, Sowa T, Schulte T, Anderson ME, Grandi E, Bers DM, Backs J, Belardinelli L, Maier LS. Reactive oxygen species-activated Ca/calmodulin kinase IIdelta is required for late I(Na) augmentation leading to cellular Na and Ca overload. *Circ Res*. 2011;108:555–565.

39. Xie LH, Chen F, Karagueuzian HS, Weiss JN. Oxidative-stress-induced afterdepolarizations and calmodulin kinase II signaling. *Circ Res*. 2009;104:79–86.

40. Onal B, Gratz D, Hund TJ. Ca(2+)/calmodulin-dependent kinase II-dependent regulation of atrial myocyte late Na(+) current, Ca(2+) cycling, and excitability: a mathematical modeling study. *Am J Physiol Heart Circ Physiol*. 2017;313:H1227–H1239.

41. Dai L, Zang Y, Zheng D, Xia L, Gong Y. Role of CaMKII and PKA in early afterdepolarization of human ventricular myocardium cell: a computational model study. *Comput Math Methods Med*. 2016;2016:4576313.

42. Lascano EC, Said M, Vittone L, Mattiazzi A, Mundina-Weilenmann C, Negroni JA. Role of CaMKII in post acidosis arrhythmias: a simulation study using a human myocyte model. *J Mol Cell Cardiol*. 2013;60:172–183.

43. Christensen MD, Dun W, Boyden PA, Anderson ME, Mohler PJ, Hund TJ. Oxidized calmodulin kinase II regulates conduction following myocardial infarction: a computational analysis. *PLoS Comput Biol*. 2009;5:e1000583.

44. Foteinou PT, Greenstein JL, Winslow RL. Mechanistic investigation of the arrhythmogenic role of oxidized CaMKII in the heart. *Biophys J*. 2015;109:838–849.

45. Zhang SZ, Li QC, Zhou LF, Wang KQ, Zhang HG. Development of a novel Markov chain model for oxidative-dependent CaMKII delta activation. *Computing in Cardiology*. 2015;42:881–884.

46. Li Q, Pogwizd SM, Prabhu SD, Zhou L. Inhibiting Na^+/K^+ ATPase can impair mitochondrial energetics and induce abnormal Ca^{2+} cycling and automaticity in guinea pig cardiomyocytes. *PLoS One*. 2014;9:e93928.

47. Li Q, Su D, O'Rourke B, Pogwizd SM, Zhou L. Mitochondria-derived ROS bursts disturb Ca(2)(+) cycling and induce abnormal automaticity in guinea pig cardiomyocytes: a theoretical study. *Am J Physiol Heart Circ Physiol*. 2015;308:H623–H636.

48. Grandi E, Puglisi JL, Wagner S, Maier LS, Severi S, Bers DM. Simulation of Ca-calmodulin-dependent protein kinase II on rabbit ventricular myocyte ion currents and action potentials. *Biophys J*. 2007;93:3835–3847.

49. Aiba T, Hesketh GG, Liu T, Carlisle R, Villa-Abrille MC, O'Rourke B, Akar FG, Tomaselli GF. Na^+ channel regulation by Ca^{2+}/calmodulin and Ca^{2+}/calmodulin-dependent protein kinase II in guinea-pig ventricular myocytes. *Cardiovasc Res*. 2010;85:454–463.

50. Cortassa S, Aon MA, O'Rourke B, Jacques R, Tseng HJ, Marban E, Winslow RL. A computational model integrating electrophysiology, contraction, and mitochondrial bioenergetics in the ventricular myocyte. *Biophys J*. 2006;91:1564–1589.

51. Cortassa S, Aon MA, Winslow RL, O'Rourke B. A mitochondrial oscillator dependent on reactive oxygen species. *Biophys J*. 2004;87:2060–2073.

52. Zhou L, Solhjoo S, Millare B, Plank G, Abraham MR, Cortassa S, Trayanova N, O'Rourke B. Effects of regional mitochondrial depolarization on electrical propagation: implications for arrhythmogenesis. *Circ Arrhythm Electrophysiol*. 2014;7:143–151.

53. Chance B, Sies H, Boveris A. Hydroperoxide metabolism in mammalian organs. *Physiol Rev*. 1979;59:527–605.

54. Backs J, Backs T, Neef S, Kreusser MM, Lehmann LH, Patrick DM, Grueter CE, Qi XX, Richardson JA, Hill JA, Katus HA, Bassel-Duby R, Maier LS, Olson EN. The delta isoform of CaM kinase II is required for pathological cardiac hypertrophy and remodeling after pressure overload. *Proc Natl Acad Sci USA*. 2009;106:2342–2347.

55. Zhao Z, Wen H, Fefelova N, Allen C, Baba A, Matsuda T, Xie LH. Revisiting the ionic mechanisms of early afterdepolarizations in cardiomyocytes: predominant by Ca waves or Ca currents? *Am J Physiol Heart Circ Physiol*. 2012;302:H1636–H1644.

56. Cortassa S, Aon MA, Marban E, Winslow RL, O'Rourke B. An integrated model of cardiac mitochondrial energy metabolism and calcium dynamics. *Biophys J*. 2003;84:2734–2755.

57. Fink M, Noble D. Pharmacodynamic effects in the cardiovascular system: the modeller's view. *Basic Clin Pharmacol Toxicol*. 2010;106:243–249.

58. Corrias A, Giles W, Rodriguez B. Ionic mechanisms of electrophysiological properties and repolarization abnormalities in rabbit Purkinje fibers. *Am J Physiol Heart Circ Physiol*. 2011;300:H1806–H1813.

59. Mason FE, Sossalla S. The significance of the late Na^+ current for arrhythmia induction and the therapeutic antiarrhythmic potential of ranolazine. *J Cardiovasc Pharmacol Ther*. 2016;22:40–50.

60. Lisman J, Schulman H, Cline H. The molecular basis of CaMKII function in synaptic and behavioural memory. *Nat Rev Neurosci*. 2002;3:175–190.

61. Song YH, Cho H, Ryu SY, Yoon JY, Park SH, Noh CI, Lee SH, Ho WK. L-type Ca^{2+} channel facilitation mediated by H_2O_2-induced activation of CaMKII in rat ventricular myocytes. *J Mol Cell Cardiol*. 2010;48:773–780.

62. Belhassen B, Horowitz LN. Use of intravenous verapamil for ventricular tachycardia. *Am J Cardiol*. 1984;54:1131–1133.

63. Gill JS, Baszko A, Xia R, Ward DE, Camm AJ. Dynamics of the QT interval in patients with exercise-induced ventricular tachycardia in normal and abnormal hearts. *Am Heart J*. 1993;126:1357–1363.

64. Gill JS, Blaszyk K, Ward DE, Camm AJ. Verapamil for the suppression of idiopathic ventricular tachycardia of left bundle branch block-like morphology. *Am Heart J*. 1993;126:1126–1133.

65. Belardinelli L, Liu G, Smith-Maxwell C, Wang WQ, El-Bizri N, Hirakawa R, Karpinski S, Li CH, Hu L, Li XJ, Crumb W, Wu L, Koltun D, Zablocki J, Yao L, Dhalla AK, Rajamani S, Shryock JC. A novel, potent, and selective inhibitor of cardiac late sodium current suppresses experimental arrhythmias. *J Pharmacol Exp Ther*. 2013;344:23–32.

66. Yang PC, Song YJ, Giles WR, Horvath B, Chen-Izu Y, Belardinelli L, Rajamani S, Clancy CE. A computational modelling approach combined with cellular electrophysiology data provides insights into the therapeutic benefit of targeting the late Na^+ current. *J Physiol*. 2015;593:1429–1442.

67. O'Hara T, Virag L, Varro A, Rudy Y. Simulation of the undiseased human cardiac ventricular action potential: model formulation and experimental validation. *PLoS Comput Biol*. 2011;7:e1002061.

68. Winslow RL, Walker MA, Greenstein JL. Modeling calcium regulation of contraction, energetics, signaling, and transcription in the cardiac myocyte. *Wiley Interdiscip Rev Syst Biol Med*. 2016;8:37–67.

69. Yang L, Xu J, Minobe E, Yu L, Feng R, Kameyama A, Yazawa K, Kameyama M. Mechanisms underlying the modulation of L-type Ca^{2+} channel by hydrogen peroxide in guinea pig ventricular myocytes. *J Physiol Sci*. 2013;63:419–426.

Supplemental Material

Table S1. Sarcolemmal membrane ionic currents

Fast Na^+ current (I_{Na})

$I_{Na} = \overline{G}_{Na}\, m^3\, h\, j\, (V - E_{Na})$	E1
$E_{Na} = \frac{RT}{F} \ln \frac{[Na^+]_o}{[Na^+]_i}$	E2
$\frac{dm_{Na}}{dt} = \alpha_m (1-m_{Na}) - \beta_m m_{Na}$	E3
$\frac{dh_{Na}}{dt} = \alpha_h (1-h_{Na}) - \beta_h h_{Na}$	E4
$\frac{dj_{Na}}{dt} = \alpha_j (1-j_{Na}) - \beta_j j_{Na}$	E5
$\alpha_m = 0.32 \frac{V + 47.13}{1 - e^{-0.1\,(V+47.13)}}$	E6
$\beta_m = 0.08\, e^{-V/11}$	E7
For $V \geq -40$ mV	
$\alpha_h = 0.0$	E8
$\alpha_j = 0.0$	E9
$\beta_h = 0.13 \left[1 + e^{\frac{V+10.66}{11.1}}\right]^{-1}$	E10
$\beta_j = 0.3 \frac{e^{-2.535 \cdot 10^{-7} V}}{1 + e^{-0.1\,(V+32)}}$	E11
For $V < -40$ mV	
$\alpha_h = 0.135\, e^{\frac{80 + V}{-6.8}}$	E12
$\alpha_j = \frac{\left(-127{,}140\, e^{0.2444\, V} - 3.474 \cdot 10^{-5}\, e^{0.04391\, V}\right) \cdot (V + 37.78)}{1 + e^{0.311\,(V+79.23)}}$	E13

$$_{h} = 3.56\ e^{0.079\ V} + 3.1 \cdot 10^{5}\ e^{0.35\ V}$$ E14

$$_{j} = 0.1212\ \frac{e^{-0.01052\ V}}{1 + e^{-0.1378\ (V+\ 40.14)}}$$ E15

Markov slow Na^{+} model ($I_{Na,L}$)

Transition rate expressions (ms^{-1})

$$IC3toIC2 = \frac{P_{1a1}}{P_{2a1} \times \exp(-V/17) + 0.2 \times \exp(-V/150)}$$ E16

$$C3toC2 = IC3toIC2$$ E17

$$LC3toLC2 = IC3toIC2$$ E18

$$LC2toIF = \frac{P_{1a1}}{P_{2a1} \times \exp(-V/12) + 0.25 \times \exp(-V/150)}$$ E19

$$C2toC1 = IC2toIF$$ E20

$$LC2toLC1 = IC2toIF$$ E21

$$LC1toLO = \frac{P_{1a1}}{P_{2a1} \times \exp(-V/12) + 0.25 \times \exp(-V/150)}$$ E22

$$C1toO = LC1toLO$$ E23

$$IC2toIC3 = P_{1b1} \times \exp(-V/P_{2b1})$$ E24

$$C2toC3 = IC2toIC3$$ E25

$$LC2toLC3 = IC2toIC3$$ E26

$$IFtoIC2 = P_{1b2} \times \exp(-\frac{V - P_{2b2}}{P_{2b1}})$$ E27

$$C1toC2 = IFtoIC2$$ E28

$$LC1toLC2 = IFtoIC2$$ E29

$$LOtoLC1 = P_{1b3} * \exp(-\frac{V - P_{2b3}}{P_{2b1}})$$ E30

$$OtoC1 = LOtoLC1$$ E31

$$IC3toC3 = P_{1a5} \times \exp(-\frac{V}{P_{2a5}})$$ E32

$IC2toC2 = IC3toC3$	E33
$IFtoC1 = IC3toC3$	E34
$C3toIC3 = P_{1b5} + P_{2b5} \times V$	E35
$C2toIC2 = C3toIC3$	E36
$C1toIF = C3toIC3$	E37
$OtoIF = P_{1a4} \times \exp(\frac{V}{P_{2a4}})$	E38
$IFtoO = \frac{LC1toLO \times OtoIF \times IC3toC3}{LOtoLC1 \times C3toIC3}$	E39
$IFtoIM1 = \frac{P_{1a4} \times \exp(V/P_{2a4}/P_{2a42})}{P_{1a6}}$	E40
$IM1toIF = P_{1b6} \times \exp(-\frac{V}{P_{2b6}})$	E41
$IM1toIM2 = P_{1a7} \times \exp(\frac{V}{P_{2a7}})$	E42
$IM2toIM1 = P_{1b7} \times \exp(-\frac{V}{P_{2b7}})$	E43
$C3toLC3 = P_{1a8}$	E44
$C2toLC2 = C3toLC3$	E45
$C1toLC1 = C3toLC3$	E46
$OtoLO = C3toLC3$	E47
$LC3toC3 = P_{1b8}$	E48
$LC2toC2 = LC3toC3$	E49
$LC1toC1 = LC3toC3$	E50
$LOtoO = LC3toC3$	E51

Balance equations of the late sodium channels

$\frac{dIC3}{dt} = C3toIC3 \times C3 + IC2toIC3 \times IC2 - (IC3toIC2 + IC3toC3) \times IC3$	E52

$$\frac{dIC2}{dt} = IC3toIC2 \times IC3 + IFtoIC2 \times IF + C2toIC2 \times C2 - (IC2toC2 + IC2toC3 + IC2toIF) \times IC2 \quad \text{E53}$$

$$\frac{dIF}{dt} = IC2toIF \times C2 + IM1toIF \times IM1 + C1toIF \times C1 + OtoIF \times O - (IFtoIC2 + IFtoIM1 + IFtoC1_IFtoO) \times IF \quad \text{E54}$$

$$\frac{dIM1}{dt} = IFtoIM1 \times IF + IM2toIM1 \times IM2 - (IM1toIF + IM1toIM2) \times IM1 \quad \text{E55}$$

$$\frac{dIM2}{dt} = IM1toIM2 \times IM1 - IM2toIM1 \times IM2 \quad \text{E56}$$

$$\frac{dC3}{dt} = IC3toC3 \times IC3 + C2toC3 \times C2 + LC3toC3 \times LC3 - (C3toIC3 + C3toC2 + C3toLC3) \times C3 \quad \text{E57}$$

$$\frac{dC2}{dt} = IC2toC2 \times IC2 + C3toC2 \times C3 + LC2toC2 \times LC2 + C1toC2 \times C1 - (C2toIC2 + C2toC3 + C2toLC2 + C2toC1) \times C2 \quad \text{E58}$$

$$\frac{dC1}{dt} = IFtoC1 \times IF + C2toC1 \times C2 + OtoC1 \times O + LC1toC1 \times LC1 - (C1toIF + C1toC2 + C1toO + C1toLC1) \times C1 \quad \text{E59}$$

$$\frac{dO}{dt} = IFtoO \times IF + C1toO \times C1 + LOtoO \times LO - (OtoIF + OtoC1 + OtoLO) \times O \quad \text{E60}$$

$$\frac{dLC3}{dt} = C3toLC3 \times C3 + LC2toLC3 \times LC2 - (LC3toC3 + LC3toLC2) \times LC3 \quad \text{E61}$$

$$\frac{dLC2}{dt} = C2toLC2 \times C2 + LC3toLC2 \times LC3 + LC1toLC2 \times LC1 - (LC2toC2 + LC2toLC3 + LC2toLC1) \times LC2 \quad \text{E62}$$

$$\frac{dLC1}{dt} = C1toLC1 \times C1 + LC2toLC1 \times LC2 + LOtoLC1 \times LO - (LC1toC1 + LC1toLC2 + LC1toLO) \times LC1 \quad \text{E63}$$

$$\frac{dLO}{dt} = OtoLO \times O + LC1toLO \times LC1 - (LOtoO + LOtoLC1) \times LO \quad \text{E64}$$

Late sodium current

$$I_{Na,L} = G_{Na,L} \cdot P_{LO} \cdot (V - E_{Na}) \quad \text{E65}$$

Time-dependent delayed rectifier K^+ current (I_K)

$$I_K = \overline{G}_K X_1 X_K^2 (V - E_K) \quad \text{E66}$$

$$E_K = \frac{RT}{F} \ln \frac{[K^+]_o + P_{Na,K}[Na^+]_o}{[K^+]_i + P_{Na,K}[Na^+]_i} \quad \text{E67}$$

$$\overline{G}_K = 0.282 \sqrt{\frac{[K^+]_o}{5.4}} \quad \text{E68}$$

$$X_1 = \left(1 + e^{(V-40)/40}\right)^{-1} \quad \text{E69}$$

$$\frac{dX_K}{dt} = (1 - X_K) - X_K \quad \text{E70}$$

$$= 7.19 \cdot 10^{-5} \frac{V + 30}{1 - e^{-0.148(V+30)}} \quad \text{E71}$$

$$= 1.31 \cdot 10^{-4} \frac{V + 30}{-1 + e^{0.0687(V+30)}} \quad \text{E72}$$

Time-independent K^+ current (I_{K1})

$$I_{K_1} = \overline{G}_{K_1} K_1 (V - E_{K_1}) \quad \text{E73}$$

$$E_{K_1} = \frac{RT}{F} \ln \frac{[K^+]_o}{[K^+]_i} \quad \text{E74}$$

$$\overline{G}_{K_1} = 0.75 \sqrt{\frac{[K^+]_o}{5.4}} \quad \text{E75}$$

$$K_1 = \frac{K_1}{K_1 + K_1} \quad \text{E76}$$

$$K_1 = \frac{1.02}{1 + e^{0.2385(V - E_{K_1} - 59.215)}} \quad \text{E77}$$

$$K_1 = \frac{0.4912 e^{0.08032(V - E_{K_1} + 5.476)} + e^{0.06175(V - E_{K_1} - 594.31)}}{1 + e^{0.5143(V - E_{K_1} + 4.753)}} \quad \text{E78}$$

Plateau K^+ current (I_{Kp})

$$I_{K_P} = \overline{G}_{K_P} K_P \left(V - E_{K_P}\right) \quad \text{E79}$$

$$E_{K_P} = E_{K_1} \quad \text{E80}$$

$$K_p = \left(1 + e^{(7.488\ V)/5.98}\right)^{-1} \quad \text{E81}$$

Na^+/Ca^{2+} exchanger current (I_{NaCa})

$$I_{NaCa} = k_{NaCa} \frac{1}{K_{m,Na}^3 + [Na^+]_o^3} \frac{1}{K_{m,Ca} + [Ca^{2+}]_o} \frac{1}{1 + k_{sat} e^{(\ -1)\frac{VF}{RT}}} e^{\frac{VF}{RT}} [Na^+]_i^3 [Ca^{2+}]_o - e^{(\ -1)\frac{VF}{RT}} [Na^+]_o^3 [Ca^{2+}]_i \quad \text{E82}$$

Na^+/ K^+ pump current (I_{NaK})

$$I_{NaK} = \bar{I}_{NaK} f_{NaK} f_{NaK}^{ATP} \left(1 + \frac{K_{m,Na_i}}{[Na^+]_i}^{1.5}\right)^{-1} \frac{[K^+]_o}{[K^+]_o + K_{m,K_o}} \quad \text{E83}$$

$$f_{NaK} = \left(1 + 0.1245\, e^{-0.1\frac{VF}{RT}} + 0.0365\, e^{-\frac{VF}{RT}} \frac{e^{[Na^+]_o/67.3}}{7}\right)^{-1} \quad \text{E84}$$

$$f_{NaK}^{ATP} = \left(1 + \frac{K_{NaK}^{1,\,ATP}}{[ATP]_i} \left(1 + \frac{[ADP]_i}{K_{NaK}^{i,\,ADP}}\right)\right)^{-1} \quad \text{E85}$$

Nonspecific Ca^{2+} activated current (I_{nsCa})

$$I_{ns(Ca)} = I_{ns(Na)} + I_{ns(K)} \quad \text{E86}$$

$$I_{ns(Na)} = \bar{I}_{ns(Na)} \left(1 + \frac{K_{m,ns(Ca)}}{[Ca^{2+}]_i}\right)^{3^{-1}} \quad \text{E87}$$

$$\bar{I}_{ns(Na)} = P_{ns(Na)} \frac{VF^2}{RT} \frac{0.75\left([Na^+]_i\, e^{VF/RT} - [Na^+]_o\right)}{e^{VF/RT} - 1} \quad \text{E88}$$

$$I_{ns(K)} = \bar{I}_{ns(K)} \left(1 + \frac{K_{m,ns(Ca)}}{[Ca^{2+}]_i}\right)^{3^{-1}} \quad \text{E89}$$

$$\bar{I}_{ns(K)} = P_{ns(K)} \frac{VF^2}{RT} \frac{0.75\left([K^+]_i\, e^{VF/RT} - [K^+]_o\right)}{e^{VF/RT} - 1} \quad \text{E90}$$

Background Ca^{2+} current ($I_{Ca,b}$)

$$I_{Ca,b} = \bar{G}_{Ca,b}\left(V - E_{Ca,N}\right) \quad \text{E91}$$

$$E_{Ca,N} = \frac{RT}{2F} \ln \frac{[Ca^{2+}]_o}{[Ca^{2+}]_i} \quad \text{E92}$$

Background Na^+ current ($I_{Na,b}$)

$$I_{Na.b} = \bar{G}_{Na,b}\left(V - E_{Na,N}\right) \quad \text{E93}$$

$$E_{Na,N} = E_{Na} \quad \text{E94}$$

Sarcolemmal Ca^{2+} pump current (I_{pCa})

$$I_{pCa} = I_{pCa\_max}\, F_{pCa}^{ATP} \frac{[Ca^{+2}]_i}{K_m^{pCa} + [Ca^{+2}]_i} \quad \text{E95}$$

$$F_{pCa}^{ATP} = \left(1+\frac{K_{m1\_pCa}^{ATP}}{[ATP]_i}\right)^{-1}\left(1+\frac{[ADP]_i}{K_{i\_pCa}^{ADP}}\right)^{-1} + \left(1+\frac{K_{m2\_pCa}^{ATP}}{[ATP]_i}\right)^{-1} \quad \text{E96}$$

SERCA pump (J_{up})

$$J_{up} = \frac{V_{max\,f}\ f_b - V_{max\,r}\ r_b}{1+f_b+r_b}\ f_{ATP}^{SERCA} \quad \text{E97}$$

$$f_b = \left(\frac{[Ca^{2+}]_i}{K_{fb}}\right)^{Nfb} \quad \text{E98}$$

$$r_b = \left(\frac{[Ca^{2+}]_{SR}}{K_{rb}}\right)^{Nrb} \quad \text{E99}$$

$$f_{ATP}^{SERCA} = \frac{K_{m,up}^{ATP}}{[ATP]_i}\cdot\left(1+\frac{[ADP]_i}{K_{i,up}} + 1 + \frac{[ADP]_i}{K_{i,up}^{'}}\right)^{-1} \quad \text{E100}$$

L-type Ca^{2+} current (I_{Ca})

$$I_{CaL} = 4\frac{N_{CaRU}}{C_m}P_{Ca}\frac{VF^2}{RT}\frac{\left[\begin{matrix}P_{(2)}\left([Ca^{2+}]_{dm}^{(2)}e^{2VF/RT}-0.314[Ca^{2+}]_0\right)+\\ P_{(4)}([Ca^{2+}]_{dm}^{(4)}e^{2VF/RT}-0.314[Ca^{2+}]_0)\end{matrix}\right]}{e^{2VF/RT}-1} \quad \text{E101}$$

Sarcolemmal membrane potential

$$\frac{dV}{dt} = -\frac{1}{C_m}\left(\begin{matrix}I_{Na}+I_{CaL}+I_{Ca,K}+I_K+I_{K1}+I_{Kp}+I_{NaCa}+I_{Na,K}\\ +I_{nsCa}+I_{pCa}+I_{Ca,b}+I_{Na,b}+I_{K,ATP}+I_{Na,L}^{*}\end{matrix}\right) \quad \text{E102}$$

Table S2. Ca^{2+} handling system

40-state LCC-RyR Model

$\alpha = 0.78133e^{(0.08(V_m-8))}$	E103
$\beta = 0.34319e^{(-0.086676(V_m-8))}$	E104
$\alpha' = a\alpha$	E105
$\beta' = \beta/b$	E106
$y_\infty = \frac{0.75}{\left(1+e^{\frac{(V_m+25)}{5}}\right)} + 0.25$	*E107
$\tau_y = \frac{500}{\left(1+e^{\frac{(V_m+28)}{10}}\right)} \times \frac{1}{\left(1+e^{\frac{-(V_m+42)}{14}}\right)} + 17$	*E108
$k_b = \frac{y_\infty}{\tau_y}$	E109
$k_f = \frac{(1-y_\infty)}{\tau_y}$	E110
$\lambda_{1,2} = \lambda_{6,7} = \alpha$	E111
$\lambda_{2,1} = \lambda_{7,6} = \beta$	E112
$\lambda_{2,3} = \lambda_{7,8} = f$	E113
$\lambda_{3,2} = \lambda_{8,7} = g$	E114
$\lambda_{1,4} = \lambda_{6,9} = \gamma_0[Ca^{2+}]_{ds}$	E115
$\lambda_{4,1} = \lambda_{9,6} = \omega$	E116
$\lambda_{4,5} = \lambda_{9,10} = \alpha'$	E117
$\lambda_{5,4} = \lambda_{10,9} = \beta'$	E118
$\lambda_{2,5} = \lambda_{7,10} = \alpha\gamma_0[Ca^{2+}]_{ds}$	E119
$\lambda_{5,2} = \lambda_{10,7} = \omega/b$	E120
$\lambda_{1,6} = \lambda_{2,7} = \lambda_{3,8} = \lambda_{4,9} = \lambda_{5,10} = k_f$	E121
$\lambda_{6,1} = \lambda_{7,2} = \lambda_{8,3} = \lambda_{9,4} = \lambda_{10,5} = k_b$	E122
$k_{1,2} = k0_{1,2}[Ca^{2+}]^2{}_{ds}$	E123
$k_{2,1} = k0_{2,1}$	E124

$k_{2,3} = k0_{2,3}[Ca^{2+}]^2{}_{ds}$	E125
$k_{3,2} = k0_{3,2}k0_{4,3}/\left(k0_{3,4}[Ca^{2+}]^2_{ds} + k0_{4,3}\right)$	E126
$k_{2,4} = k0_{2,5}[Ca^{2+}]^2{}_{ds}$	E127
$k_{4,2} = k0_{5,2}k0_{6,5}/\left(k0_{5,6}[Ca^{2+}]^2_{ds} + k0_{6,5}\right)$	E128
$k_{3,4} = k0_{4,5}k0_{3,4}[Ca^{2+}]^2_{ds}/\left(k0_{3,4}[Ca^{2+}]^2_{ds} + k0_{4,3}\right)$	E129
$k_{4,3} = k0_{6,5}k0_{5,4}[Ca^{2+}]^2_{ds}/\left(k0_{5,6}[Ca^{2+}]^2_{ds} + k0_{6,5}\right)$	E130
$\dot{x}_1 = -\left(\lambda_{1,2} + \lambda^{(1)}_{1,4} + \lambda_{1,6} + k^{(1)}_{1,2}\right)x_1 + \lambda_{2,1}x_2 + \lambda_{4,1}x_4 + \lambda_{6,1}x_6 + k_{2,1}x_{11}$	E131
$\dot{x}_2 = \lambda_{1,2}x_1 - \left(\lambda_{2,1} + \lambda_{2,3} + \lambda^{(1)}_{2,5} + \lambda_{2,7} + k^{(1)}_{1,2}\right)x_2 + \lambda_{3,2}x_3 + \lambda_{5,2}x_5 + \lambda_{7,2}x_7 + k_{2,1}x_{12}$	E132
$\dot{x}_3 = \lambda_{2,3}x_2 - \left(\lambda_{3,2} + \lambda_{3,8} + k^{(2)}_{1,2}\right)x_3 + \lambda_{8,3}x_8 + k_{2,1}x_{13}$	E133
$\dot{x}_4 = \lambda^{(1)}_{1,4}x_1 - \left(\lambda_{4,1} + \lambda_{4,5} + \lambda_{4,9} + k^{(2)}_{1,2}\right)x_4 + \lambda_{5,4}x_5 + \lambda_{9,4}x_9 + k_{2,1}x_{14}$	E134
$\dot{x}_5 = \lambda^{(1)}_{2,5}x_2 + \lambda_{4,5}x_4 - \left(\lambda_{5,2} + \lambda_{5,4} + \lambda_{5,10} + k^{(1)}_{1,2}\right)x_5 + \lambda_{10,5}x_{10} + k_{2,1}x_{15}$	E135
$\dot{x}_6 = \lambda_{1,6}x_1 + \lambda_{7,6}x_7 - \left(\lambda_{6,1} + \lambda_{6,7} + \lambda^{(1)}_{6,9} + k^{(1)}_{1,2}\right)x_6 + \lambda_{9,6}x_9 + k_{2,1}x_{16}$	E136
$\dot{x}_7 = \lambda_{2,7}x_2 + \lambda_{6,7}x_6 - \left(\lambda_{7,2} + \lambda_{7,6} + \lambda_{7,8} + \lambda^{(1)}_{7,10} + k^{(1)}_{1,2}\right)x_7 + \lambda_{8,7}x_8 + \lambda_{10,7}x_{10} + k_{2,1}x_{17}$	E137
$\dot{x}_8 = \lambda_{3,8}x_3 + \lambda_{7,8}x_7 - \left(\lambda_{8,3} + \lambda_{8,7} + k^{(1)}_{1,2}\right)x_8 + k_{2,1}x_{18}$	E138
$\dot{x}_9 = \lambda_{4,9}x_4 + \lambda^{(1)}_{6,9}x_6 - \left(\lambda_{9,4} + \lambda_{9,6} + \lambda_{9,10} + k^{(1)}_{1,2}\right)x_9 + \lambda_{10,9}x_{10} + k_{2,1}x_{19}$	E139
$\dot{x}_{10} = \lambda_{5,10}x_5 + \lambda_{9,10}x_9 + \lambda^{(1)}_{7,10}x_7 - \left(\lambda_{10,5} + \lambda_{10,7} + \lambda_{10,9} + k^{(1)}_{1,2}\right)x_{10} + k_{2,1}x_{20}$	E140
$\dot{x}_{11} = k^{(1)}_{1,2}x_1 - \left(\lambda_{1,2} + \lambda^{(1)}_{1,4} + \lambda_{1,6} + k_{2,1} + k^{(1)}_{2,3} + k^{(1)}_{2,4}\right)x_{11} + \lambda_{2,1}x_{12} + \lambda_{4,1}x_{14} + \lambda_{6,1}x_{16} + k^{(3)}_{3,2}x_{21} + k^{(1)}_{4,2}x_{31}$	E141
$\dot{x}_{12} = k^{(1)}_{1,2}x_2 - \left(\lambda_{2,1} + \lambda_{2,3} + \lambda^{(1)}_{2,5} + \lambda_{2,7} + k_{2,1} + k^{(1)}_{2,3} + k^{(1)}_{2,4}\right)x_{12} + \lambda_{3,2}x_{13} + \lambda_{5,2}x_{15} + \lambda_{7,2}x_{17} + k^{(1)}_{4,2}x_{32} + k^{(3)}_{3,2}x_{22}$	E142
$\dot{x}_{13} = k^{(2)}_{1,2}x_3 + \lambda_{2,3}x_{12} - \left(\lambda_{3,2} + \lambda_{3,8} + k_{2,1} + k^{(2)}_{2,3} + k^{(2)}_{2,4}\right)x_{13} + \lambda_{8,3}x_{18} + k^{(2)}_{4,2}x_{33} + k^{(4)}_{3,2}x_{23}$	E143
$\dot{x}_{14} = k^{(2)}_{1,2}x_4 + \lambda^{(1)}_{1,4}x_{11} - \left(\lambda_{4,1} + \lambda_{4,5} + \lambda_{4,9} + k_{2,1} + k^{(1)}_{2,3} + k^{(1)}_{2,4}\right)x_{14} + \lambda_{5,4}x_{15} + \lambda_{9,4}x_{19} + k^{(1)}_{4,2}x_{34} + k^{(3)}_{3,2}x_{24}$	E144

$$\dot{x}_{15} = k_{1,2}^{(1)} x_5 + \lambda_{2,5}^{(1)} x_{12} + \lambda_{4,5} x_{14} - \left(\lambda_{5,2} + \lambda_{5,4} + \lambda_{5,10} + k_{2,1} + k_{2,3}^{(1)} + k_{2,4}^{(1)}\right) x_{15} + \lambda_{10,5} x_{20} + k_{4,2}^{(1)} x_{35} + k_{3,2}^{(3)} x_{25} \quad \text{E145}$$

$$\dot{x}_{16} = k_{1,2}^{(1)} x_6 + \lambda_{1,6} x_{11} - \left(\lambda_{6,1} + \lambda_{6,7} + \lambda_{6,9}^{(1)} + k_{2,1} + k_{2,3}^{(1)} + k_{2,4}^{(1)}\right) x_{16} + \lambda_{7,6} x_{17} + \lambda_{9,6} x_{19} + k_{4,2}^{(1)} x_{36} + k_{3,2}^{(3)} x_{26} \quad \text{E146}$$

$$\dot{x}_{17} = k_{1,2}^{(1)} x_7 + \lambda_{2,7} x_{12} + \lambda_{6,7} x_{16} - \left(\lambda_{7,2} + \lambda_{7,6} + \lambda_{7,8} + \lambda_{7,10}^{(1)} + k_{2,1} + k_{2,3}^{(1)} + k_{2,4}^{(1)}\right) x_{17} + \lambda_{8,7} x_{18} + \lambda_{10,7} x_{20} + k_{4,2}^{(1)} x_{37} + k_{3,2}^{(3)} x_{27} \quad \text{E147}$$

$$\dot{x}_{18} = k_{1,2}^{(1)} x_8 + \lambda_{3,8} x_{13} + \lambda_{7,8} x_{17} - \left(\lambda_{8,3} + \lambda_{8,7} + k_{2,1} + k_{2,3}^{(1)} + k_{2,4}^{(1)}\right) x_{18} + k_{4,2}^{(1)} x_{38} + k_{3,2}^{(3)} x_{28} \quad \text{E148}$$

$$\dot{x}_{19} = k_{1,2}^{(1)} x_9 + \lambda_{4,9} x_{14} + \lambda_{6,9}^{(1)} x_{16} - \left(\lambda_{9,4} + \lambda_{9,6} + \lambda_{9,10} + k_{2,1} + k_{2,3}^{(1)} + k_{2,4}^{(1)}\right) x_{19} + \lambda_{10,9} x_{20} + k_{4,2}^{(1)} x_{39} + k_{3,2}^{(3)} x_{29} \quad \text{E149}$$

$$\dot{x}_{20} = k_{1,2}^{(1)} x_{10} + \lambda_{5,10} x_{15} + \lambda_{7,10}^{(1)} x_{17} + \lambda_{9,10} x_{19} - \left(\lambda_{10,5} + \lambda_{10,7} + \lambda_{10,9} + k_{2,1} + k_{2,3}^{(1)} + k_{2,4}^{(1)}\right) x_{20} + k_{4,2}^{(1)} x_{40} + k_{3,2}^{(3)} x_{30} \quad \text{E150}$$

$$\dot{x}_{21} = k_{2,3}^{(1)} x_{11} - \left(\lambda_{1,2} + \lambda_{1,4}^{(3)} + \lambda_{1,6} + k_{3,2}^{(3)} + k_{3,4}^{(3)}\right) x_{21} + \lambda_{2,1} x_{22} + \lambda_{4,1} x_{24} + \lambda_{6,1} x_{26} + k_{4,3}^{(1)} x_{31} \quad \text{E151}$$

$$\dot{x}_{22} = k_{2,3}^{(1)} x_{12} + \lambda_{1,2} x_{21} - \left(\lambda_{2,1} + \lambda_{2,3} + \lambda_{2,5}^{(3)} + \lambda_{2,7} + k_{3,2}^{(3)} + k_{3,4}^{(3)}\right) x_{22} + \lambda_{3,2} x_{23} + \lambda_{5,2} x_{25} + \lambda_{7,2} x_{27} + k_{4,3}^{(1)} x_{32} \quad \text{E152}$$

$$\dot{x}_{23} = k_{2,3}^{(2)} x_{13} + \lambda_{2,3} x_{22} - \left(\lambda_{3,2} + \lambda_{3,8} + k_{3,2}^{(4)} + k_{3,4}^{(4)}\right) x_{23} + \lambda_{8,3} x_{28} + k_{4,3}^{(2)} x_{33} \quad \text{E153}$$

$$\dot{x}_{24} = k_{2,3}^{(1)} x_{14} + \lambda_{1,4}^{(3)} x_{21} - \left(\lambda_{4,1} + \lambda_{4,5} + \lambda_{4,9} + k_{3,2}^{(3)} + k_{3,4}^{(3)}\right) x_{24} + \lambda_{5,4} x_{25} + \lambda_{9,4} x_{29} + k_{4,3}^{(1)} x_{34} \quad \text{E154}$$

$$\dot{x}_{25} = k_{2,3}^{(1)} x_{15} + \lambda_{2,5}^{(3)} x_{22} + \lambda_{4,5} x_{24} - \left(\lambda_{5,2} + \lambda_{5,4} + \lambda_{5,10} + k_{3,2}^{(3)} + k_{3,4}^{(3)}\right) x_{25} + \lambda_{10,5} x_{30} + k_{4,3}^{(1)} x_{35} \quad \text{E155}$$

$\dot{x}_{26} = k_{2,3}^{(1)} x_{16} + \lambda_{1,6} x_{21} - \left(\lambda_{6,1} + \lambda_{6,7} + \lambda_{6,9}^{(3)} + k_{3,2}^{(3)} + k_{3,4}^{(3)}\right) x_{26} + \lambda_{7,6} x_{27} + \lambda_{9,6} x_{29} + k_{4,3}^{(1)} x_{36}$	E156
$\dot{x}_{27} = k_{2,3}^{(1)} x_{17} + \lambda_{2,7} x_{22} + \lambda_{6,7} x_{26} - \left(\lambda_{7,2} + \lambda_{7,6} + \lambda_{7,8} + \lambda_{7,10}^{(3)} + k_{3,2}^{(3)} + k_{3,4}^{(3)}\right) x_{27} + \lambda_{8,7} x_{28} + \lambda_{10,7} x_{30} + k_{4,3}^{(1)} x_{37}$	E157
$\dot{x}_{28} = k_{2,3}^{(1)} x_{18} + \lambda_{3,8} x_{23} + \lambda_{7,8} x_{27} - \left(\lambda_{8,3} + \lambda_{8,7} + k_{3,2}^{(3)} + k_{3,4}^{(3)}\right) x_{28} + k_{4,3}^{(1)} x_{38}$	E158
$\dot{x}_{29} = k_{2,3}^{(1)} x_{19} + \lambda_{4,9} x_{24} + \lambda_{6,9}^{(1)} x_{26} - \left(\lambda_{9,4} + \lambda_{9,6} + \lambda_{9,10} + k_{3,2}^{(3)} + k_{3,4}^{(3)}\right) x_{29} + \lambda_{10,9} x_{30} + k_{4,3}^{(1)} x_{39}$	E159
$\dot{x}_{30} = k_{2,3}^{(1)} x_{20} + \lambda_{5,10} x_{25} + \lambda_{7,10}^{(3)} x_{27} + \lambda_{9,10} x_{29} - \left(\lambda_{10,5} + \lambda_{10,7} + \lambda_{10,9} + k_{3,2}^{(3)} + k_{3,4}^{(3)}\right) x_{30} + k_{4,3}^{(1)} x_{40}$	E160
$\dot{x}_{31} = k_{2,4}^{(1)} x_{11} + k_{3,4}^{(3)} x_{21} - \left(\lambda_{1,2} + \lambda_{1,4}^{(1)} + \lambda_{1,6} + k_{4,2}^{(1)} + k_{4,3}^{(1)}\right) x_{31} + \lambda_{2,1} x_{32} + \lambda_{4,1} x_{34} + \lambda_{6,1} x_{36}$	E161
$\dot{x}_{32} = k_{2,4}^{(1)} x_{12} + k_{3,4}^{(3)} x_{22} + \lambda_{1,2} x_{31} - \left(\lambda_{2,1} + \lambda_{2,3} + \lambda_{2,5}^{(1)} + \lambda_{2,7} + k_{4,2}^{(1)} + k_{4,3}^{(1)}\right) x_{32} + \lambda_{3,2} x_{33} + \lambda_{5,2} x_{35} + \lambda_{7,2} x_{37}$	E162
$\dot{x}_{33} = k_{2,4}^{(2)} x_{13} + k_{3,4}^{(3)} x_{23} + \lambda_{2,3} x_{32} - \left(\lambda_{3,2} + \lambda_{3,8} + k_{4,2}^{(2)} + k_{4,3}^{(2)}\right) x_{33} + \lambda_{8,3} x_{38}$	E163
$\dot{x}_{34} = k_{2,4}^{(1)} x_{14} + k_{3,4}^{(3)} x_{24} + \lambda_{1,4}^{(1)} x_{31} - \left(\lambda_{4,1} + \lambda_{4,5} + \lambda_{4,9} + k_{4,2}^{(1)} + k_{4,3}^{(1)}\right) x_{34} + \lambda_{5,4} x_{35} + \lambda_{9,4} x_{39}$	E164
$\dot{x}_{35} = k_{2,4}^{(1)} x_{15} + k_{3,4}^{(3)} x_{25} + \lambda_{2,5}^{(1)} x_{32} + \lambda_{4,5} x_{34} - \left(\lambda_{5,2} + \lambda_{5,4} + \lambda_{5,10} + k_{4,2}^{(1)} + k_{4,3}^{(1)}\right) x_{35} + \lambda_{10,5} x_{40}$	E165
$\dot{x}_{36} = k_{2,4}^{(1)} x_{16} + k_{3,4}^{(3)} x_{26} + \lambda_{1,6} x_{31} - \left(\lambda_{6,1} + \lambda_{6,7} + \lambda_{6,9}^{(1)} + k_{4,2}^{(1)} + k_{4,3}^{(1)}\right) x_{36} + \lambda_{7,6} x_{37} + \lambda_{9,6} x_{39}$	E166
$\dot{x}_{37} = k_{2,4}^{(1)} x_{17} + k_{3,4}^{(3)} x_{27} + \lambda_{2,7} x_{32} + \lambda_{6,7} x_{36} - \left(\lambda_{7,2} + \lambda_{7,6} + \lambda_{7,8} + \lambda_{7,10}^{(1)} + k_{4,2}^{(1)} + k_{4,3}^{(1)}\right) x_{38} + \lambda_{10,7} x_{40}$	E167
$\dot{x}_{38} = k_{2,4}^{(1)} x_{18} + k_{3,4}^{(3)} x_{28} + \lambda_{3,8} x_{33} + \lambda_{7,8} x_{37} - \left(\lambda_{8,3} + \lambda_{8,7} + k_{4,2}^{(1)} + k_{4,3}^{(1)}\right) x_{38}$	E168
$\dot{x}_{39} = k_{2,4}^{(1)} x_{19} + k_{3,4}^{(3)} x_{29} + \lambda_{4,9} x_{34} + \lambda_{6,9}^{(1)} x_{36} - \left(\lambda_{9,4} + \lambda_{9,6} + \lambda_{9,10} + k_{4,2}^{(1)} + k_{4,3}^{(1)}\right) x_{39} + \lambda_{10,9} x_{40}$	E169

$$\dot{x}_{40} = k_{2,4}^{(1)} x_{20} + k_{3,4}^{(3)} x_{30} + \lambda_{5,10} x_{35} + \lambda_{7,10}^{(3)} x_{37} + \lambda_{9,10} x_{39} - \left(\lambda_{10,5} + \lambda_{10,7} + \lambda_{10,9} + k_{4,2}^{(1)} + k_{4,3}^{(1)}\right) x_{40} \quad \text{E170}$$

$$p_{(1)} = x_1 + x_2 + x_4 + x_5 + x_6 + x_7 + x_8 + x_9 + x_{10} + x_{11} + x_{12} + x_{14} + x_{15} + x_{16} + x_{17} + x_{18} + x_{19} + x_{20} + x_{31} + x_{32} + x_{33} + x_{34} + x_{35} + x_{36} + x_{37} + x_{38} + x_{39} + x_{40} \quad \text{E171}$$

$$P_{(2)} = x_3 + x_{13} + x_{33} \quad \text{E172}$$

$$P_{(3)} = x_{21} + x_{22} + x_{24} + x_{25} + x_{26} + x_{27} + x_{28} + x_{29} + x_{30} \quad \text{E173}$$

$$P_{(4)} = x_{23} \quad \text{E174}$$

The notation $\lambda_{i,j}$ is used to denote the transition rate from state i to state j for the LCC. The notation k_{ij} is used to denote the transition rate from state i to state j for the RyR. x_i denotes i^{th} state, $\dot{x}_i$ denotes the time derivative of the i^{th} state. $P_{(n)}$ denotes the probability that a CaRU is in the n^{th} (n=1,2,3,4) open-closed configuration. * The equations are modified to provide better fit of I_{CaL} to experimental data [3]. LCC: L-type Ca^{2+} channel, RyR: ryanodine receptor, CaRU: Ca^{2+} release unit.

Whole-cell Ca^{2+} flux through the LCCs (J_{LCC})

$$J_{LCC} = N_{CaRU} J_L \; V_m \frac{(p_{(2)}([Ca^{2+}]_{dm}^{(2)} e^{\;V_m} \quad 0.341[Ca^{2+}]_0) + p_{(4)}([Ca^{2+}]_{dm}^{(4)} e^{\;V_m} \quad 0.341[Ca^{2+}]_0))}{1 \quad e^{\;V_m}} \quad \text{E175}$$

Whole-cell Ca^{2+} release through the RyRs (J_{rel})

$$J_{rel} = N_{CaRU} r_{RyR} (p_{(3)}([Ca^{2+}]_{JSR} \quad [Ca^{2+}]_{dm}^{(3)}) + p_{(4)}([Ca^{2+}]_{JSR} \quad [Ca^{2+}]_{dm}^{(4)})) \quad \text{E176}$$

The Ca^{2+} flux diffused from the dyadic microdomain (dm) to the cytoplasm (J_{xfer})

$$J_{xfer} = N_{CaRU} r_{xfer} \sum_{i=1}^{4} p_{(i)}([Ca^{2+}]_{dm}^{(i)} - [Ca^{2+}]_i) \quad \text{E177}$$

Table S3. Sarcoplasmic Reticulum (SR) Ca^{2+} dynamics

SR Ca^{2+} model equations

$_{JSR} = 1 + \frac{K_m^{CSQN}[CSQN]_{tot}}{\left(K_m^{CSQN} + [Ca^{2+}]_{JSR}\right)^2}^{1}$	E178
$_{NSR} = 1 + \frac{K_m^{CSQN}[CSQN]_{tot}}{\left(K_m^{CSQN} + [Ca^{2+}]_{NSR}\right)^2}^{1}$	E179
$_{i} = 1 + \frac{K_m^{CMDN}[CMDN]_{tot}}{\left(K_m^{CMDN} + [Ca^{2+}]_{i}\right)^2}^{1}$	E180
$J_{trpn} = \frac{d[HTRPNCa]}{dt} + \frac{d[LTRPNCa]}{dt}$	E181
$J_{tr} = \frac{[Ca^{2+}]_{NSR} \quad [Ca^{2+}]_{JSR}}{tr}$	E182
$J_{up} = \frac{V_{max\,f} \; f_b - V_{max\,r} \; r_b}{1 + f_b + r_b} \; f_{ATP}^{SERCA}$	E183
$f_b = \frac{[Ca^{2+}]_i}{K_{fb}}^{Nfb}$	E184
$r_b = \frac{[Ca^{2+}]_{SR}}{K_{rb}}^{Nrb}$	E185
$f_{ATP}^{SERCA} = \frac{K_{m,up}^{ATP}}{[ATP]_i} \cdot \left(1 + \frac{[ADP]_i}{K_{i,up}} + 1 + \frac{[ADP]_i}{K'_{i,up}}\right)^{1}$	E186
$\frac{d[LTRPNCa]}{dt} = k_{ltrpn}^{+}[Ca^{2+}]_i\left([LTRPN]_{tot} \quad [LTRPNCa]\right)$ $k_{ltrpn} \; 1 \; \frac{2}{3} Force_{Norm} \; [LTRPNCa]$	E187

$$\frac{d[HTRPNCa]}{dt} = k^{+}_{htrpn}\,[Ca^{2+}]_i\,([HTRPN]_{tot} \quad [HTRPNCa]) \quad k_{htrpn}\,[HTRPNCa]$$ E188

$$\frac{d[Ca^{2+}]_i}{dt} = {}_i\left(J_{xfer} - J_{up} - J_{trpn} - \left(I_{Ca,b} - 2\,I_{NaCa} + I_{pCa}\right)\frac{A_{cap}}{2V_{myo}F} + \left(V_{NaCa} - V_{uni}\right)\frac{V_{mito}}{V_{myo}}\right)$$ E189

$$\frac{d[Ca^{2+}]_{NSR}}{dt} = {}_{NSR}\left(\frac{V_{myo}}{V_{NSR}}J_{up} \quad J_{tr}\right)$$ E190

$$\frac{d[Ca^{2+}]_{JSR}}{dt} = {}_{JSR}\left(\frac{V_{NSR}}{V_{JSR}}J_{tr} \quad \frac{V_{SS}}{V_{JSR}}J_{rel}\right)$$ E191

SR Ca^{2+} model parameters

Symbol	Value	Units	Description	Ref.
V_{NSR}	1.4	pL	NSR volume	4
V_{JSR}	0.16	pL	JSR volume	4
K_m^{CSQN}	0.8	mM	Ca^{2+} half saturation constant for calsequestrin	4
K_m^{CMDN}	2.38×10^{-3}	mM	Ca^{2+} half saturation constant for calmodulin	4
k^{+}_{htrpn}	20	mM^{-1} ms^{-1}	Ca^{2+} on-rate for troponin high affinity sites	5
k_{htrpn}	3.3×10^{-4}	ms^{-1}	Ca^{2+} off-rate for troponin high affinity sites	4
k^{+}_{ltrpn}	40	mM^{-1} ms^{-1}	Ca^{2+} on-rate for troponin low affinity sites	5
k_{ltrpn}	$4x10^{-2}$	ms^{-1}	Ca^{2+} off-rate for troponin low affinity sites	4
$[HTRPN]_{tot}$	0.14	mM	Total troponin high-affinity sites	4
$[LTRPN]_{tot}$	0.07	mM	Total troponin low-affinity sites	4
$[CMDN]_{tot}$	5.0×10^{-2}	mM	Total myoplasmic calmoduling concentration	4
$[CSQN]_{tot}$	5	mM	Total SR calsequestrin concentration	*
$_{tr}$	0.5747	ms	Time constant for transfer from NSR to JSR	4

J_{RyR_max}	16.6	ms^{-1}	RyR flux channel constant	*
N_{CaRU}	300000		Number of Ca2+ release units	*
$V_{max,f}$	2.989×10^{-4}	ms^{-1}	SERCA forward rate parameter	[4]
$V_{max,r}$	3.979×10^{-4}	ms^{-1}	SERCA reverse rate parameter	[4]
K_{fb}	1.5×10^{-4}	mM	Forward Ca^{2+} half saturation constant of SERCA	**
K_{rb}	3.3	mM	Reverse Ca^{2+} half saturation constant of SERCA	**
N_{fb}	0.5		Forward cooperativity constant of SERCA	**
N_{rb}	0.5		Reverse cooperativity constant of SERCA	**
$K_{m,up}^{ATP}$	0.01	mM	ATP half saturation constant for SERCA	[4]
$K_{i,up}$	0.1	mM	ADP first inhibition constant for SERCA	[4]
$K_{i,up}^{'}$	1	mM	ADP second inhibition constant for SERCA	[4]

* These parameters were adjusted to achieve a ~37% of SR Ca^{2+} depletion during a normal AP cycle.

**These parameters were adjusted to maintain $[Ca^{2+}]_{NSR}$ at 0.45mM [6-8] while avoiding net reverse SERCA flux.

Effect of ROS on RyR open probability and SR Ca^{2+} release

$$J_{rel\_ROS} = N_{CaRU} r_{RyR} (p_{(3)\_ROS}([Ca^{2+}]_{SR} - [Ca^{2+}]_{dm}^{(3)}) + p_{(4)\_ROS}([Ca^{2+}]_{SR} - [Ca^{2+}]_{dm}^{(4)}))$$
$$= N_{CaRU} r_{RyR} \frac{P_{O\_ryr\_ROS}}{P_{O\_ryr}} \left(p_{(3)} \left([Ca^{2+}]_{SR} - [Ca^{2+}]_{dm}^{(3)} \right) + p_{(4)} \left([Ca^{2+}]_{SR} - [Ca^{2+}]_{dm}^{(4)} \right) \right) \quad \text{E192}$$

where $\frac{P_{Oryr\_ROS}}{P_{Oryr}}$ is the ROS-dependent scaling factor of RyR opening probability.

Table S4. CaMKII Activation Module

Transition rate expression (ms^{-1})

$$ItoB = k_{asso} \times [CaMCa4] \quad \text{E193}$$

$AtoP = k_{asso} \times [CaMCa4]$	E194
$OxAtoOxP = k_{asso} \times [CaMCa4]$	E195
$BtoI = k_{disso} \times (1 - \frac{K_{m,CaM}^3}{[[Ca^{2+}]_i^3 + K_{m,CaM}^3}) + k_{dissoCa} \times \frac{K_{m,CaM}^3}{[Ca^{2+}]_i^3 + K_{m,CaM}^3})$	E196
$PtoA = k_{disso2} \times (1 - \frac{K_{m,CaM}^3}{[Ca^{2+}]_i^3 + K_{m,CaM}^3}) + k_{dissoCa2} \times \frac{K_{m,CaM}^3}{[Ca^{2+}]_i^3 + K_{m,CaM}^3})$	E197
$OxPtoOxA = k_{disso2} \times (1 - \frac{K_{m,CaM}^3}{[Ca^{2+}]_i^3 + K_{m,CaM}^3}) + k_{dissoCa2} \times \frac{K_{m,CaM}^3}{[Ca^{2+}]_i^3 + K_{m,CaM}^3})$	E198
$BtoP = k_{cat} \times [1 - (\frac{[I]}{[CaMKII_{total}]})^2] \times \frac{[ATP]}{[ATP] + K_{m,ATP}}$	E199
$OxBtoOxP = k_{cat} \times [1 - (\frac{[I]}{[CaMKII_{total}]})^2] \times \frac{[ATP]}{[ATP] + K_{m,ATP}}$	E200
$PtoB = k_{cat,PP1} \times \frac{1}{[P] + K_{m,PP1}} \times [PP1]$	E201
$OxPtoOxB = k_{cat,PP1} \times \frac{1}{[OxP] + K_{m,PP1}} \times [PP1]$	E202
$BtoOxB = k_{ox} \times [ROS]_i$	E203
$BtoOxP = k_{ox} \times [ROS]_i$	E204
$AtoOxA = k_{ox} \times [ROS]_i$	E205

CaMKII Activation Balance Equations

$\frac{d[CaMCa]}{dt} = k_1 \times [Ca^{2+}]_i \times [CaM] + k_{-2} \times [CaMCa2] - k_{-1} \times [CaMCa] - k_2 \times [Ca^{2+}]_i \times [CaMCa]$	E206
$\frac{d[CaMCa2[}{dt} = k_2 \times [Ca^{2+}]_i \times [CaCaM] + k_{-3} \times [CaMCa3] - k_{-2} \times [CaMCa2] - k_3 \times [Ca^{2+}]_i \times [CaMCa2]$	E207
$\frac{d[CaMCa3]}{dt} = k_3 \times [Ca^{2+}]_i \times [CaCaM2] + k_{-4} \times [CaMCa4] - k_{-3} \times [CaMCa3] - k_4 \times [Ca^{2+}]_i \times [CaMCa3]$	E208
$\frac{d[CaMCa4]}{dt} = k_4 \times [Ca^{2+}]_i \times [CaCaM3] - k_{-4} \times [CaMCa4]$	E209
$\frac{d[B]}{dt} = ItoB \times [I] + PtoB \times [P] + OxBtoB \times [OxB] - (BtoI + BtoP + BtoOxB) \times [B]$	E210
$\frac{d[P]}{dt} = BtoP \times [B] + AtoP \times [A] + OxPtoP \times [OxP] - (PtoB + PtoA + PtoOxP) \times [P]$	E211
$\frac{d[A]}{dt} = PtoA \times [P] + OxAtoA \times [OxA] - (AtoI + AtoP + AtoOxA) \times [A]$	E212
$\frac{d[OxB]}{dt} = BtoOxB \times [B] + OxPtoOxB \times [OxP] - (OxBtoB + OxBtoOxP) \times [OxB]$	E213
$\frac{d[OxA]}{dt} = AtoOxA \times [A] + OxPtoOxA \times [OxP] - (OxAtoA + OxAtoOxP) \times [OxA]$	E214
$\frac{d[OxP]}{dt} = OxBtoOxP \times [OxB] + PtoOxP \times [P] + OxAtoOxP \times [OxA] - (OxPtoOxB + OxPtoP + OxPtoOxA) \times [OxP]$	E215
$[CaM] = [CaM_{total}] - [CaMCa] - [CaMCa2] - [CaMCa3] - [CaMCa4]$	E216
$[CaMKII_{active}] = [CaMKII_{total}] - [B] - [P] - [A] - [OxA] - [OxP] - [OxB]$	E217

$$CaMKII_{active} = \frac{[CaMKII_{active}]}{[CaMKII_{total}]} \times 100\% \quad \text{E218}$$

where $CaMKII_{active}$ represents the percentage of activated CaMKII.

Table S5. Ionic concentrations balance equations

$\frac{d[Ca^{2+}]_m}{dt} = \left(V_{uni} - V_{NaCa}\right)$	E219
$\frac{d[Na^+]_i}{dt} = \circ\ (I_{Na} + I_{Na;L} + I_{Na;b} + I_{ns;Na} + 3I_{NaCa} + 3I_{NaK})\frac{A_{cap}}{V_{myo}F}$	E220
$\frac{d[K^+]_i}{dt} = -\left(I_K + I_{K_1} + I_{Kp} + I_{ns,K} + I_{Ca,K} - 2\,I_{NaK}\right)\frac{A_{cap}}{V_{myo}F}$	E221

Table S6. Force generation model [5]

$\frac{d[P_o]}{dt} = \left(k_{pn}^{trop} + f_{01}\right)[P_o] + k_{np}^{trop}[N_0] + g_{01}(SL)[P_1]$	E222
$\frac{d[P_2]}{dt} = \left(f_{23} + g_{12}(SL)\right)[P_2] + f_{12}[P_1] + g_{23}(SL)[P_3]$	E224
$\frac{d[P_3]}{dt} = g_{23}(SL)[P_3] + f_{23}[P_2]$	E225
$\frac{d[N_1]}{dt} = k_{pn}^{trop}[P_1] + \left(k_{np}^{trop} + g_{01}^{'}(SL)\right)[N_1]$	E226
$\frac{d[N_0]}{dt} = \frac{d[N_1]}{dt} + \frac{d[P_0]}{dt} + \frac{d[P_1]}{dt} + \frac{d[P_2]}{dt} + \frac{d[P_3]}{dt}$	E227

$$f_{01} = 3 \cdot f_{XB}$$ E228

$$f_{12} = 10 \cdot f_{XB}$$ E229

$$f_{23} = 7 \cdot f_{XB}$$ E230

$$g_{01} = 1 \cdot g_{XB}^{min}$$ E231

$$g_{12} = 2 \cdot g_{XB}^{min}$$ E232

$$g_{23} = 3 \cdot g_{XB}^{min}$$ E233

$$g_{01}(SL) = 1 \cdot \quad \cdot g_{XB}^{min}$$ E234

$$g_{12}(SL) = 2 \cdot \quad \cdot g_{XB}^{min}$$ E235

$$g_{23}(SL) = 3 \cdot \quad \cdot g_{XB}^{min}$$ E236

$$= 1 + \frac{2.3 - SL}{(2.3 - 1.7)^{1.6}}$$ E237

$$k_{np}^{trop} = k_{pn}^{trop} \left(\frac{[LTRPNCa]}{K_{1/2}^{trop} [LTRPN]_{tot}} \right)^{N^{trop}}$$ E238

$$K_{1/2}^{trop} = 1 + \frac{K_{Ca}^{trop}}{1.7 \cdot 10^{-3} - 0.8 \cdot 10^{-3} \frac{(SL - 1.7)}{0.6}}$$ E239

$$N^{trop} = 3.5 \cdot SL - 2.0$$ E240

$$K_{Ca}^{trop} = \frac{k_{ltrpn}}{k_{ltrpn}^{+}}$$ E241

$$PATHS = g_{01}\, g_{12}\, g_{23} + f_{01}\, g_{12}\, g_{23} + f_{01}\, f_{12}\, g_{23} + f_{01}\, f_{12}\, f_{23}$$ E242

$$Pl_{max} = \frac{f_{01}\, g_{12}\, g_{23}}{PATHS}$$ E243

$$P2_{max} = \frac{f_{01}\, f_{12}\, g_{23}}{PATHS} \qquad \text{E244}$$

$$P3_{max} = \frac{f_{01}\, f_{12}\, f_{23}}{PATHS} \qquad \text{E245}$$

$$Force = \frac{P_1 + N_1 + 2\,P_2 + 3\,P_3}{P1_{max} + 2\,P2_{max} + 3\,P3_{max}} \qquad \text{E246}$$

$$Force_{Norm} = \frac{P_1 + N_1 + P_2 + P_3}{P1_{max} + P2_{max} + P3_{max}} \qquad \text{E247}$$

$$V_{AM} = V_{AM}^{max} \frac{f_{01}\,[P_0] + f_{12}\,[P_1] + f_{23}\,[P_2]}{f_{01} + f_{12} + f_{23}} \cdot \left(1 + \frac{K_{M,AM}^{ATP}}{[ATP]_i}\right)^{1} \left(1 + \frac{[ADP]_i}{K_{i,AM}}\right) \qquad \text{E248}$$

Table S7. Mitochondrial membrane potential ($\Delta\Psi_m$)

$$\frac{d\ \ _m}{dt} = \frac{V_{He} + V_{He(F)} - V_{Hu} - V_{ANT} - V_{HLeak} - V_{NaCa} - 2\,V_{uni}\quad V_{IMAC}}{C_{mito}} \qquad \text{E249}$$

Table S8. Energy metabolism system

Mitochondrial metabolites balance equations

$$\frac{d\,[ATP]_i}{dt} = V_{ANT}\frac{V_{mito}}{V_{myo}} - V_{CK}^{mito} - V_{AM} - \frac{1}{2}J_{up} - \left(I_{pCa} + I_{NaK}\right)\frac{A_{cap}}{V_{myo}F} \qquad \text{E250}$$

$$\frac{d\,[ATP]_{ic}}{dt} = -V_{CK}^{cyto} - V_{ATPase}^{cyto} \qquad \text{E251}$$

$$\frac{d\,[CrP]_i}{dt} = V_{CK}^{mito} - V_{tr}^{CrP} \qquad \text{E252}$$

$$\frac{d\,[CrP]_{ic}}{dt} = V_{tr}^{CrP} + V_{CK}^{cyto} \qquad \text{E253}$$

$$\frac{d\,[ADP]_m}{dt} = V_{ANT} - V_{ATPase} - V_{SL} \qquad \text{E254}$$

$$[ATP]_m = C_A - [ADP]_m \qquad \text{E255}$$

$$\frac{d[NADH]}{dt} = - V_{O2} + V_{IDH} + V_{KGDH} + V_{MDH} \qquad \text{E256}$$

$$\frac{d[ISOC]}{dt} = V_{ACO} - V_{IDH} \qquad \text{E257}$$

$$\frac{d[\ \ KG]}{dt} = V_{IDH} - V_{KGDH} + V_{AAT} \qquad \text{E258}$$

$$\frac{d[SCoA]}{dt} = V_{KGDH} - V_{SL} \qquad \text{E259}$$

$$\frac{d[Suc]}{dt} = V_{SL} - V_{SDH} \qquad \text{E260}$$

$$\frac{d[FUM]}{dt} = V_{SDH} - V_{FH} \qquad \text{E261}$$

$$\frac{d[MAL]}{dt} = V_{FH} - V_{MDH} \qquad \text{E262}$$

$$\frac{d[OAA]}{dt} = V_{MDH} - V_{CS} \quad V_{AAT} \qquad \text{E263}$$

$$[CIT] = C_{Kint} - [ISOC] + [\ \ KG] + [SCoA] + [Suc] + [FUM] + [MAL] + [OAA] \qquad \text{E264}$$

Cytosolic metabolic reaction rate

$$V_{ANT} = V_{maxANT} \frac{0.75\left(1 - \frac{0.25[ATP]_i \cdot 0.45[ADP]_m}{0.17[ADP]_i \cdot 0.025[ATP]_m} e^{\frac{F}{RT}\Delta\psi_m}\right)}{1 + \frac{0.25[ATP]_i}{0.225[ADP]_i} e^{\frac{-h^{ANT} F}{RT}\Delta\psi_m}\left(1 + \frac{0.45[ADP]_m}{0.025[ATP]_m}\right)}$$ E265

$$V_{CK}^{cyto} = k_{CK}^{cyto}\left([ATP]_{ic}[Cr]_{ic} - \frac{[ADP]_{ic}[CrP]_{ic}}{K_{EQ}}\right)$$ E266

$$V_{CK}^{mito} = k_{CK}^{mito}\left([ATP]_{i}[Cr]_{i} - \frac{[ADP]_{i}[CrP]_{i}}{K_{EQ}}\right)$$ E267

$$V_{tr}^{CrP} = k_{tr}^{Cr}\left([CrP]_i - [CrP]_{ic}\right)$$ E268

Tricarboxylic acid cycle reaction rate

$$V_{CS} = k_{cat}^{CS} E_T^{CS}\left(1 + \frac{K_M^{AcCoA}}{[AcCoA]} + \frac{K_M^{OAA}}{[OAA]} + \frac{K_M^{AcCoA}}{[AcCoA]}\frac{K_M^{OAA}}{[OAA]}\right)^{-1}$$ E269

$$V_{ACO} = k_f^{ACO}\left([CIT] - \frac{[ISOC]}{K_E^{ACO}}\right)$$ E270

$$f_a^{IDH} = \left(1 + \frac{[ADP]_m}{K_{ADP}^a}\right)^{-1}\left(1 + \frac{[Ca^{2+}]_m}{K_{Ca}^a}\right)^{-1}$$ E271

$$f_i^{IDH} = 1 + \frac{[NADH]}{K_{i,NADH}}$$ E272

$$V_{IDH} = k_{cat}^{IDH} E_T^{IDH}\left(1 + \frac{[H^+]}{k_{h,1}} + \frac{k_{h,2}}{[H^+]} + f_i^{IDH}\frac{K_M^{NAD}}{[NAD]} + f_a^{IDH}\left(\frac{K_M^{ISOC}}{[ISOC]}\right)^{ni} + f_a^{IDH} f_i^{IDH}\left(\frac{K_M^{ISOC}}{[ISOC]}\right)^{ni}\frac{K_M^{NAD}}{[NAD]}\right)^{-1}$$ E273

$$f_a^{KGDH} = \left(1 + \frac{[Mg^{2+}]}{K_D^{Mg^{2+}}}\right)^{-1} \left(1 + \frac{[Ca^{2+}]_m}{K_D^{Ca^{2+}}}\right)^{-1} \quad \text{E274}$$

$$V_{KGDH} = \frac{k_{cat}^{KGDH} E_T^{KGDH}}{\left(1 + f_a^{KGDH} \frac{K_M^{KG}}{[KG]} + f_a^{KGDH} \frac{K_M^{NAD}}{[NAD]}\right)^{n_{aKG}}} \quad \text{E275}$$

$$V_{SL} = k_f^{SL} [SCoA][ADP]_m - \frac{[Suc][ATP]_m[CoA]}{K_E^{SL}} \quad \text{E276}$$

$$V_{SDH} = \frac{k_{cat}^{SDH} E_T^{SDH}}{\left(1 + \frac{K_M^{Suc}}{[Suc]}\right)\left(1 + \frac{[OAA]}{K_{i,sdh}^{OAA}}\right)\left(1 + \frac{[FUM]}{K_i^{FUM}}\right)} \quad \text{E277}$$

$$V_{FH} = k_f^{FH} [FUM] - \frac{[MAL]}{K_E^{FH}} \quad \text{E278}$$

$$f_{h,a} = \left(1 + \frac{[H^+]}{k_{h1}} + \frac{[H^+]^2}{k_{h1} k_{h2}}\right)^{-1} + k_{offset} \quad \text{E279}$$

$$f_{h,i} = \left(1 + \frac{k_{h3}}{[H^+]} + \frac{k_{h3} k_{h4}}{[H^+]^2}\right)^{-2} \quad \text{E280}$$

$$V_{MDH} = \frac{k_{cat}^{MDH} E_T^{MDH} f_{h,a} f_{h,i}}{\left(1 + \frac{K_M^{MAL}}{[MAL]}\right)\left(1 + \frac{[OAA]}{K_i^{OAA}}\right) + \frac{K_M^{NAD}}{[NAD]} + \frac{K_M^{MAL}}{[MAL]}\left(1 + \frac{[OAA]}{K_i^{OAA}}\right)\frac{K_M^{NAD}}{[NAD]}} \quad \text{E281}$$

$$V_{AAT} = k_f^{AAT}[OAA][GLU] \frac{k_{ASP} K_E^{AAT}}{\left(k_{ASP} K_E^{AAT} + [KG] k_f^{AAT}\right)} \quad \text{E282}$$

Oxidative phosphorylation reaction rates

$$V_{O_2} = 0.5^{res} \frac{r_a + r_{c1} e^{\frac{6F\Delta\psi_B}{RT}} e^{\frac{A_{res}F}{RT}} - r_a e^{\frac{g6F\Delta\psi_H}{RT}} + r_{c2} e^{\frac{A_{res}F}{RT}} e^{\frac{g6F\Delta\psi_H}{RT}}}{1 + r_1 e^{\frac{FA_{res}}{RT}} e^{\frac{6F\Delta\psi_B}{RT}} + r_2 + r_3 e^{\frac{FA_{res}}{RT}} e^{\frac{g6F\Delta\psi_H}{RT}}} \quad \text{E283}$$

$$V_{He} = 6^{\text{res}} \frac{r_a\, e^{\frac{A_{res}\,F}{R\,T}} \quad (r_a + r_b)\, e^{\frac{g\,6F_{H}}{R\,T}}}{1 + r_1\, e^{\frac{F\,A_{res}}{R\,T}} \quad e^{\frac{6\,F_{B}}{R\,T}} \quad + \quad r_2 + r_3\, e^{\frac{F\,A_{res}}{R\,T}} \quad e^{\frac{g\,6\,F_{H}}{R\,T}}} \qquad \text{E284}$$

$$A_{res} = \frac{R\,T}{F} \ln \quad K_{res} \sqrt{\frac{[NADH]}{[NAD^+]}} \qquad \text{E285}$$

$$[NAD^+] = C_{PN} - [NADH] \qquad \text{E286}$$

$$V_{He(F)} = 4^{\text{res(F)}} \frac{r_a\, e^{\frac{A_{res(F)}\,F}{R\,T}} \quad (r_a + r_b)\, e^{\frac{g\,6F_{H}}{R\,T}}}{1 + r_1\, e^{\frac{F\,A_{res(F)}}{R\,T}} \quad e^{\frac{6\,F_{B}}{R\,T}} \quad + \quad r_2 + r_3\, e^{\frac{F\,A_{res(F)}}{R\,T}} \quad e^{\frac{g\,6\,F_{H}}{R\,T}}} \qquad \text{E287}$$

$$A_{res(F)} = \frac{R\,T}{F} \ln \quad K_{res(F)} \sqrt{\frac{[FADH_2]}{[FAD]}} \qquad \text{E288}$$

$$V_{ATPase} = -^{\text{F1}} \frac{10^2\, p_a + p_{c1}\, e^{\frac{3F_{B}}{R\,T}} \quad e^{\frac{A_{F1}\,F}{R\,T}} \; - \; p_a\, e^{\frac{3F_{H}}{R\,T}} + p_{c2}\, e^{\frac{A_{F1}\,F}{R\,T}} \quad e^{\frac{3F_{H}}{R\,T}}}{1 + p_1\, e^{\frac{F\,A_{F1}}{R\,T}} \quad e^{\frac{3F_{B}}{R\,T}} \quad + \quad p_2 + p_3\, e^{\frac{F\,A_{F1}}{R\,T}} \quad e^{\frac{3F_{H}}{R\,T}}} \qquad \text{E289}$$

$$V_{Hu} = -3^{\text{F1}} \frac{10^2 p_a \quad 1 + e^{\frac{F\,A_{F1}}{R\,T}} \quad -(p_a + p_b)\, e^{\frac{3F_{H}}{R\,T}}}{1 + p_1\, e^{\frac{F\,A_{F1}}{R\,T}} \quad e^{\frac{3F_{B}}{R\,T}} \quad + \quad p_2 + p_3\, e^{\frac{F\,A_{F1}}{R\,T}} \quad e^{\frac{3F_{H}}{R\,T}}} \qquad \text{E290}$$

$$A_{F1} = \frac{R\,T}{F} \ln \quad K_{F1} \frac{[ATP]_m}{[ADP]_m\, Pi} \qquad \text{E291}$$

$$V_{Hleak} = g_H \qquad _H \qquad \text{E292}$$

$$_H \; = \; -2.303 \frac{R\,T}{F} \quad pH \; + \qquad _m \qquad \text{E293}$$

Mitochondrial Ca^{2+} handling rates

E294

$$V_{uni} = V_{max}^{uni} \frac{\frac{[Ca^{2+}]_i}{K_{trans}} \left(1 + \frac{[Ca^{2+}]_i}{K_{trans}}\right)^3 \frac{2F\left(\Delta\Psi_m - \Delta\Psi^o\right)}{RT}}{\left(1 + \frac{[Ca^{2+}]_i}{K_{trans}}\right)^4 + \frac{L}{\left(1 + \frac{[Ca^{2+}]_i}{K_{act}}\right)^{n_a}}} \left(1 - e^{\frac{-2F\left(\Delta\Psi_m - \Delta\Psi^o\right)}{RT}}\right)$$

E295

$$V_{NaCa} = V_{max}^{NaCa} \frac{e^{\frac{b F\left(\Delta\Psi_m - \Psi^o\right)}{RT}} e^{\ln\frac{[Ca^{2+}]_m}{[Ca^{2+}]_i}}}{\left(1+\frac{K_{Na}}{[Na^+]_i}\right)^n \left(1+\frac{K_{Ca}}{[Ca^{2+}]_m}\right)}$$

ROS-induced-ROS-release rates

E296

$$V_{SOD\_mito} = \frac{2 \cdot k_{SOD}^1 k_{SOD}^5 \left(k_{SOD}^1 + k_{SOD}^3\right)\left(1 + \frac{[H_2O_2]}{K_i^{H2O2}}\right) E_{SOD}^T [O_2^{\cdot -}]_{p\_mito}}{k_{SOD}^5 \left(2 \cdot k_{SOD}^1 + k_{SOD}^3\right)\left(1 + \frac{[H_2O_2]}{K_i^{H2O2}}\right) + [O_2^{\cdot -}]_{p\_mito} k_{SOD}^1 k_{SOD}^3 \left(1 + \frac{[H_2O_2]}{K_i^{H2O2}}\right)}$$

E297

$$f([O_2^{\cdot -}]_{SR}) = V_{SOD\_SR} = \frac{2 \cdot k_{SOD}^1 k_{SOD}^5 \left(k_{SOD}^1 + k_{SOD}^3\right)\left(1 + \frac{[H_2O_2]}{K_i^{H2O2}}\right) E_{SOD}^T [O_2^{\cdot -}]_{SR}}{k_{SOD}^5 \left(2 \cdot k_{SOD}^1 + k_{SOD}^3\right)\left(1 + \frac{[H_2O_2]}{K_i^{H2O2}}\right) + [O_2^{\cdot -}]_{SR} k_{SOD}^1 k_{SOD}^3 \left(1 + \frac{[H_2O_2]}{K_i^{H2O2}}\right)} \frac{2585.8986}{X^{1.82}}$$

E298

$$V_{CAT} = 2\ k_{CAT}^1\ E_{CAT}^T [H_2O_2]\, e^{\ fr\,[H_2O_2]}$$

E299

$$V_{GPX} = \frac{E_{GPX}^T [H_2O_2][GSH]}{{}_1[GSH] + {}_2[H_2O_2]}$$

$$V_{GR} = \frac{k_{GR}^{1} \; E_{GR}^{T}}{1 + \frac{K_M^{GSSG}}{[GSSG]} + \frac{K_M^{NADPH}}{[NADPH]} + \frac{K_M^{GSSG}}{[GSSG]} \frac{K_M^{NADPH}}{[NADPH]}}$$ E300

$$V_{ROS}^{Tr} = j \cdot \frac{V_{IMAC}}{m} \quad {}_m - \frac{RT}{F} \log \frac{[O_2^{\cdot -}]_{mito}}{[O_2^{\cdot -}]_{p\_mito}}$$ E301

$$V_{IMAC} = a + \frac{b}{1 + \frac{K_{cc}}{[O_2^{\cdot -}]_i}} \quad G_L + \frac{G_{max}}{1 + e^{\left(\begin{smallmatrix} b \\ m \end{smallmatrix} \quad m \right)}} \quad {}_m$$ E302

$$G_T = [GSH] + 2 \cdot [GSSG]$$ E303

ROS-induced-ROS-release metabolites balance equations

$$\frac{d[O_2^{\cdot -}]_{mito}}{dt} = \text{shunt} \; V_{O_2} \quad V_{ROS}^{Tr}$$ E304

$$\frac{d[O_2^{\cdot -}]_{p\_mito}}{dt} = V_{ROS}^{Tr} - V_{SOD\_mito}$$ E305

$$\frac{d[H_2O_2]}{dt} = V_{SOD\_mito} - V_{CAT} - V_{GPX}$$ E306

$$\frac{d[GSH]}{dt} = V_{GR} - V_{GPX}$$ E307

ROS diffusion between mitochondrion and SR

$$\frac{d[O_2^{-}]_{SR}(t)}{dt} = D_{O_2^-} \cdot \frac{[O_2^{-}]_{p\_mito}(t) - [O_2^{-}]_{SR}(t)}{X^2} + \nu_{cyto\_MSM} \cdot f([O_2^{-}]_{SR}(t))$$ E308

Table S9. General parameters

Symbol	Value	Units	Description	Ref.
F	96.5	$C \cdot mmol^{-1}$	Faraday constant	
T	310	K	Absolute temperature	
R	8.31	$J \cdot mol^{-1} \cdot K^{-1}$	Universal gas constant	
C_m	1.0	$\mu F \cdot cm^{-2}$	Membrane capacitance	7
A_{cap}	1.54×10^{-4}	cm^2	Capacitative cell surface area	7
V_{myo}	25.84	pL	Cytosolic volume	7
V_{mito}	15.89	pL	Mitochondrial volume	7
V_{ss}	2.5×10^{-7}	pL	SS volume	**
$[K^+]_o$	5.4	mM	Extracellular K^+ concentration	7
$[Na^+]_o$	140.0	mM	Extracellular Na^+ concentration	7
$[Ca^{2+}]_o$	2.0	mM	Extracellular Ca^{2+} concentration	7

* estimated. ** was slightly modified to achieve ~37% of SR Ca^{2+} depletion during a normal AP cycle.

Table S10. Sarcolemmal membrane current parameters

Symbol	Value	Units	Description	Ref.
$\overline{G}_{Na}$	12.8	$mS \cdot \mu F^{-1}$	Maximal Na channel conductance	7
$\overline{G}_{K_p}$	8.28×10^{-3}	$mS \cdot \mu F^{-1}$	Maximal plateau K^+ channel conductance	4
$P_{Na,K}$	0.0183		Na^+ permeability of K^+ channel	4
k_{NaCa}	9000	$\mu A \cdot \mu F^{-1}$	Scaling factor of Na^+/Ca^+ exchange	4
$k_{m,Na}$	87.5	mM	Na half saturation constant NCX	4
$k_{m,Ca}$	1.38	mM	Na half saturation constant NCX	4
k_{sat}	0.1		Na^+/Ca^{2+} exchange saturation factor at negative potentials	4
η	0.35		Controls voltage dependence of NCX	4

Table S11. Na^+/K^+ pump parameters

Symbol	Value	Units	Description	Ref.
$\bar{I}_{NaK}$	3.247	$\mu A \cdot \mu F^{-1}$	Maximum Na^+/K^+ pump current	4
$K_{m,Nai}$	10	mM	Na half saturation for Na^+/K^+ pump	4
$K_{m,Ko}$	1.5	mM	K half saturation for Na^+/K^+ pump	4
$K_{NaK}^{l,ATP}$	8.0×10^{-3}	mM	ATP half saturation constant for Na^+/K^+ pump	4
$K_{NaK}^{i,ADP}$	0.1	mM	ADP inhibition constant for Na^+/K^+ pump	4

Table S12. Non-specific channel current parameters

Symbol	Value	Units	Description	Ref.
$P_{ns(Na)}$	1.75×10^{-7}	$cm \cdot s^{-1}$	Non-specific channel current Na permeability	4
$K_{m,ns(Ca)}$	1.2×10^{-3}	mM	Ca^{2+} half saturation constant for non-specific current	4
$P_{ns(K)}$	0	$cm \cdot s^{-1}$	Non-specific channel current K permeability	4

Table S13 Background Ca^{2+} current parameters

Symbol	Value	Units	Description	Ref.
$\bar{G}_{Ca,b}$	3.22×10^{-3}	$mS \cdot \mu F^{-1}$	Maximum background current Ca^{2+} conductance	4
$\bar{G}_{Na,b}$	3.5e-3	$mS \cdot \mu F^{-1}$	Maximum background current Na^+ conductance	*

* The parameters were adjusted to maintain $[Na^+]$ at 8.5 mM under normal condition.

Table S14. Sarcolemmal Ca^{2+} current parameters

Symbol	Value	Units	Description	Ref.
I_{pCa_max}	0.575	$\mu A \cdot \mu F^{-1}$	Maximum sarcolemmal Ca^{2+} pump current	4
K_m^{pCa}	5×10^{-4}	mM	Ca^{2+} half saturation constant for sarcolemmal Ca^{2+} pump	4
$K_{m1\_pCa}^{ATP}$	0.012	mM	First ATP half saturation constant for sarcolemmal Ca^{2+} pump	4
$K_{m2\_pCa}^{ATP}$	0.23	mM	Second ATP half saturation constant for sarcolemmal Ca^{2+} pump	4
$K_{i\_pCa}^{ADP}$	1.0	mM	ADP inhibition constant for sarcolemmal Ca^{2+} pump	4

Table S15. Sarcoplasmic reticulum Ca^{2+} ATPase parameters

Symbol	Value	Units	Description	Ref.
$V_{max,f}$	2.99×10^{-4}	ms^{-1}	SERCA forward rate parameter	4
$V_{max,r}$	3.98×10^{-4}	ms^{-1}	SERCA reverse rate parameter	4
K_{fb}	1.5×10^{-4}	mM	Forward Ca^{2+} half saturation constant of SERCA	*
K_{rb}	3.3	mM	Reverse Ca^{2+} half saturation constant of SERCA	*
N_{fb}	0.5		Forward cooperativity constant of SERCA	*
N_{rb}	0.5		Reverse cooperativity constant of SERCA	*
$K_{m,up}^{ATP}$	0.01	mM	ATP half saturation constant for SERCA	4
$K_{i,up}$	0.14	mM	ADP first inhibition constant for SERCA	4
$K_{i,up}^{'}$	5.1	mM	ADP second inhibition constant for SERCA	4

*These parameters were adjusted to maintain diastolic $[Ca^{2+}]_i$ near 60 nM and $[Ca^{2+}]_{SR}$ near 0.45 mM while avoiding net reverse SERCA flux at 1 Hz pacing.

Table S16. L-type Ca^{2+} current parameters

Symbol	Value	Units	Description	Ref.
$\bar{P}_{Ca}$	9.13×10^{-13}	$cm\cdot s^{-1}$	L-type Ca^{2+} channel permeability to Ca^{2+}	[7]
N_{CaRU}	300000		Number of Ca2+ release units	*
f	0.85	ms^{-1}	Transit rate into open state	[7]
g	2	ms^{-1}	Transit rate out of open state	[7]
a	5.0		LCC mode transition parameter	[7]
b	10.0		Mode transition parameter	[7]
γ_0	7.5		Mode transition parameter	[7]
ω	0.068		Mode transition parameter	*

* These parameters are modified to provide better fit of I_{CaL} to experimental data [3].

Table S17. Ca^{2+} release channel parameters

Symbol	Value	Units	Description	Ref.
$k0_{1,2}$	5265	ms^{-1}	RyR channel rate parameter	[7]
$k0_{2,1}$	1500	ms^{-1}	RyR channel rate parameter	[7]
$k0_{2,3}$	$2.36e^{8}$	ms^{-1}	RyR channel rate parameter	[7]
$k0_{3,2}$	9.6	ms^{-1}	RyR channel rate parameter	[7]
$k0_{4,3}$	13.65	ms^{-1}	RyR channel rate parameter	[7]
$k0_{3,4}$	$1.42e^{6}$	ms^{-1}	RyR channel rate parameter	[7]
$k0_{2,5}$	$2.36e^{6}$	ms^{-1}	RyR channel rate parameter	[7]
$k0_{5,2}$	0.0013	ms^{-1}	RyR channel rate parameter	[7]
$k0_{6,5}$	30	ms^{-1}	RyR channel rate parameter	[7]
$k0_{5,6}$	$1.89e^{7}$	ms^{-1}	RyR channel rate parameter	[7]
$k0_{4,5}$	0.07	ms^{-1}	RyR channel rate parameter	[7]
$k0_{5,4}$	93.39	ms^{-1}	RyR channel rate parameter	[7]

Table S18. Force generation parameters

Symbol	Value	Units	Description	Ref.
k_{pn}^{trop}	0.04	ms^{-1}	Transition rate from tropomyosin permissive to non-permissive	5
SL	2.15	μm	Sarcomere length	5
f_{XB}	0.05	ms^{-1}	Transition rate from weak to strong cross bridge	9
g_{XB}^{min}	0.1	ms^{-1}	Minimum transition rate from strong to weak cross bridge	9
g_{off}	0.01	ms^{-1}	Minimium transition rate from strong to weak cross bridge for non-permissive tropomyosin	5
ζ	0.1	$N{\cdot}mm^{-2}$	Conversion factor normalizing to physiological force	5
V_{AM}^{max}	4.8×10^{-4}	$mM{\cdot}ms^{-1}$	Maximal rate of ATP hydrolysis by myofibrils (AM ATPase)	10
$K_{M,AM}^{ATP}$	0.03	mM	ATP half saturation constant of AM ATPase	10
$K_{i,AM}$	0.26	mM	ADP inhibition constant of AM ATPase	10

Table S19. Cytoplasmic energy handling parameters

Symbol	Value	Units	Description	Ref.
C_T	25	mM	Total concentration of creatine metabolites (both compartments)	11, 12
k_{CK}^{cyto}	1.4×10^{-4}	ms^{-1}	Forward rate constant of cytoplasmic CK	13
k_{CK}^{mito}	1.33×10^{-6}	ms^{-1}	Forward rate constant of mitochondrial CK	13
k_{tr}^{Cr}	2.0×10^{-3}	ms^{-1}	Transfer rate constant of CrP	13
K_{EQ}	0.0095		Equilibrium constant of CK	9, 11

V_{ATPase}^{cyto}	$1.0x10^{-5}$	$mM \cdot ms^{-1}$	Constitutive cytosolic ATP consumption rate	14

Table S20. Tricarboxylic acid cycle parameters

Symbol	Value	Units	Description	Ref.
[AcCoA]	1.0	mM	Acetyl CoA concentration	15
k_{cat}^{CS}	0.5	ms^{-1}	Catalytic constant of CS	4
E_T^{CS}	0.4	mM	Concentration of CS	7, 15
K_M^{AcCoA}	1.26×10^{-2}	mM	Michaelis constant for AcCoA	15
K_M^{OAA}	6.4×10^{-4}	mM	Michaelis constant for OAA	15
C_{Kint}	1.0	mM	Sum of TCA cycle intermediates' concentration	15
k_f^{ACO}	1.25×10^{-2}	ms^{-1}	Forward rate constant of ACO	15
K_E^{ACO}	2.22		Equilibrium constant of ACO	15
K_{ADP}^{a}	0.62	mM	Activation constant by ADP	4
K_{Ca}^{a}	0.0005	mM	Activation constant for Ca^{2+}	4
$K_{i,NADH}$	0.19	mM	Inhibition constant by NADH	15
k_{cat}^{IDH}	0.05	ms^{-1}	Rate constant of IDH	4
E_T^{IDH}	0.109	mM	Concentration of IDH	15
$[H^+]$	2.5×10^{-5}	mM	Matrix proton concentration	15
$k_{h,1}$	8.1×10^{-5}	mM	Ionization constant of IDH	15
$k_{h,2}$	5.98×10^{-5}	mM	Ionization constant of IDH	15
K_M^{ISOC}	1.52	mM	Michaelis constant for isocitrate	15
ni	2.0		Cooperativity for isocitrate	15

K_M^{NAD}	0.92	mM	Michaelis constant for NAD^+	15
$K_D^{Mg^{2+}}$	0.031	mM	Activation constant for Mg^{2+}	15
$K_D^{Ca^{2+}}$	1.27×10^{-3}	mM	Activation constant for Ca^{2+}	15
E_T^{KGDH}	0.5	mM	Concentration of KGDH	15
k_{cat}^{KGDH}	0.075	ms^{-1}	Rate constant of KGDH	4
K_M^{KG}	1.94	mM	Michaelis constant for αKG	15
K_M^{NAD}	38.7	mM	Michaelis constant for NAD	15
$n_{\alpha KG}$	1.2		Hill coefficient of KGDH for αKG	15
Mg^{2+}	0.4	mM	Mg^{2+} concentration in mitochondria	15
k_f^{SL}	5.0×10^{-3}	$mM^{-1}\cdot ms^{-1}$	Forward rate constant of SL	4
K_E^{SL}	3.12		Equilibrium constant of the SL reaction	15
[CoA]	0.02	mM	Coenzyme A concentration	15
k_{cat}^{SDH}	5.0×10^{-3}	ms^{-1}	Rate constant of SDH	4
E_T^{SDH}	0.5	mM	SDH enzyme concentration	15
K_M^{Suc}	0.03	mM	Michaelis constant for succinate	15
K_i^{FUM}	1.3	mM	Inhibition constant by fumarate	15
$K_{i,sdh}^{OAA}$	0.15	mM	Inhibition constant by oxalacetate	15
k_f^{FH}	3.32×10^{-3}	ms^{-1}	Forward rate constant for FH	4
K_E^{FH}	1.0		Equilibrium constant of FH	15
k_{h1}	1.13×10^{-5}	mM	Ionization constant of MDH	15
k_{h2}	26.7	mM	Ionization constant of MDH	15
k_{h3}	6.68×10^{-9}	mM	Ionization constant of MDH	15
k_{h4}	5.62×10^{-6}	mM	Ionization constant of MDH	15
k_{offset}	3.99×10^{-2}		pH-independent term in the pH activation factor of MDH	15
k_{cat}^{MDH}	0.11	ms^{-1}	Rate constant of MDH	4

E_T^{MDH}	0.15	mM	Total MDH enzyme concentration	15
K_M^{MAL}	1.49	mM	Michaelis constant for malate	15
K_i^{OAA}	3.1×10^{-3}	mM	Inhibition constant for oxalacetate	15
K_M^{NAD}	0.22	mM	Michaelis constant for NAD^+	15
[GLU]	1	mM	Glutamate concentration	15
k_f^{AAT}	6.44×10^{-4}	ms^{-1}	Forward rate constant of AAT	15
K_E^{AAT}	6.6		Equilibrium constant of AAT	15
k_{ASP}	1.5×10^{-6}	ms^{-1}	Rate constant of aspartate consumption	4

Table S21. Oxidative phosphorylation parameters

Symbol	Value	Units	Description	Ref.
r_a	6.39×10^{-13}	ms^{-1}	Sum of products of rate constants	15
r_b	1.76×10^{-16}	ms^{-1}	Sum of products of rate constants	15
r_{c1}	2.66×10^{-22}	ms^{-1}	Sum of products of rate constants	15
r_{c2}	8.63×10^{-30}	ms^{-1}	Sum of products of rate constants	15
r_1	2.08×10^{-18}		Sum of products of rate constants	15
r_2	1.73×10^{-9}		Sum of products of rate constants	15
r_3	1.06×10^{-26}		Sum of products of rate constants	15
ρ^{res}	0.1×10^{-3}	mM	Concentration of electron carriers (respiratory complexes I-III-IV)	4
K_{res}	1.35×10^{18}		Equilibrium constant of respiration	15
$\rho^{res(F)}$	3.75×10^{-4}	mM	Concentration of electron carriers (respiratory complexes II-III-IV)	4
$\Delta\Psi_B$	50	mV	Phase boundary potential	15
g	0.85		Correction factor for voltage	15
$K_{res(F)}$	5.77×10^{13}		Equilibrium constant of $FADH_2$ oxidation	15
[FADH2]	1.24	mM	Concentration of $FADH_2$ (reduced)	15
[FAD]	0.01	mM	Concentration of FAD (oxidized)	15

p_a	1.66×10^{-8}	ms^{-1}	Sum of products of rate constants	15
p_b	3.37×10^{-10}	ms^{-1}	Sum of products of rate constants	15
p_{c1}	9.65×10^{-17}	ms^{-1}	Sum of products of rate constants	15
p_{c2}	4.59×10^{-17}	ms^{-1}	Sum of products of rate constants	15
p_1	1.35×10^{-8}		Sum of products of rate constants	15
p_2	7.74×10^{-7}		Sum of products of rate constants	15
p_3	6.65×10^{-15}		Sum of products of rate constants	15
ρ^{F1}	0.05	mM	Concentration of F_1F_0-ATPase	4
K_{F1}	1.71×10^{6}		Equilibrium constant of ATP hydrolysis	15
Pi	2.0	mM	Inorganic phosphate concentration	4
C_A	1.5	mM	Total sum of mito adenine nucleotides	4
V_{maxANT}	0.005	$mM\cdot ms^{-1}$	Maximal rate of the ANT	4, 15
h^{ANT}	0.5		Fraction of $\Delta\Psi_m$	15
g_H	1.0×10^{-8}	$mM\cdot ms^{-1}\cdot mV^{-1}$	Ionic conductance of the inner membrane	15
ΔpH	-0.6	pH units	pH gradient across the inner memb.	15
C_{PN}	1.0	mM	Total sum of mito pyridine nucleotides	15
C_{mito}	1.81×10^{-3}	$mM\cdot mV^{-1}$	Inner membrane capacitance	15

Table S22. Mitochondrial Ca^{2+} handling parameters

Symbol	Value	Units	Description	Ref.
V_{max}^{uni}	0.028	$mM\cdot ms^{-1}$	Vmax uniport Ca^{2+} transport	4
$\Delta\Psi°$	91	mV	Offset membrane potential	15
K_{act}	3.8×10^{-4}	mM	Activation constant	15
K_{trans}	0.019	mM	K_d for translocated Ca^{2+}	15
L	110.0		Keq for conformational transitions in uniporter	15

n_a	2.8		Uniporter activation cooperativity	[15]
V_{max}^{NaCa}	1×10^{-4}	$mM\cdot ms^{-1}$	Vmax of Na^+/Ca^{2+} antiporter	*
b	0.5		$\Delta\Psi_m$ dependence of Na^+/Ca^{2+} antiporter	[15]
K_{Na}	9.4	mM	Antiporter Na^+ constant	[15]
K_{Ca}	3.75×10^{-4}	mM	Antiporter Ca^{2+} constant	[15]
n	3		Na^+/Ca^{2+} antiporter cooperativity	[15]
δ	$3.0x10^{-4}$		Fraction of free $[Ca^{2+}]_m$	[15]

*: The maximal rate of the Na^+/Ca^{2+} antiporter was adjusted to balance the mitochondrial Ca^{2+} level.

Table S23. ROS-induced-ROS-release parameters

Symbol	Value	Units	Description	Ref.
af	1×10^{-4}		Activation factor by cytoplasmic $O_2^{\cdot-}$	[4]
Kcc	0.01	mM	Activation constant of IMAC by $O_2^{\cdot-}$	[4]
G_L	3.50×10^{-8}	$mM\cdot ms^{-1}\cdot mV^{-1}$	Leak conductance for IMAC	[4]
G_max	3.91×10^{-6}	$mM\cdot ms^{-1}\cdot mV^{-1}$	Integral conductance of IMAC at saturation	[4]
	0.07	mV^{-1}	Steepness factor	[4]
$^{b}_{m}$	4	mV	Potential at half-saturation	[4]
k1_SOD	1.2×10^{3}	$mM\cdot ms^{-1}$	Second-order rate constant of conversion between native oxidized and reduced SOD	[4]
k5_SOD	2.5×10^{-4}	$mM^{-1}\cdot ms^{-1}$	First-order rate constant for conversion between inactive and active oxidized SOD	[4]
k3_SOD	24	$mM^{-1}\cdot ms^{-1}$	Second-order rate constant of conversion between native reduced SOD and its inactive form	[4]
etSOD	1.43×10^{-3}	mM	Intracellular concentration of SOD	[4]
K_i^{H2O2}	0.5	mM	Inhibition constant for H_2O_2	[4]
k_{CAT}^1	17	$mM^{-1}\cdot ms^{-1}$	Rate constant of CAT	[4]
E_{CAT}^T	0.01	mM	Intracellular CAT concentration	[4]
fr	0.05		Hydrogen peroxide inhibition factor for CAT	[4]
E_{GPX}^T	0.01	mM	Intracellular GPX concentration	[4]
$_1$	5×10^{-3}	mM·ms	Constant for GPX activity	[4]
$_2$	0.75	mM·ms	Constant for GPX activity	[4]

k^1_{GR}	5×10^{-3}	ms^{-1}	Rate constant of GR	[4]
E^T_{GR}	0.01	mM	Intracellular GR concentration	[4]
K^{GSSG}_M	0.06	mM	Michaelis constant for oxidized glutathione of GR	[4]
K^{NADPH}_M	0.015	mM	Michaelis constant for NADH for GR	[4]
NADPH	1	mM	Total NADH pool	[4]
G_T	1	mM	Total glutathione pool	[4]
shunt	0.02		Fraction of O^2 to form superoxide.	[4]
j	0.1		Fraction of IMAC conductance.	[4]

*: The ROS diffusion coefficient and the distance between SR and mitochondria were adjusted to be inconsistent with previous experimental studies [16, 17].

Table S24. ROS diffusion model parameters

Symbol	Value	Units	Description	Ref.
$D_{O2.-}$	0.295	$\mu m^2 \cdot ms^{-1}$	$O_2^{\cdot-}$ diffusion coefficient	*
X	75	nm	Distance between SR and mitochondria	*
c_{ryr}	0.2		ROS enhancement coefficient	**
k_{ryr}	19.55	mM^{-1}	ROS enhancement effective factor	**
c_{SERCA}	1.02		ROS inhibition coefficient	**
k_{SERCA}	43.67	mM^{-1}	ROS inhibition effective factor	**
V_{cyto_MSM}	2.05×10^5		Cytosolic/MSM effective volume ratio	***

*: The ROS diffusion coefficient and the distance between SR and mitochondria were adjusted to be inconsistent with previous experimental studies [16, 17].

**: The values of model parameter were obtained using the least-square curve fitting method, as described in the text.

***: estimated.

Table S25. CaMKII activation parameters

Symbol	Value	Units	description	Ref.
k_1	2.5	$mM^{-1} \cdot ms^{-1}$	The kinetic rate constant	[1, 18, 19]
k_{-1}, k_{-2}	0.05	ms^{-1}	The kinetic rate constant	[1, 18, 19]
k_2	88.25	$mM^{-1} \cdot ms^{-1}$	The kinetic rate constant	[1, 18, 19]

k_3	12.5	$mM^{-1}\cdot ms^{-1}$	The kinetic rate constant	[1, 18, 19]
k_{-3}, k_{-4}	1.25	ms^{-1}	The kinetic rate constant	[1, 18, 19]
k_{asso}	2.1	$mM^{-1}\cdot ms^{-1}$	The association rate constant	[1, 18, 19]
k_{disso}	0.7×10^{-4}	ms^{-1}	The dissociation rate constant	[1, 18, 19]
$k_{dissoCa}$	0.95×10^{-3}	ms^{-1}	The dissociation rate constant	[1, 18, 19]
$k_{dissoCa2}$	0.95×10^{-6}	ms^{-1}	The dissociation rate constant	[1, 18, 19]
k_{cat}	5.4×10^{-3}	ms^{-1}	The phosphorylation rate constant	[1, 18, 19]
$k_{cat,PP1}$	1.72×10^{-3}	ms^{-1}	The dephosphorylation rate constant	[1, 18, 19]
$K_{m,ATP}$	19.1×10^{-3}	mM	The binding affinity for ATP	[1, 18, 19]
$K_{m,PP1}$	11.0×10^{-3}	mM	The binding affinity for PP1	[1, 18, 19]
k_{ox}	0.013	$mM^{-1}\cdot ms^{-1}$	The oxidation rate by ROS	[1]
k_{MrsA}	1.0×10^{-4}	ms^{-1}	The reduction rate by MrsA	[1]
$[PP1]$	14.3×10^{-3}	mM	The concentration of protein phosphatases	[1]
$[CaM_{total}]$	50.0×10^{-3}	mM	The concentration of total CaM	[1]
$[CaMKII_{total}]$	3.15×10^{-6}	mM	The concentration of total CaMKII	[1]

Table S26. Markov late sodium channels parameters

Parameter	Unphosphorylated	Phosphorylated	Ref.
P1a1	3.99	3.99	[20]
P2a1	0.02	0.02	
P1a4	5.76	5.76	
P2a4	107.67	1.67	
P1a5	1.63×10^{-8}	2.5×10^{-8}	
P2a5	6.21	6.21	
P1b1	0.03	0.03	
P2b1	9.35	9.35	
P1b2	0.037	0.037	
P2b2	6.66	6.66	
P1b3	1.67×10^{-3}	1.67×10^{-3}	
P2b3	17.33	17.33	
P1b5	0.013	0.013	

P2b5	-7.2×10^{-6}	-1.82×10^{-6}
P1a6	27.27	1.99
P1b6	$2.45^{\times}10^{-6}$	3.77×10^{-6}
P2b6	11.79	11.79
P1a7	0.0047	0.0018
P2a7	25.91	151.60
P1b7	0.03	0.03
P2b7	53.44	53.44
P1a8	1.62×10^{-6}	7.24×10^{-6}
P1b8	1.54×10^{-3}	1.54×10^{-3}
P1a42	1.21	0.10

Table S27. Sodium channels Phosphorylation Parameters

Symbol	Value	Units	description	Ref.
$G_{Na,Late}$	8	$mS/\mu F$	Conduction rate of late sodium channels	[20]
K_{Dephos}	7.19×10^{-4}	ms^{-1}	The unphosphorylation rate of Na^+ channels	[21]
k_{Phos_MAX}	1.07	ms^{-1}	The phosphorylation rate of Na^+ channels	*

*The dephosphorylation rate was fit using the experiment data [2]

Table S28. States variables initial values

Symbol	Unit	Description	Value
V	mV	Sarcolemmal membrane potential	-84.24
m_{Na}		Sodium channel activation gate	0.033
h_{Na}		Sodium channel inactivation gate	0.98
j_{Na}		Sodium channel slow inactivation gate	0.99
X_k		Potassium channel activation gate	1.89×10^{-4}
$[Na^+]_i$	mM	Intracellular Na^+ concentration	8.12

$[K^+]_i$	mM	Intracellular K^+ concentration	136.9
$[Ca^{2+}]_i$	mM	Intracellular Ca^{2+} concentration	5.08×10^{-5}
$[Ca^{2+}]_{JSR}$	mM	JSR Ca^{2+} concentration	0.47
$[Ca^{2+}]_{NSR}$	mM	NSR Ca^{2+} concentration	0.47
$[Ca^{2+}]_m$	mM	Mitochondrial free Ca^{2+} concentration	1.44×10^{-4}
x_1		State 1 of Calcium release	6.9×10^{-4}
x_2		State 2 of Calcium release	1.89×10^{-1}
x_3		State 3 of Calcium release	7.91×10^{-2}
x_4		State 4 of Calcium release	5.41×10^{-6}
x_5		State 5 of Calcium release	5.15×10^{-2}
x_6		State 6 of Calcium release	1.35×10^{-3}
x_7		State 7 of Calcium release	3.71×10^{-1}
x_8		State 8 of Calcium release	1.58×10^{-1}
x_9		State 9 of Calcium release	8.17×10^{-6}
x_{10}		State 10 of Calcium release	7.77×10^{-2}
x_{11}		State 11 of Calcium release	6.09×10^{-10}
x_{12}		State 12 of Calcium release	1.77×10^{-7}
x_{13}		State 13 of Calcium release	1.26×10^{-6}
x_{14}		State 14 of Calcium release	8.14×10^{-11}
x_{15}		State 15 of Calcium release	7.52×10^{-7}
x_{16}		State 16 of Calcium release	1.71×10^{-10}
x_{17}		State 17 of Calcium release	4.67×10^{-8}
x_{18}		State 18 of Calcium release	2.22×10^{-8}
x_{19}		State 19 of Calcium release	1.71×10^{-11}
x_{20}		State 20 of Calcium release	1.62×10^{-7}
x_{21}		State 21 of Calcium release	8.74×10^{-6}
x_{22}		State 22 of Calcium release	2.55×10^{-3}

x_{23}		State 23 of Calcium release	2.86×10^{-3}
x_{24}		State 24 of Calcium release	1.33×10^{-6}
x_{25}		State 25 of Calcium release	1.23×10^{-2}
x_{26}		State 26 of Calcium release	4.84×10^{-7}
x_{27}		State 27 of Calcium release	1.30×10^{-4}
x_{28}		State 28 of Calcium release	9.42×10^{-5}
x_{29}		State 29 of Calcium release	2.62×10^{-7}
x_{30}		State 30 of Calcium release	2.48×10^{-3}
x_{31}		State 31 of Calcium release	3.54×10^{-5}
x_{32}		State 32 of Calcium release	9.74×10^{-3}
x_{33}		State 33 of Calcium release	4.19×10^{-3}
x_{34}		State 34 of Calcium release	1.16×10^{-6}
x_{35}		State 35 of Calcium release	1.10×10^{-2}
x_{36}		State 36 of Calcium release	4.47×10^{-5}
x_{37}		State 37 of Calcium release	1.23×10^{-2}
x_{38}		State 38 of Calcium release	5.23×10^{-3}
x_{39}		State 39 of Calcium release	8.87×10^{-7}
x_{40}		State 40 of Calcium release	8.46×10^{-3}
[LTRPNCa]	mM	Ca^{2+} bound to low affinity troponin sites	3.29×10^{-3}
[HTRPNCa]	mM	Ca^{2+} bound to high affinity troponin sites	0.11
$[N_0]$		Non-permissive tropomyosin with 0 cross bridges	0.99
$[N_1]$		Non-permissive tropomyosin with 1 cross bridges	7.91×10^{-7}
$[P_0]$		Permissive tropomyosin with 0 cross bridges	9.07×10^{-7}
$[P_1]$		Permissive tropomyosin with 1 cross bridges	9.88×10^{-7}
$[P_2]$		Permissive tropomyosin with 2 cross bridges	1.47×10^{-6}
$[P_3]$		Permissive tropomyosin with 3 cross bridges	1.28×10^{-6}
$[ATP]_i$	mM	EC coupling linked ATP concentration	7.97

$[ATP]_{ic}$	mM	Cytosolic ATP concentration not linked to EC coupling	7.95
$[CrP]_{i}$	mM	Mitochondrial linked creatine phosphate concentration	15.27
$[CrP]_{ic}$	mM	Cytosolic creatine phosphate concentration	15.28
$[ADP]_{m}$	mM	Mitochondrial ADP concentration	0.010
[NADH]	mM	Mitochondrial NADH concentration	9.18
$\Delta\Psi_{m}$	mV	Inner mitochondrial membrane potential	131.3
[ISOC]	mM	Isocitrate concentration (mitochondrial)	0.55
[αKG]	mM	α ketoglutarate concentration (mitochondrial)	3.79×10^{-5}
[SCoA]	mM	Succinyl CoA concentration (mitochondrial)	0.18
[Suc]	mM	Succinate concentration (mitochondrial)	1.15×10^{-4}
[FUM]	mM	Fumarate concentration (mitochondrial)	0.013
[MAL]	mM	Malate concentration (mitochondrial)	9.67×10^{-3}
[OAA]	mM	Oxalacetate concentration (mitochondrial)	3.35×10^{-8}
$[O_2^{\cdot-}]_{p\_mito}$	mM	$O_2^{\cdot-}$ concentration (peri_mito)	9.45×10^{-7}
$[O_2^{\cdot-}]_{SR}$	mM	$O_2^{\cdot-}$ concentration (peri-SR)	1.39×10^{-10}
$[O_2^{\cdot-}]_{mito}$	mM	$O_2^{\cdot-}$ concentration (mitocondrial)	0.29
$[H_2O_2]$	mM	Hydrogen peroxdize (cytoplasmic)	6.70×10^{-7}
[GSH]	mM	Reduced glutathione (cytoplasmic)	0.99
[CaMCa]	mM	CaM with one Ca^{2+} ion binded	1.35×10^{-4}
[CaMCa2]	mM	CaM with two Ca^{2+} ion binded	1.29×10^{-5}
[CaMCa3]	mM	CaM with three Ca^{2+} ion binded	7.02×10^{-9}
[CaMCa4]	mM	CaM with four Ca^{2+} ion binded	7.62×10^{-11}
[B]	mM	CaMKII with Ca^{2+}/CaM binded	7.62×10^{-11}
[P]	mM	CaMKII with Ca^{2+}/CaM binded and being phosphorylated	1.05×10^{-12}
[A]	mM	CaMKII with being phosphorylated	1.03×10^{-16}

[OxB]	mM	CaMKII with Ca^{2+}/CaM binded and being oxidated	4.04×10^{-14}
[OxP]	mM	CaMKII with Ca^{2+}/CaM binded and being phosphorylated and oxidated	5.13×10^{-17}
[OxA]	mM	CaMKII with being phosphorylated and oxidated	1.00×10^{-19}
IC3		State of unphosphorylated sodium channels	5.21×10^{-1}
IC2		State of unphosphorylated sodium channels	2.98×10^{-2}
IF		State of unphosphorylated sodium channels	3.71×10^{-5}
IM1		State of unphosphorylated sodium channels	8.37×10^{-3}
IM2		State of unphosphorylated sodium channels	1.33×10^{-4}
C3		State of unphosphorylated sodium channels	4.16×10^{-1}
C2		State of unphosphorylated sodium channels	2.38×10^{-2}
C1		State of unphosphorylated sodium channels	2.96×10^{-5}
O		State of unphosphorylated sodium channels	6.78×10^{-8}
LC3		State of unphosphorylated sodium channels	3.92×10^{-4}
LC2		State of unphosphorylated sodium channels	2.24×10^{-5}
LC1		State of unphosphorylated sodium channels	2.79×10^{-8}
LO		State of unphosphorylated sodium channels	6.39×10^{-11}
$IC3'$		State of phosphorylated sodium channels	4.19×10^{-1}
$IC2'$		State of phosphorylated sodium channels	2.39×10^{-2}
IF'		State of phosphorylated sodium channels	2.98×10^{-5}
$IM1'$		State of phosphorylated sodium channels	7.33×10^{-4}
$IM2'$		State of phosphorylated sodium channels	7.39×10^{-5}
$C3'$		State of phosphorylated sodium channels	5.24×10^{-1}
$C2'$		State of phosphorylated sodium channels	2.99×10^{-2}
$C1'$		State of phosphorylated sodium channels	3.73×10^{-5}

O'	State of phosphorylated sodium channels	8.54×10^{-8}
$LC3'$	State of phosphorylated sodium channels	2.29×10^{-3}
$LC2'$	State of phosphorylated sodium channels	1.31×10^{-4}
$LC1'$	State of phosphorylated sodium channels	1.63×10^{-7}
LO'	State of phosphorylated sodium channels	3.74×10^{-10}
ϕ_{Na}	The fraction of unphosphorylated Na^+ channels	7.81×10^{-1}
$\phi_{Na,CaMKII}$	The fraction of phosphorylated Na^+ channels	2.2×10^{-1}

Figure S1. Top: The Scheme of CaMKII activation model modified from Foteinou *et al.* [1]. In this model, there is only one inactive state (state I). CaMKII can be activated *via* binding Ca^{2+}/CaM, autophosphorylating, and oxidizing. Bottom: The scheme of Markov model for CaMKII activation-dependent sodium channel phosphorylation. We hypothesized that the phosphorylated rate was proportional to CaMKII autophosphorylation rate and the fraction of activated CaMKII. The dephosphorylation rate was a constant which was fit using the experiment data from Wagner *et al.* [2]. CaMKII: Ca^{2+}/calmodulin-dependent protein kinase II; CaM: calmodulin.

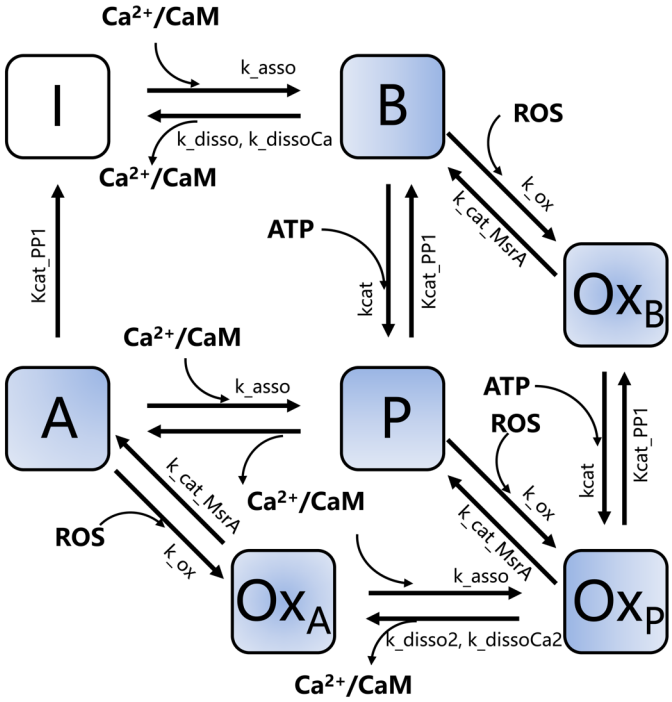

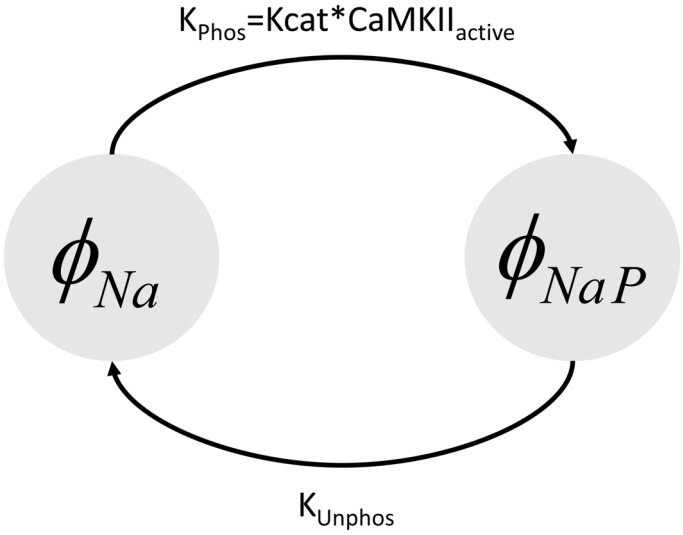

Figure S2. (A): Increasing *shunt* from 0.02 to 0.1 caused sustained mitochondrial oscillations and cyclic reactive oxygen species (ROS) bursts in a cardiomyocyte. (B): Dynamics of cytosolic Na^+ concentration ($[Na^+]_i$) during mitochondrial oscillations in the presence of oxidative CaMKII oxidation. (C): Dynamics of cytosolic Na^+ concentration during mitochondrial oscillations in the absence of oxidative CaMKII oxidation. CaMKII: Ca^{2+}/calmodulin-dependent protein kinase II.

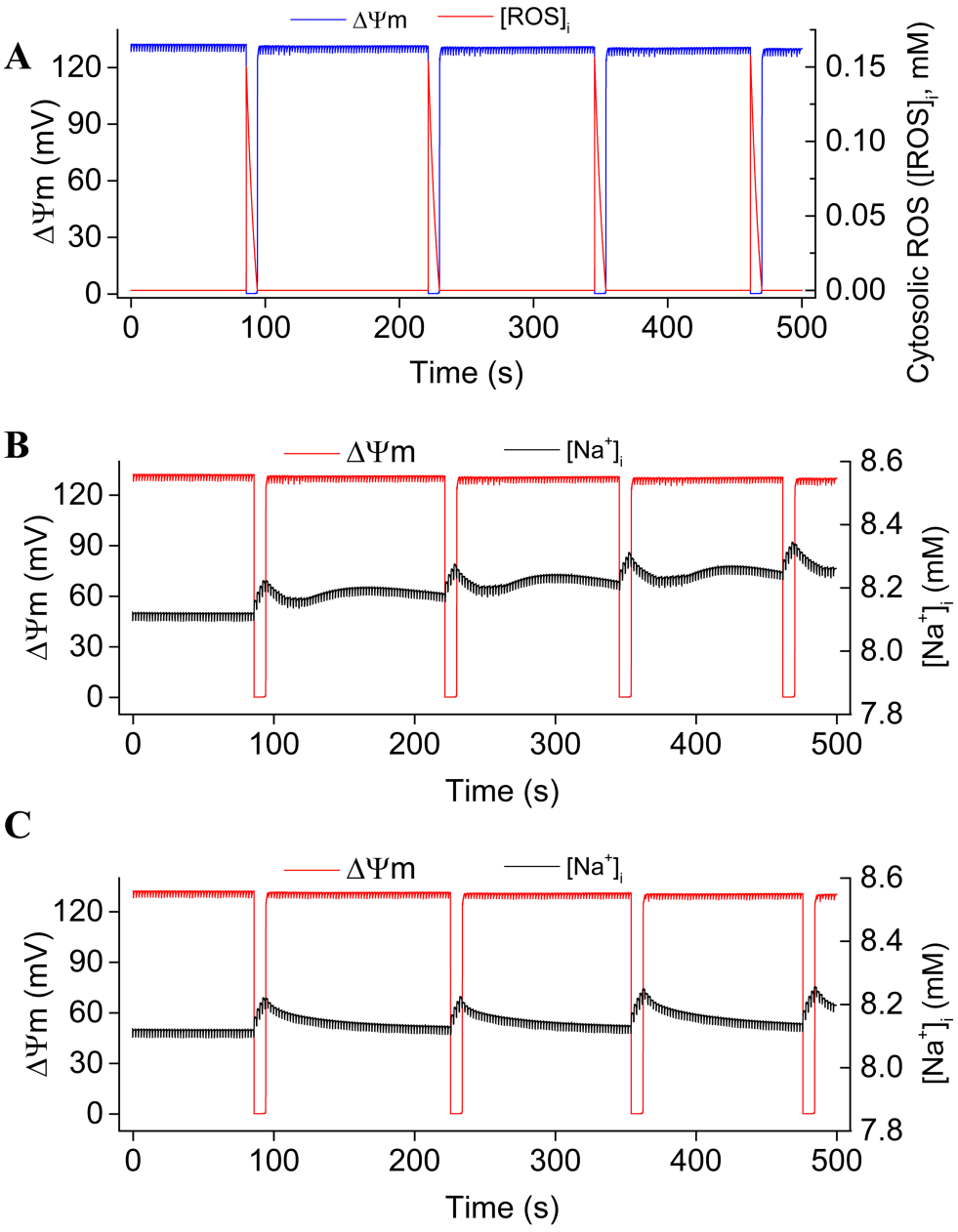

Figure S3. After the 3rd depolarization, the EADs sustained throughout the whole repolarization phase. *Shunt* = 0.14, PCL = 2s. EADs: early afterdepolarizations; PCL: pacing cycle length.

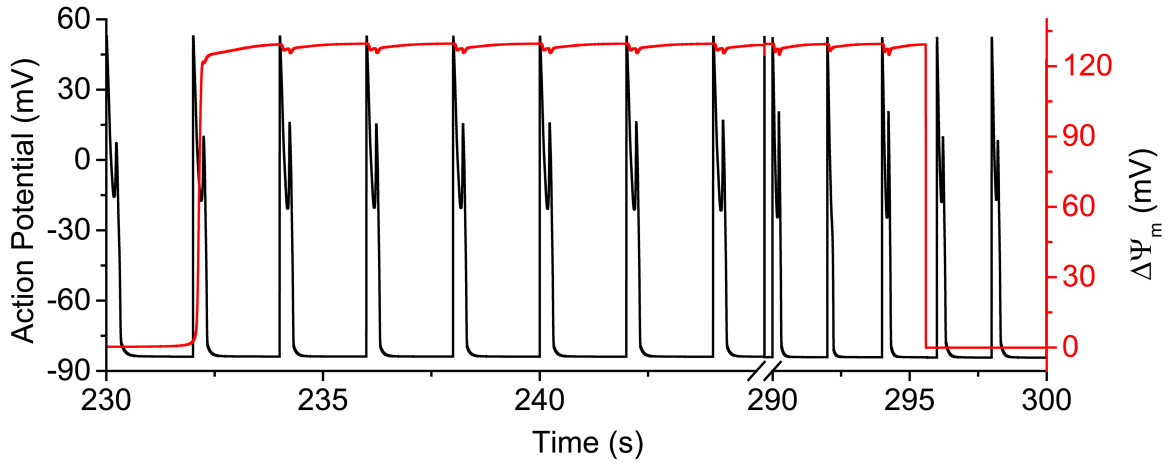

Figure S4. Effect of increasing ROS scavenging (i.e. *et_SOD*) on mdROS-CaMKII activation-induced EADs. *et_SOD* was increased from 1.43 x 10^{-3} mM (baseline value) to 1.8 x 10^{-3} mM at 200s (black line), 300s (red line), or 700s (blue line). (A): The fraction of phosphorylation sodium channels. (B): Action potentials of the last two beats. *shunt* = 0.14 and PCL = 2s. mdROS: mitochondrial-derived reactive oxygen species; CaMKII: Ca^{2+}/calmodulin-dependent protein kinase II; EADs: early afterdepolarizations; PCL: pacing cycle length.

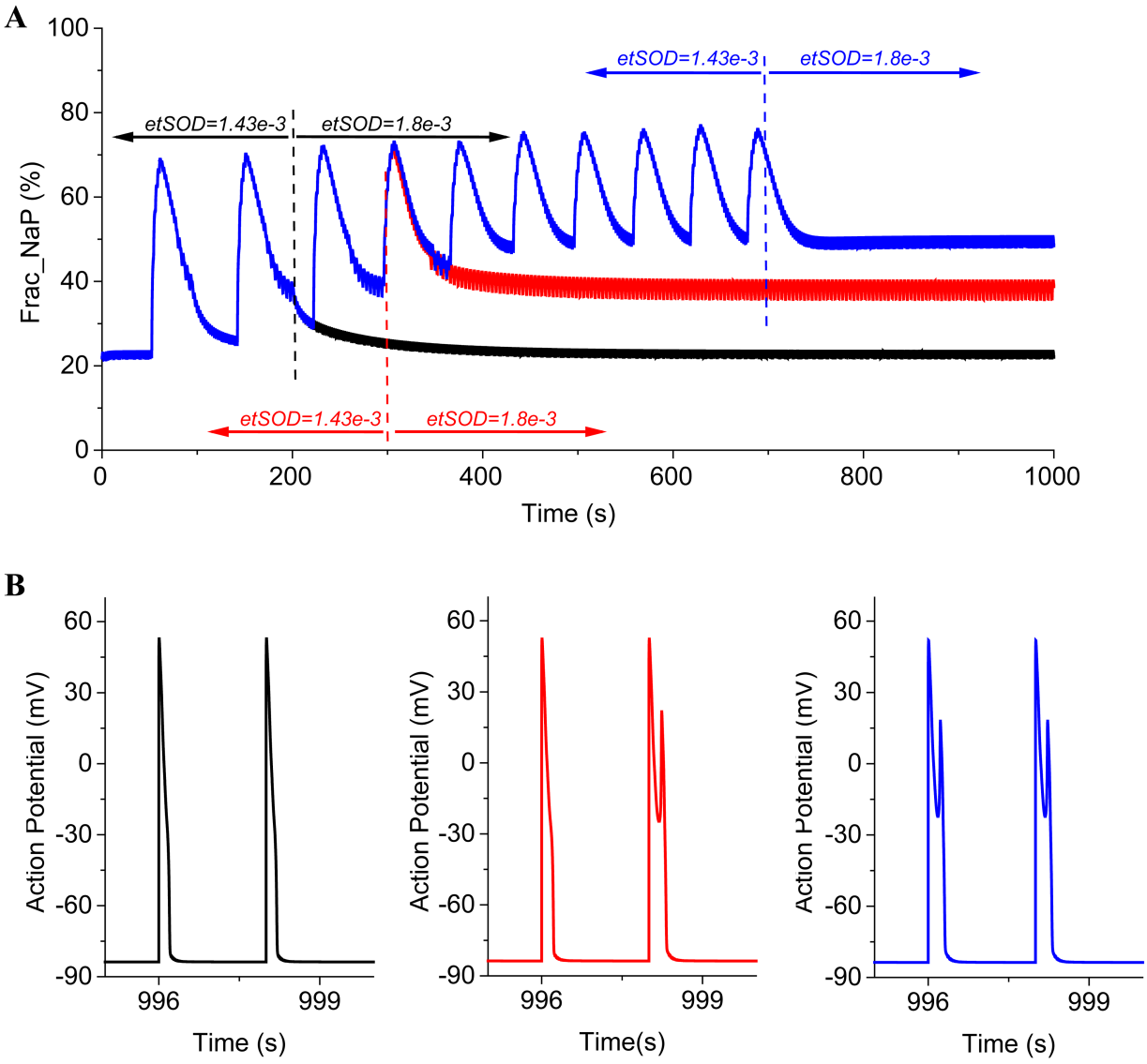

Supplemental References:

1. Foteinou PT, Greenstein JL, Winslow RL. Mechanistic investigation of the arrhythmogenic role of oxidized camkii in the heart. *Biophys J*. 2015;109:838-849
2. Wagner S, Ruff HM, Weber SL, Bellmann S, Sowa T, Schulte T, Anderson ME, Grandi E, Bers DM, Backs J, Belardinelli L, Maier LS. Reactive oxygen species-activated ca/calmodulin kinase iidelta is required for late i(na) augmentation leading to cellular na and ca overload. *Circulation research*. 2011;108:555-565
3. Grantham CJ, Cannell MB. Ca2+ influx during the cardiac action potential in guinea pig ventricular myocytes. *Circulation research*. 1996;79:194-200
4. Zhou L, Cortassa S, Wei AC, Aon MA, Winslow RL, O'Rourke B. Modeling cardiac action potential shortening driven by oxidative stress-induced mitochondrial oscillations in guinea pig cardiomyocytes. *Biophys J*. 2009;97:1843-1852
5. Rice JJ, Jafri MS, Winslow RL. Modeling short-term interval-force relations in cardiac muscle. *Am. J. Physiol. Heart Circ. Physiol.* 2000;278:H913-931
6. Terracciano CM, Naqvi RU, MacLeod KT. Effects of rest interval on the release of calcium from the sarcoplasmic reticulum in isolated guinea pig ventricular myocytes. *Circulation research*. 1995;77:354-360
7. Gauthier LD, Greenstein JL, Winslow RL. Toward an integrative computational model of the guinea pig cardiac myocyte. *Front Physiol*. 2012;3:244
8. Bers D. *Excitation-contraction coupling and cardiac contractile force*. Springer; 2001.
9. Ruf T, Hebisch S, Gross R, Alpert N, Just H, Holubarsch C. Modulation of myocardial economy and efficiency in mammalian failing and non-failing myocardium by calcium channel activation and beta-adrenergic stimulation. *Cardiovasc. Res.* 1996;32:1047-1055
10. Karatzaferi C, Myburgh KH, Chinn MK, Franks-Skiba K, Cooke R. Effect of an adp analog on isometric force and atpase activity of active muscle fibers. *Am. J. Physiol. Cell Physiol.* 2003;284:C816-825
11. Selivanov VA, Alekseev AE, Hodgson DM, Dzeja PP, Terzic A. Nucleotide-gated katp channels integrated with creatine and adenylate kinases: Amplification, tuning and sensing of energetic signals in the compartmentalized cellular environment. *Mol. Cell. Biochem.* 2004;256-257:243-256
12. Joubert F, Gillet B, Mazet JL, Mateo P, Beloeil J, Hoerter JA. Evidence for myocardial atp compartmentation from nmr inversion transfer analysis of creatine kinase fluxes. *Biophys J*. 2000;79:1-13
13. Clark JF, Kuznetsov AV, Radda GK. Adp-regenerating enzyme systems in mitochondria of guinea pig myometrium and heart. *Am. J. Physiol.* 1997;272:C399-404
14. Ingwall JS, Weiss RG. Is the failing heart energy starved? On using chemical energy to support cardiac function. *Circ. Res.* 2004;95:135-145
15. Cortassa S, Aon MA, Marban E, Winslow RL, O'Rourke B. An integrated model of cardiac mitochondrial energy metabolism and calcium dynamics. *Biophys J*. 2003;84:2734-2755
16. Cortassa S, Aon MA, Winslow RL, O'Rourke B. A mitochondrial oscillator dependent on reactive oxygen species. *Biophys J*. 2004;87:2060-2073

17. Sharma VK, Ramesh V, Franzini-Armstrong C, Sheu SS. Transport of ca2+ from sarcoplasmic reticulum to mitochondria in rat ventricular myocytes. *Journal of bioenergetics and biomembranes*. 2000;32:97-104

18. Chiba H, Schneider NS, Matsuoka S, Noma A. A simulation study on the activation of cardiac camkii delta-isoform and its regulation by phosphatases. *Biophys J*. 2008;95:2139-2149

19. Zhang SZ, Li QC, Zhou LF, Wang KQ, Zhang HG. Development of a novel markov chain model for oxidative-dependent camkii delta activation. *2015 Computing in Cardiology Conference (Cinc)*. 2015;42:881-884

20. Hashambhoy YL, Winslow RL, Greenstein JL. Camkii-dependent activation of late ina contributes to cellular arrhythmia in a model of the cardiac myocyte. *Conf Proc IEEE Eng Med Biol Soc*. 2011;2011:4665-4668

21. Hashambhoy YL, Winslow RL, Greenstein JL. Camkii-induced shift in modal gating explains l-type ca(2+) current facilitation: A modeling study. *Biophys J*. 2009;96:1770-1785